

# **Stimuli Responsive Hybrid Microgels Functionalized with Metal Nanoparticles**

Von der Fakultät für Mathematik, Informatik und Naturwissenschaften der RWTH  
Aachen University zur Erlangung des akademischen Grades eines Doktors der  
Naturwissenschaften genehmigte Dissertation

vorgelegt von

M. Sc. Volodymyr Palchyk

aus Schostka, Ukraine

Berichter: Universitätsprofessor Prof. Dr. Andrij Pich

Universitätsprofessor Prof. Dr. Magnus Rueping

Tag der mündlichen Prüfung: 07.12.2016

Diese Dissertation ist auf der Internetseite der Hochschulbibliothek online verfügbar.



*To my parents*



## Table of Content

1	Introduction .....	1
1.1	Goals .....	1
1.2	Dissertation outline .....	2
2	Theoretical background .....	3
2.1	Introduction.....	3
2.2	Synthesis of microgels .....	4
2.2.1	Precipitation polymerization .....	4
2.2.2	Emulsion polymerization .....	5
2.3	Functionalization of microgels .....	7
2.3.1	Direct modification with functional monomers.....	7
2.3.2	Post modification of microgels.....	7
2.3.3	Integration of NPs.....	8
2.4	Stimuli responsive microgels.....	11
2.4.1	Microgels in aqueous solutions.....	11
2.4.2	Microgels in organic solvents .....	12
2.5	Microgels in catalysis.....	14
2.5.1	Metal complexes in microgels.....	14
2.5.2	Metal nanoparticles in microgels .....	15
2.6	Design of functional films .....	17
2.6.1	Film formation .....	17
2.6.2	Microgel films.....	18
2.6.3	Hybrid microgel films.....	19
2.6.4	Thin conductive films.....	19

3	Microgel-based catalysts.....	21
3.1	Experimental part .....	21
3.2	Synthesis and characterization of microgels.....	24
3.3	Microgels with metal complexes and organocatalyst .....	37
3.4	Microgels loaded with metal nanoparticles.....	51
3.5	Application of hybrid microgels in catalysis.....	58
4	Microgel-based conductive films.....	67
4.1	Experimental part .....	67
4.2	Synthesis and characterization of microgels.....	68
4.3	Post modification of microgels.....	74
4.4	Loading of the microgels with metal nanoparticles.....	85
4.5	Design and characterization of composite films .....	96
5	Conclusions and outlook .....	109
	References.....	112

## Nomenclature

AAC	acrylic acid
AAEM	2-(methacryloyloxy)ethyl acetoacetate
ACMA	2,2'-azobis[N-(2-carboxyethyl)-2-methylpropionamidine]
AMPA	2,2'-azobis(2-methylpropionamidine) dihydrochloride
BIS	<i>N,N'</i> -methylenebisacrylamide
BuOH	1-butanol
c	concentration
CAT	critical aggregation temperature
CTAB	hexadecyltrimethyl-ammonium bromide
D <sub>h</sub>	hydrodynamic diameter
DLS	dynamic light scattering
EA	ethyl acrylate
EtOH	ethanol
FTIR	fourier transform infrared
HEMA	2-hydroxyethyl methacrylate
i-PrOH	2-propanol
LCST	lower critical solution temperature
MEAK	[2-(methacryloyloxy)ethyl]trimethylammonium chloride
MeOH	methanol
mol-%	mole percent
NPs	nanoparticles
PDI	polydispersity index

PrOH	1-propanol
PVP	poly(vinylpyrrolidone)
R <sub>h</sub>	hydrodynamic radius
RPM	rounds per minute
SDS	sodium dodecyl sulfate
T	temperature
TEM	transmission electron microscopy
TGA	thermal gravimetric analysis
UCST	upper critical solution temperature
UV-Vis	ultraviolet-visible spectroscopy
V	volume
VCL	<i>N</i> -vinylcaprolactam
vol-%	volume percent
VP	1-vinyl-2-pyrrolidone
VPTT	volume phase transition temperature
V <sub>s</sub>	sedimentation velocity
wt-%	weight percent
XPS	X-ray photoelectron spectroscopy
XRD	X-ray diffraction
ζ	zeta potential



## **1 Introduction**

### **1.1 Goals**

The aim of the current work was to synthesize and modify (in direct or indirect way) functional microgels with controlled chemical structure and incorporated functional groups, which can act as containers for ions or nanoparticles. The stability of the microgels in different solvents and stimuli responsive properties were of big importance. First part of the work was focused on the production of new catalytic colloidal reactors. The challenge was to combine the advantages of the homogeneous and heterogeneous catalysis using the hybrid microgel concept, combining high catalytic activity and convenient recycling. The way to solve this problem was the application of the temperature responsive hybrid microgels loaded with catalytic active centers. Microgels should be able to easily transfer in different solvents, which expands applications in catalysis. At the reaction temperatures, hybrid microgels should exhibit a big surface area, be well redispersed and swollen in the solvent. Each catalytic active center must be open and accessible for the reactants (advantage of the homogeneous catalysis). After the catalytic reaction, the catalyst must be easily removed from the reaction mixture (advantage of the heterogeneous catalysis). This can be achieved through the application of the microgels with temperature induced aggregation properties. After performing the reaction and cooling down the reaction mixture, hybrid microgel should aggregate and can be easily removed by decantation. The second part of the work focused on the production of the conductive inks based on the water dispersed conductive hybrid microgels. They can be used for the fabrication of thin flexible conductive films for creation of highly flexible electrical circuit for different applications. Nowadays the fabrication of smart textiles occurs through integration of wires or conductive fibers in the textiles by fabrication step or subsequent embroider of the final product. The inks, based on the microgels and metal nanoparticles, should combine high metal loading, define size of the metal nanoparticles and colloidal stability. The resulting films should be highly flexible and conductive. This may significantly reduce production costs and wear ability of the functional textiles.

### 1.2 Dissertation outline

This dissertation consists of five major chapters. The performing of this work would not be possible without the previous theoretical background described in the chapter two. The recent literature summarizes state of the art in synthesis of microgels by precipitation and emulsion polymerization. The major attention was paid to functionalization of the microgels with metal ions and metal nanoparticles. The application of the hybrid microgels in catalysis and for producing of the conductive films were described.

The third chapter is dedicated to the development of the stimuli responsive microgels and their application in the catalysis. In this chapter, synthesis conditions and influence of the microgel structure on the resulting properties of the microgel were described. Temperature-responsive microgels containing different metal complexes and nanoparticles were synthesized. Through the copolymerization of the different comonomers it was possible to shift a critical aggregation temperature in a broad temperature range. Finally, new hybrid microgels were tested over many catalytic runs to evaluate their catalytic activity.

The fourth chapter of this work describes the synthesis of different microgels highly loaded with metal nanoparticles by two approaches. A methodology to load the microgels up to 90 wt-% of metal nanoparticles was developed. The film-forming ability of the hybrid microgel dispersions was proven. Additionally conductive and mechanical properties of the hybrid films were investigated.

Finally, the conclusions of this work and the possible further investigations and applications of the functional hybrid microgels were summarized in the chapter 5. The references are listed in the last part of this work.

## 2 Theoretical background

### 2.1 Introduction

Stimuli responsive polymers and three-dimensional polymeric networks on their basis attracted big interest due to their unique properties in recent years. Microgels consist of crosslinked polymer chains, which are swollen in a solvent. Exciting properties of microgels can be explained with special architecture, which is lying between linear polymers and three-dimensional polymer networks (hydrogels) <sup>[1-6]</sup>. Stimuli responsive microgels can change the size, morphology, surface charge and softness with the changing of the temperature, pH, ionic strength or a solvent <sup>[7-11]</sup>. The modification of microgels with metal or metal oxide nanoparticles, proteins, ions or enzymes, provides unique properties such as catalytic activity, magnetic response or conductivity <sup>[12-14]</sup>. Due to their porosity, microgels are very attractive for the catalysis. The open structure of the microgel allows diffusion of the substrates to the catalytic center and allows the products to come out. At the same time, functional groups and crosslinked structures hold the catalytic species in their places <sup>[15-18]</sup>. Due to the amphiphilic character of the microgels, they can operate in different environments and can be easily transferred from the water to organic media <sup>[19]</sup>. Through the modification of the surface or core of the microgels, they can be further functionalized with catalytic or conductive units. By changing the synthesis conditions, size and shape of the microgels can be tuned in a wide range. The swelling degree may influence the reaction kinetic <sup>[20-21]</sup>. The relatively big size of the microgels compared to the metal ions or nanoparticles simplify the separation of the catalyst from the substrate or solvent.

### 2.2 Synthesis of microgels

#### 2.2.1 Precipitation polymerization

Precipitation polymerization is one of the most used techniques for the microgel synthesis [22]. Generally, water is used as common solvent in the polymerization process. All monomers, crosslinker and initiator in this system must be water-soluble. The resulting polymer at the same time is not soluble at the reaction temperature. The polymerization starts by decomposition of the initiator at the reaction temperature (50-70 °C), which leads to the formation of free radicals. Free radicals react with the monomers, building oligoradicals. At critical length, the polymer chains collapse, building the precursor particles (Figure 2.1). The particle growth happens by aggregation of the precursor particles, sedimentation on the big particles or addition of monomers or oligoradicals. The growth of the particles stops at reaching the electrostatic point, due to the electrostatic stabilizing of the particles. The charge on the particle surface is possible due to the presence of charged initiator fragments at the end of the polymer chain. Unlike emulsion polymerization, microgels synthesized by using precipitation polymerization contain a big amount of the solvent in the microgel core. After stopping the reaction by cooling the reaction mixture to room temperature, the microgel size increases due to the swelling. The swelling occurs due to the formation of hydrogen bonds between the carbonyl or amide groups of polymer chains and water molecules.

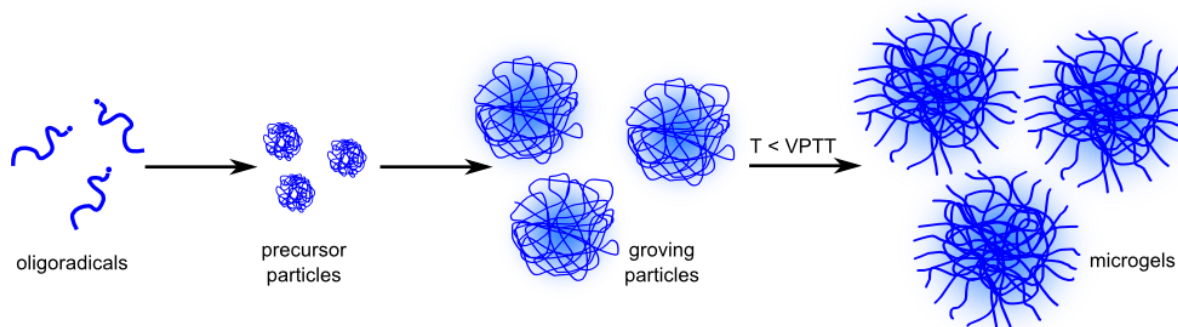


Figure 2.1 Scheme of the precipitation polymerization [22]

One of the big advantages of the precipitation polymerization is a possibility to perform the surfactant free polymerization. The control of the microgel size can be provided by changing the mixing speed as well as the nature and concentration of the crosslinker [23-26].

## 2. Theoretical Background

---

For a more accurate control of the microgel size especially in the small particles direction, the addition of surfactants is necessary. Although initiator fragments stabilize the microgels, this charge is not enough to stabilize the big surface area of the precursor particles and they aggregate to big stable particles. The addition of surfactants stabilizes the small precursor particles and prevent their aggregation. Pelton et al. demonstrated, that the application of the SDS in PNIPAAm microgel synthesis can decrease the size of the microgel by a factor of 10<sup>[27]</sup>.

### 2.2.2 Emulsion polymerization

Emulsion polymerization is known for a long time and was first reported in 1932 by Luther and Heuck<sup>[28]</sup>. By emulsion polymerization, the particles growth happens in a heterogeneous system using a free radical mechanism. In general, the polymerization system consists of monomers, a dispersing medium (water), emulsifier and a water-soluble free radical initiator. In this work additionally to these components, crosslinker was added to the system in order to produce microgels. Usually the solubility of the monomers in the dispersing phase is quite low. Harkins described the mechanism of the emulsion polymerization<sup>[29]</sup>. Due to this mechanism, the reaction mixture after mixing consists of big monomer droplets, stabilized by emulsifier, small surfactant micelles loaded with monomers, free surfactant molecules and a small amount of the dissolved monomer. After addition of the initiator to the preheated reaction mixture, the initiator starts to decompose building free radicals (Figure 2.2).

The polymerization process does not take place in the monomer droplets because of the very small surface area of the droplets compared to the large surface area of the surfactant micelles. The size of the polymer particles is constantly growing due to the constant transport of the monomer molecules from the droplets to the monomer-swollen micelle. When all monomers are polymerized, the reaction is finished.

## 2. Theoretical Background

---

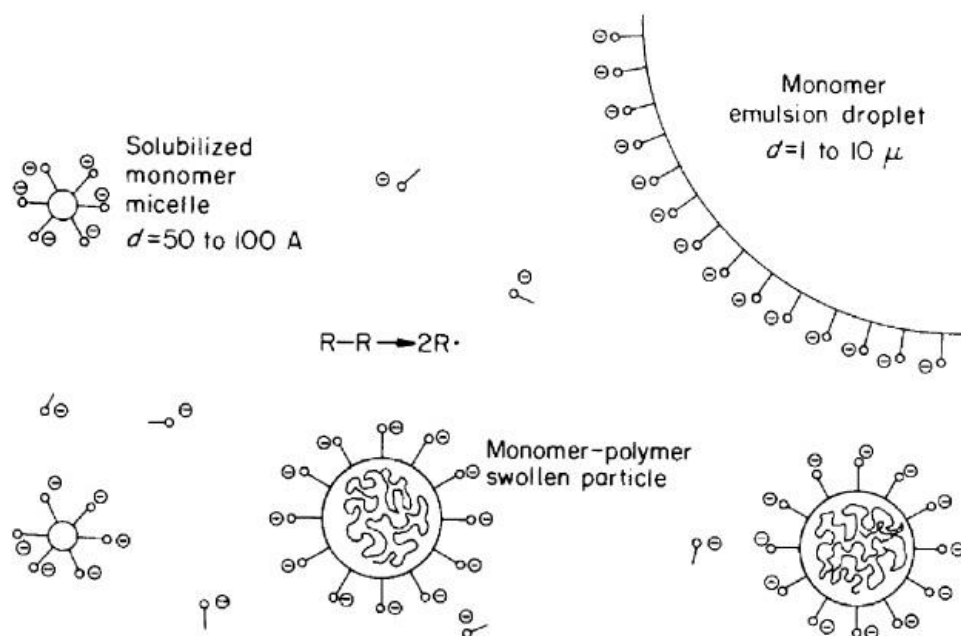


Figure 2.2 Schematic presentation of the emulsion polymerization mechanism <sup>[30]</sup>.

### 2.3 Functionalization of microgels

#### 2.3.1 Direct modification with functional monomers

The easiest way to produce the microgels with a desired functionality is the direct modification during the polymerization process using functional monomers. The use of functional comonomers ensures a covalent bonding of the functional groups to the microgel structure. Besides the functionality, comonomers can additionally improve the colloidal stability of the microgels and have an influence on the microgel size and swelling.

Copolymerization of the standard monomers with ionic monomers by precipitation polymerization (VCL or NIPAM) can lead to the formation of the pH sensitive microgels, which can change the size and the colloidal stability upon variation of pH <sup>[31-35]</sup>. Boyko et al. described an interesting system consisting of VCL and AAEM <sup>[36]</sup>. It was shown that the increase of the AAEM content leads to the decrease of the microgel size due to the formation of a crosslinked core. Hoare and coworkers studied the distribution of functional groups in thermo-sensitive carboxylic-acid-functionalized poly(*N*-isopropylacryl-amide) based microgels <sup>[37-38]</sup>. Amalvy et al. reported about the synthesis and characterization of pH-responsive microgels based on tertiary amine methacrylates <sup>[39]</sup>. The resulting microgels had size of 250-700 nm and could switch from microgels to latex due to the protonation of the tertiary amine groups at a critical pH of 6.6-7.0. Eichenbaum et al. investigated the influence of the crosslinking density on the swelling degree and size of the ionic poly(methacrylic acid-co-acrylic acid) microgels <sup>[40]</sup>.

The direct modification technique was broadly used in this work to produce catalytic active microgels in a one-step synthesis. It was possible to copolymerize ethyl acrylate with metal complex-based functional monomer without further modification.

#### 2.3.2 Post modification of microgels

Microgels cannot always be modified with desired functional groups by direct copolymerization. The possible reasons for this can be:

- low solubility of the comonomer in water (in case of aqueous precipitation polymerization)
- destruction of the comonomer at the polymerization reaction temperature
- large difference in copolymerization parameters which may lead to undesirable distribution of the functional groups in microgel structure.

## 2. Theoretical Background

---

Post modification can be an alternative to the application of direct co-polymerization. Most of the literature is based on the post modification of two types of microgels based on either PVCL or PNIPAAm. The post modification can bring unique properties and functionalities to the resulting microgels. Garcia et al. functionalized PNIPAAm-Allylamine microgels with spiropyran photochrome containing a carboxylic acid group via an amide bond <sup>[41]</sup>. The resulting microgel had photo-, thermal-, and pH-responsive properties. Xu and coworkers <sup>[42]</sup> synthesized poly(*N*-isopropylacrylamide) thermo-responsive microgel particles with an amine-rich corona by hydrolysis of the PNIPAAm microgels at the temperatures above VPTT and pH 1.5. The amine-functionalized microgel was coupled with iodine-terminated poly(*N*-vinylformamide) and hydrolyzed one more time. Hu et al. described the grafting of linear poly(*N*-isopropylacrylamide) (PNIPAAm) chains onto a spherical PNIPAAm-HEA microgel, using RAFT polymerization, in order to form a core-shell nanostructure <sup>[43]</sup>. Richter's group reported about the modification of the negatively charged Poly(*N*-isopropylacrylamide)-co-acrylic/methacrylic acid microgels with positively charged polyelectrolyte poly(diallyldimethylammonium chloride) <sup>[44-46]</sup>. Interestingly, besides the building the new layers on the surface, the addition of the polyelectrolytes leads to the decrease of the microgel size.

Häntzschel et al. reported the functionalization of the PVCL/GMA microgels by modification of the epoxy groups using 2-aminoethanethiol at low pH values <sup>[47]</sup>. An amino functionalized microgel was used as a container for silver nanoparticles. Cheng et al. presented a simple way to modify hydrophilic PVCL/AAEM/VIm microgels with amphiphilic wedge-shaped 4-*N*-[3',4',5'-tris(dodecyloxy)benzamido]benzene-4-sulfonic acid. The resulting microgel exhibit changed values of the swelling degree, surface charge, and responsiveness toward temperature and pH <sup>[48]</sup>. Microgels were tested on their ability to uptake hydrophobic molecules in aqueous media.

### 2.3.3 Integration of NPs

In recent years the amount of publications about the incorporation of nanoparticles in microgels is constantly growing. Due to the porous structure of the microgels, they are perfectly suitable as a carrier for the nanoparticles. The use of microgels as nanoparticle carriers has many advantages. The nanoparticles can be loaded into the microgels or directly synthesized inside the microgels. The nanoparticles can be held inside the microgels due to hydrophobic forces, hydrogen bonding or electrostatic interactions. By using the microgels as nano-reactors, they can act as stabilizers, stabilizing the nanoparticles from the aggregation.



## 2. Theoretical Background

---

Beside the aggregation stability, microgel pores can influence the size and shape of nanoparticles, or distance between the nanoparticles. By using the microgels with a different crosslinking density, the accessibility to the particles can be tuned. By using thermo-responsive microgels, the distance between the particles can change, due to the swelling or deswelling of the microgels. The same is possible for pH sensitive microgels with changing of the pH. The overloading of the microgels should be prevented, as the high loading of the microgels with nanoparticles leads to the reduction of the microgel chains movements and as a result reduces the colloidal stability of the hybrid microgels.

Gong et al. investigated the incorporation of CdTe nanoparticles capped with thioglycerol and thioglycolic acid by mixing them with microgels based on *N*-isopropylacrylamide [49]. The incorporation was possible due to the hydrogen bonds between microgels and the capping agent of the CdTe nanoparticles. The incorporation of the nanoparticles influenced the size of the hybrid microgels, while microgels remained thermosensitive. Lu and coworkers modified the polystyrene core, poly(*N*-isopropylacrylamide) shell core@shell microgels with silver, gold and palladium nanoparticles by direct reduction of the metal salts inside the microgel [16]. The hybrid microgels were used for catalytic application, the influence of the temperature on the catalytic activity was investigated. Kuang et al. reported the incorporation of water-soluble CdTe nanocrystals in *N*-isopropylacrylamide-co-4-vinylpyridine microgels [50]. The hybrid microgels stay temperature- and pH- sensitive and can take up or release the nanoparticles depending on pH. Gorelikov et al. loaded *N*-isopropylacrylamide-co-acrylic acid microgels with gold nanorods [51]. The loading was performed by mixing the microgel and gold nanorod dispersions. The holding of the particles inside the microgel was possible due to the electrostatic forces between acrylic acid and the gold surface. Biffis et al. reported about the modification of the methyl methacrylate-co-*N,N*-dimethylaminoethyl methacrylate-co-ethylene dimethacrylate microgels with palladium nanoparticles [52]. The synthesis of the palladium nanoparticles was performed inside the microgel by reducing the palladium acetate using ethanol as reducing agent. The size of the palladium nanoparticles can be controlled by changing the crosslinking degree of the microgels. Zhang et al. reported about the loading of the *N*-isopropylacrylamide-co-4-vinylpyridine microgels with calcium carbonate nanoparticles [53-54]. Zhang et al. synthesized silver nanoparticles in *N*-isopropylacrylamide-co-acrylic acid-co-2-hydroxyethyl acrylate microgels applying UV irradiation to the microgel-silver nitrate mixture [55]. The influence of the irradiation time on nanoparticles properties was investigated. Tang with coworkers loaded *N*-isopropylacrylamide-co-acrylic acid microgels in-situ with silver nanoparticles using sodium borohydride for the reduction of the microgel-

## 2. Theoretical Background

---

silver nitrate solution <sup>[56]</sup>. The hybrid microgel is used for the production of sensors. Suzuki and coworkers loaded NIPAAm-co-GMA core-shell microgels post modified with 2-Aminoethanethiol with gold nanoparticles by reducing the chloroauric acid inside the microgel particles by using sodium borohydride <sup>[57]</sup>. The gold nanoparticles were additionally increased in size by application of the electroless gold plating using gold precursor and hydroxylamine hydrochloride. Tehrani and coworkers reported the incorporation of lanthanide (Ln = La, Nd, Eu, Tb, Ho, Tm) phosphate nanocrystals inside of poly(NIPAAm/VCL/MAA) microgels by reaction of the lanthanide ions inside the microgel with PBS buffer as precipitant <sup>[58]</sup>. Resulting microgels can be suitable for mass cytometry applications. Pich and coworkers presented the in-situ synthesis of silver nanoparticles in PVCL-AAEM microgels <sup>[59]</sup>. The incorporation and holding of the silver nanoparticles was possible due to the complexation ability of the AAEM groups. It was possible to load the microgels with different amounts of silver nanoparticles. The resulting microgels were thermosensitive, the shrinking-swelling behavior was reversible. Also in a Pich group the PVCL-AAEM microgels were loaded with zinc sulfide nanoparticles <sup>[60]</sup>. For the modification of the microgels with ZnS, a microgel dispersion was mixed with zinc acetate and thioacetamide. The formation of ZnS was performed by applying ultra-sonication. The influence of the zinc sulfide on the microgel morphology and swelling properties was studied. Schachschal and coworkers loaded PVCL-PAAEM-PVIm microgels with different amounts of hydroxyapatite nanoparticles <sup>[61]</sup>. The synthesis of the hydroxyapatite crystals was performed inside the microgels by mixing of the calcium nitrate with diammonium hydrogenphosphate. The influence of the nanoparticles content on microgel properties was studied. Häntzschel et al. reported about the amine modification of the *N*-vinylcaprolactam-co-glycidyl methacrylate with final in situ synthesis of the silver nanoparticles by reduction with sodium borohydride <sup>[47]</sup>. The resulting product was tested as application in medicine as an anti-microbial agent. Jia et al. synthesized hybrid microgels based on PVCL-co-cyclodextrin microgels loaded with gold nanoparticles <sup>[62]</sup>. It was shown that only PVCL-co-cyclodextrin microgel, compared to pure PVCL microgel, can efficiently incorporate gold nanoparticles due to the coordination of the cyclodextrin to the gold nanoparticle surface. Contin et al. reported about the in-situ synthesis of palladium, platinum and gold nanoparticles inside the Laponite nanoclay loaded PVCL-AAEM microgel <sup>[63]</sup>. Palladium loaded microgels were used for catalytic activity tests. Shen and coworkers reported about the incorporation of CdSe semiconductor nanoparticles in PNIPAAm/VIm and PVCL/VIm <sup>[19]</sup>. The incorporation was performed by a CdSe capping agent replacement in THF.

### 2.4 Stimuli responsive microgels

Microgels have the ability to swell and collapse in response to changes in the external environment, for example: temperature, pH, light, solvent or magnetic field. The crosslinker holds the particles together, gives them shape and controls the swelling of the particles. The ability of the microgels to change the size depending on the stimuli from outside attract the interest of research in different areas. Unlike linear polymers which show LCST and UCST depending on the used monomers, microgels have a volume phase transition temperature (VPTT). Microgels with a VPTT at low temperatures are swollen (Figure 2.3). With an increase of the temperature hydrogen bonds between the polymer chains and water break and the microgel shrinks and decreases in size. If the microgels are composed of polymers which exhibit UCST, at low temperatures they collapse and swell upon heating. Typical polymers with UCST behavior are poly acrylates in alcohol solvents <sup>[64-68]</sup>. In this work, both VPTT and CAT properties were of big importance. VPTT properties should be taken in account by loading the microgels with nanoparticles. In the case of conductive inks, loading of microgels was performed at low temperature to insure the maximal load density. However, for catalytic applications of the microgel, CAT properties were used. At a high reaction temperature microgels are swollen and catalytic centers are accessible for the reagent; after cooling down, collapsed and precipitated microgels can be removed. The loading of microgels with nanoparticles in this case should be done at high temperatures.

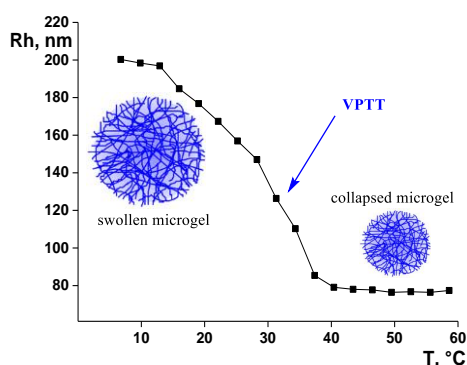


Figure 2.3 Hydrodynamic radius  $R_h$  of PVCL-AAEM-AAC microgel as a function of temperature

#### 2.4.1 Microgels in aqueous solutions

The majority of modern microgel research is based on systems where the microgels are dispersed in water. The microgels swollen in water can respond with collapsing to the variety

## 2. Theoretical Background

---

of the stimuli from outside. The most common type of the smart microgels described in the literature are thermo-sensitive microgels.

Most microgels described in the literature use polymers that present a lower critical solution temperature (LCST). The most common microgels are based on poly(*N*-isopropylacrylamide) [2,23]. PNIPAAm has a LCST of around 32 °C, a very useful temperature for biomedical applications since it is close to the body temperature (37 °C). Adjustment of the VPTT of PNIPAAm can be achieved by copolymerizing it with hydrophilic or hydrophobic monomers changing the overall hydrophilicity of the polymer [69]. Other microgels with thermoresponsive properties include poly(*N*-vinylcaprolactam) [36,70,71] with an VPTT between 25 and 35 °C, poly(*N,N*-diethylacrylamide) [24,72] with an VPTT over the range of 25 to 32 °C and poly[2-(dimethylamino)ethyl methacrylate] [39] with an VPTT of around 50 °C. The microgels can also respond to pH changes of the solvent by incorporation of the anionic or cationic copolymers like as acrylic acid or vinylimidazole in the microgel structure [35,38,71-77], ionic strength by incorporation of the polyelectrolyte groups [31,78], addition of the organic solvent such as alcohol [27,79-83] or light [84-86].

### 2.4.2 Microgels in organic solvents

The majority of modern microgel research is based on systems where the microgels are dispersed in water. However, there are few reports about non-aqueous microgels systems. There are two approaches for the synthesis of non-aqueous microgels. First one is the indirect synthesis of the non-aqueous microgels based on emulsion, surfactant free or microemulsion polymerization in water. The product can be transferred to the organic solvent by using dialysis, centrifugation, evaporation or freeze-drying. The second approach is direct synthesis of the microgels in organic solvents using precipitation or dispersion polymerization.

Cui et al. synthesized polystyrene microgels with a size of 1-2.5 µm in diameter, using precipitation polymerization in acetonitrile. The microgel can be transferred to toluene or isopropanol [87]. Butun and coworkers reported the polymerization of the 2-(*N*-morpholino)ethyl methacrylate in *n*-hexane [88]. Changing the synthesis condition the size of the microgels can be varied from 120 to 720 nm. The microgel build stable dispersions in THF, acetone and chloroform. Clarke et al. made and characterized polystyrene microgels with a size of 400-1150 nm by a transfer of polystyrene latex in ethylbenzene [89]. Nur and coworkers synthesized poly(*N*-isopropylacrylamide) and PNIPAAm-co-acrylic acid microgels using surfactant-free emulsion polymerization. Finally, freeze-dried microgels were redispersed in hexane and methanol [90]. Antonietti et al. synthesized polystyrene latex in

## 2. Theoretical Background

---

water using mini emulsion polymerization with the size of 60-200 nm. The microgel dispersion was achieved by transporting the product in toluene <sup>[91]</sup>. Cragg et al. reported about the synthesis of polystyrene particles in water using emulsion polymerization <sup>[92]</sup>. The product was washed using butanone; the polystyrene microgels were made by redispersing the latex in benzene. Nie and coworkers synthesized poly(methyl methacrylate) based microgels using ethylene glycidyl methacrylate (GMA) or hydroxyl ethyl methacrylate (HEMA) as comonomers in water by micro emulsion polymerization <sup>[93]</sup>. The resulting microgel was transferred in butyl acetate. Frank et al. reported about the synthesis of the divinylbenzene-co-maleic anhydride microgels using precipitation polymerization in methyl ethyl ketone/heptane mixtures. Depending on the solvent ratios it was possible to synthesize the microgels in a size range of 100-500 nm <sup>[94]</sup>. Jiang and coworkers synthesized polystyrene microgels using precipitation polymerization in ethanol <sup>[95]</sup>. Influence of the monomer concentration on microgel formation was investigated. The size of the microgel particles was in a range of 580-750 nm. Lu et al. reported about the preparation of poly(divinylbenzene-co-acrylonitrile) microgels in acetonitrile using precipitation polymerization <sup>[96]</sup>. Changing the monomer ratios, it was possible to synthesize the microgels with sizes between 2.3 and 3.1  $\mu\text{m}$ . Downey and coworkers synthesized copolymer based on mixtures of divinylbenzene and 4-methylstyrene using emulsion polymerization in methyl ethyl ketone and heptane mixture <sup>[97]</sup>. Adjusting the solvent and monomers ratios was possible to change the microgels size in a range of 1800-4600 nm. Goh et al. reported about the synthesis of methacrylic acid and ethylene glycol methyl ether methacrylate based microgels using precipitation polymerization in methyl ethyl ketone and heptane mixture. Resulting microgels have sizes in a range of 450-2900 nm <sup>[98]</sup>. Machatova et al. reported about the synthesis of copolymer microgels with different cross-linking densities by the semi-batch emulsion copolymerisation of methyl methacrylate, butyl methacrylate, 2-hydroxyethyl methacrylate and allyl methacrylate in water, with further transferring to acetone or 5-methyl-2-hexanone <sup>[99]</sup>. The size of the resulting microgels was in a range of 109-235 nm.

### 2.5 Microgels in catalysis

Since last time microgels find more and more applications in catalysis. To introduce the catalytic functionality, microgels can be loaded with metal complexes, metal nanoparticles or enzymes. The role of the microgels in microgel based catalysts, is to improve the stability and the recyclability of the catalytic centers without the loss of their catalytic activity. Nowadays there are a lot of publications about the usage of solid and not soluble silica spheres or polystyrene latex as carriers for catalysts. These systems are great for catalyst recovery, but insolubility in the solvent leads to the decrease of the contact area, accessibility of substrates to catalysts and loss of the catalytic activity at the same time. Another approach is the use of the linear polymers as a carrier for catalyst. They have slightly less recyclability, but offer perfect accessibility of the catalytic units to reagents. The main problem in use of the linear polymers as catalyst carriers is not strong bonding of the catalysts to the polymer chains. The weak binding leads to the loss of the catalyst over a few recycling runs. The application of the microgels as a catalyst carrier can solve these issues. The catalytic units in swollen microgels are easily accessible for the reactants. The surface area of the swollen microgels is comparable to the linear polymer catalysts. The crosslinking of the microgels can be precisely adjusted in order to get the desirable pore sizes. The catalytic units can be reliably held in the microgel pores without leaching by the recycling process.

#### 2.5.1 Metal complexes in microgels

Metal ions due to the high activity and huge surface area have broad applications for catalytic reactions in the organic synthesis. The metals, which are used in catalysis, have usually a very high price. The usage of the noble and transition metals in catalysis is always combined with difficulty, time and recourse consuming recycling procedure to remove the catalyst. To avoid these steps metal ions can be incorporated in microgels. Microgels with incorporated metal complexes show a high catalytic activity, selectivity, a big surface area and accessibility, and they can be easily removed from the reaction media <sup>[100,101]</sup>.

There are two ways to synthesize the microgel@metal-complex systems. Post modification is the first approach for functional microgels synthesis. The problem, which can appear is the steric hindrance of the ligands by the backbones of the microgels, which can lead to the incomplete incorporation of the metal ions. The second strategy is the direct modification of the microgels with functional monomers, which already contain metal complexes. The usage of this approach requires the modification of the polymerization procedure.

## 2. Theoretical Background

---

Terashima et al. reported about the direct synthesis of functional methyl methacrylate microgels loaded with a ruthenium complex <sup>[102-109]</sup>. The final catalyst was used for the ruthenium-catalyzed oxidation of 1-phenylethanol to acetophenone in acetone. Deng et al. synthesized polystyrene-co-TsDPEN derivatives based microgels <sup>[110]</sup>, which due to the amine functionality were able to build the complexes with ruthenium salts. The final microgel was applied in asymmetric hydrogenation reactions of aromatic ketones to give enantioenriched secondary alcohols in quantitative yield. Haraguchi et al. reported about a precipitation polymerization of polystyrene-co-TsDPEN derivatives and polymethacrylic acid-co-TsDPEN derivatives in acetonitrile with further complexation of ruthenium ions <sup>[111]</sup>. The final product showed good reactivity and enantioselectivity in the catalytic asymmetric transfer hydrogenations.

### 2.5.2 Metal nanoparticles in microgels

Similar to the metal complexes metal nanoparticles have a big surface area. Metal nanoparticles find many applications in organic synthesis. Compared to the bulk metals metal nanoparticles exhibit higher catalytic activity. Pure metal nanoparticles are colloiddally unstable which leads to aggregation, decrease of the active surface and as a result decreasing of the catalytic activity. To prevent aggregation, metal nanoparticles can be covered with different types of protective layers such as: surfactants, linear or branched polymers networks or microgels. As in the case of metal complexes, the stabilization of metal nanoparticles using microgels has significant advantages. The combination of metal nanoparticles with sensitive microgels open great opportunities in catalytic applications, due to the convenient separation of the products and recycling of the catalyst.

There are three main approaches to synthesize hybrid microgel@MeNPs colloids. The first one is more common and convenient, and based on the in situ formation of metal nanoparticles inside the microgel. The second approach is based on the direct encapsulation of the metal nanoparticles in microgels during the polymerization process. The last one is the incorporation of the metal particles inside of the microgel by mixing the microgel and metal nanoparticle dispersions together. The formation of the hybrid microgels in this case is possible due to the ligand exchange on the metal nanoparticle surface.

In Ballauff's work group verities of hybrid polystyrene-core poly(*N*-isopropylacrylamid)-shell thermo-sensitive microgels with different crosslinking densities, loaded with silver and palladium nanoparticles were synthesized <sup>[19,112,113]</sup>. The catalytic activity of the hybrid microgels was investigated by monitoring photometrically the reduction of 4-nitrophenol by

## 2. Theoretical Background

---

an excess of  $\text{NaBH}_4$ . Zhang et al. reported about the synthesis of poly-*N*-isopropylacrylamide-(maleated carboxymethylchitosan) microgels with further loading of silver nanoparticles <sup>[114]</sup>. The catalytic activity of hybrid microgels was proven by the catalytic reduction of 4-nitrophenol. The influence of the pH and temperature on catalytic activity was investigated. Sahiner et al. reported about the catalytic reduction of 4-nitrophenol using copper nanoparticle loaded poly(4-vinylpyridine-co-1-vinylimidazole) hybrid microgels using sodium borohydride <sup>[115]</sup>. Kanaoka et al. reported about the catalyzed aerobic oxidation of alcohols such as benzyl alcohol using thermo-sensetive poly-2-(2-ethoxy)ethoxyethyl vinyl ether microgels loaded with gold nanoparticles <sup>[116]</sup>. After the catalysis, hybrid microgels could be easily separated from the reaction mixture by utilizing their thermosensitive nature, allowing for repeated usage. Lu and coworkers reported about the oxidation of alcohols to the corresponding aldehydes or ketones using gold, platinum and rhodium nanoparticle loaded polystyrene-core poly(*N*-isopropylacrylamid)-shell thermo-sensitive microgels <sup>[17]</sup>. It has been found that the catalytic activity of the metal nanocomposite can be modulated by the volume transition of microgel particles for the oxidation reaction of benzyl alcohol. Biffis and coworkers reported about the application of palladium and platinum nanoparticle loaded polymethyl methacrylate-co-ethylene dimetacrylate based microgels in catalysis <sup>[52,117,118]</sup>. The hybrid microgels were active in the catalytic vinylation of aryl iodides and bromides (Heck reaction) and Suzuki coupling of aryl bromides and chlorides with phenylboronic acid.



### 2.6 Design of functional films

#### 2.6.1 Film formation

The film formation in water based dispersions of polymer particles can be divided in 3 steps (Figure 2.4) <sup>[119]</sup>.

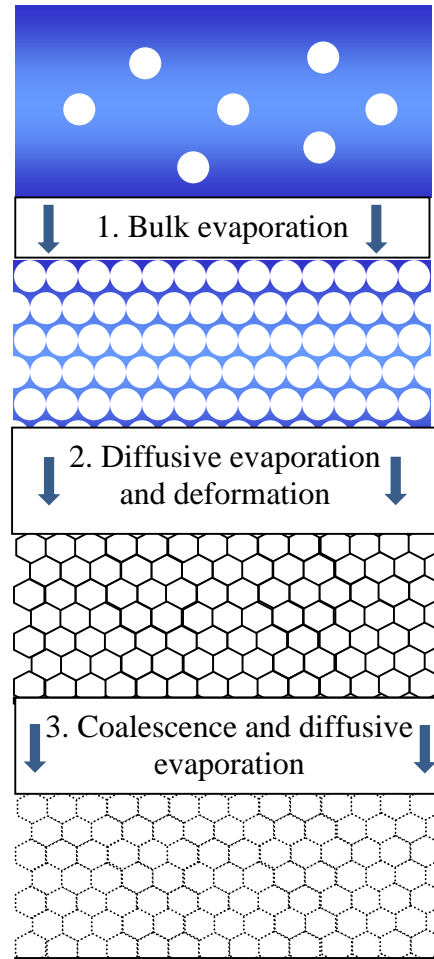


Figure 2.4 Film formation process of water based polymer dispersions <sup>[119]</sup>.

In the first step, the big part of the solvent evaporates and the particles organize themselves in concentrated dispersion. Even at perfect particle packing in the film, at least 36 % of water remains in the holes between the particles. In the second step water from the space between the particles slowly evaporates, which leads to the deformation and as a result to the coalescence of the polymer particles <sup>[120-124]</sup>. The deformation of the particles is caused by capillary and osmotic forces. The electrostatic, repulsion and elastic deformation of the particles act opposite. After the drying of the films the particles form the polyhedral structure. The slowest third step leads to the final dried homogeneous film through the coalescence and diffusion of the polymer chains from the polymer particles <sup>[125,126]</sup>. Unlike hard latex

## 2. Theoretical Background

---

particles, swollen microgel particles shrink and decrease in diameter when they are drying. In case of the hybrid microgels this leads to the decrease of the distance between the loaded nanoparticles. At high loadings this ensures the direct contact between the nanoparticles, which is important for the synthesis of conductive inks.

### 2.6.2 Microgel films

Yue et al. made a film from poly(*N*-isopropylacrylamide-co-*N*-[3-(dimethylamino)-propyl]methacrylamide) simply by casting a microgel solution onto the surface of a solid substrate <sup>[127]</sup>. Due to the amino functionalities the resulting microgel film can be used for removing carbon dioxide from the air. Sorrell et al. reported about the film formation of poly(*N*-isopropylacrylamide-co-acrylic acid) by actively spreading a concentrated solution of microgels onto an Au surface at 30 °C <sup>[128]</sup>. Zavorodnya et al. thoroughly characterized the films based on poly(*N*-isopropylacrylamide-co-acrylic acid) microgels, deposited on glass substrates coated with polyelectrolyte multilayers composed of the polycation poly(allylamine hydrochloride) and the polyanion poly(sodium 4-styrenesulfonate) <sup>[129]</sup>. The microgel density and structure of the resultant films were investigated as a function of: polyanion, polycation layer thickness, charge of the polyelectrolyte multilayer film and pH of the microgel deposition solution. The Lyon group prepared films based on poly(*N*-isopropylacrylamide-co-acrylic acid) microgels using a layer-by-layer spin coating (scLbL) polyelectrolyte assembly approach using poly(allylamine hydrochloride) as a polycationic “glue” on glass substrates <sup>[130-135]</sup>. The films were used for thermally regulated uptake and release of the chemotherapeutic drug doxorubicin and insulin. Xia et al. reports the formation of thermoresponsive poly(*N*-isopropylacrylamide-co-styrene) microgel films and their use for cell growth and detachment via temperature stimuli <sup>[136]</sup>. Spin coating or drop coating of microgel dispersions was used for the production of thermo-responsive films. Glass coverslips, cell culture plates, and flasks can be used as a substrate. Horigome et al. thoroughly investigated the drying mechanism of poly(*N*-isopropylacrylamide) microgel dispersions <sup>[137]</sup>. Digital camera and an optical microscope were used for the observation of the microgel dispersion drying processes. The dried microgel film structures were observed by scanning electron microscopy. Schmidt et al. investigated the film formation of the stimuli responsive poly(*N*-isopropylacrylamide) and poly(*N*-isopropylacrylamide-co-acrylic acid) microgels using dip coating and dropping on pre-modified silicon wafers <sup>[138,139]</sup>. The influence of the pH value of the dipping solutions on the particle density at the surface was investigated. Wei et al. reported about film formation of thermo-responsive poly(*N*-isopropylacrylamide) microgels <sup>[140]</sup>. Uniform microgel surfaces were fabricated by drop-

## 2. Theoretical Background

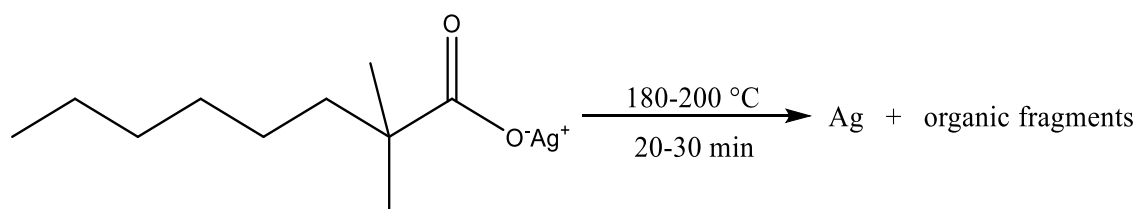
coating on silicon wafers, glass dishes, or gold coated glass slides with the polyethylenimine (PEI) layer. The final microgel films can act as a non-toxic substrate for cell growth.

### 2.6.3 Hybrid microgel films

Berger et al. reported about the film formation of microgel-clay composites based on poly(*N*-vinylcaprolactam-co-acetoacetoxyethyl methacrylate) containing different amounts of incorporated clay nanoparticles <sup>[141]</sup>. The obtained hybrid microgels had spherical shape and exhibited a strong tendency to form films on solid substrates. Bhattacharya and coworkers described the film formation of hybrid microgels based on poly(*N*-vinylcaprolactam-co-acetoacetoxyethyl methacrylate-co-vinylimidazole) loaded with magnetite nanoparticles by a simple drying process <sup>[142]</sup>. Highly porous films were achieved by drying the magnetic hybrid microgels under the application of magnetic field. Pich et al. reported about the film formation of hybrid poly(*N*-vinylcaprolactam-co-acetoacetoxyethyl methacrylate) microgels loaded with magnetite, zinc sulfide or silver nanoparticles <sup>[59,60,143]</sup>. Simple drying at room temperature leads to the formation of highly flexible and transparent dense film even at high nanoparticles loading. Xia et al. reported about film building of the hybrid poly(*N*-isopropylacrylamide) microgels and poly(*N*-isopropylacrylamide-co-acrylic acid) microgels loaded with calcium carbonate <sup>[144]</sup>. The microgels formed stable monolayer films on bare silica and glass substrates upon drying.

### 2.6.4 Thin conductive films

As described in the literature conductive inks can be divided in two groups. The first group is made of solutions of metal salt with organic anions, generally in organic solvents (metal organic decomposition inks MOD) <sup>[145-149]</sup>. These salts can be decomposed into the metal and organic fragments by applying temperature. The small size of the resulting metal particles requires low temperature for their melting and a building of conductive patterns (Scheme 2.1).



Scheme 2.1 Building of the metallic silver from a MOD.

Another approach in the synthesis of conductive inks is the application of metal nanoparticles. To improve the sedimentation stability, usually various surfactants are used. The disadvantage of the surfactant use is the increase of distance between the metal nanoparticles in the

## 2. Theoretical Background

resulting films, which lead to high electrical resistance. To minimize the resistance, metal particles can be sintered together <sup>[150]</sup> (Figure 2.5).

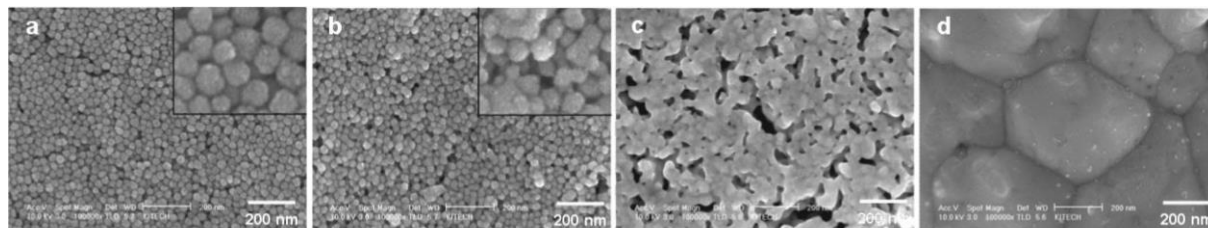


Figure 2.5 SEM images of the Ag nanoparticles (21 nm) at different sintering temperatures: 100 °C (a), 140 °C (b), 200 °C (c) and 300 °C (d) <sup>[150]</sup>

Low sintering temperatures are possible because of the high surface energies of the metal nanoparticles. It is noticeable, that the decrease of the particle size leads to a decrease in the melting point. Gold nanoparticles with a diameter below 2 nm are able to melt already at 150-200 °C <sup>[151,152]</sup> (Figure 2.6).

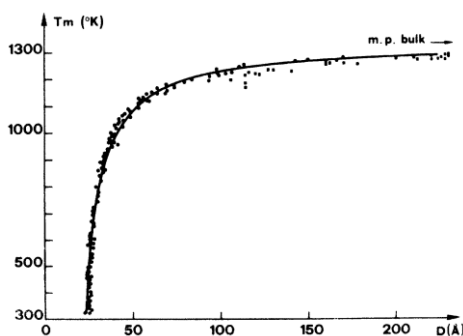


Figure 2.6 Melting point of gold nanoparticles related to their diameter <sup>[151,152]</sup>.

## 3 Microgel-based catalysts

### 3.1 Experimental part

#### Materials

The following chemicals were purified by distillation at reduced pressure in order to remove the inhibitors and stored at 4 °C

1. Acrylic acid, 99% (Sigma-Aldrich)

Purified by passing through the syringe filled with Al<sub>2</sub>O<sub>3</sub> powder were:

2. 2-(Methacryloyloxy)ethyl acetoacetate, 95% (Sigma-Aldrich)
3. Ethyl acrylate, 99% (Sigma-Aldrich)
4. 2-Hydroxyethyl methacrylate, 97% (Acros Organics)

All other reagents were used as received:

5. 2-Propanol, 99.7% (VWR BDH Prolabo)
6. Aluminum oxide, purum p.a. (Fluka)
7. Methanol, 99.8% (VWR BDH Prolabo)
8. Ethanol, 99.8% (VWR BDH Prolabo)
9. 1-Propanol, 99.8% (VWR BDH Prolabo)
10. 1-Butanol, 99.8 (VWR BDH Prolabo)
11. Hydrazine monohydrate, 98% (Sigma-Aldrich)
12. Metal precursors

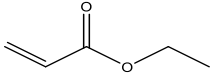
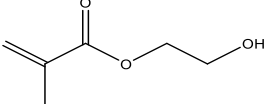
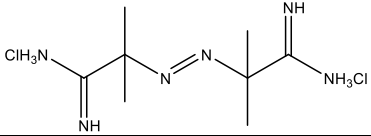
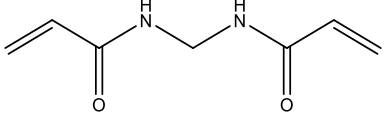
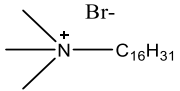
Distilled water was used for all polymerization and purification processes.

### 3. Microgel-Based Catalysts

#### Microgel synthesis and purification

For the synthesis of the temperature sensitive microgels, classical emulsion polymerization was used. For the big scale synthesis, the procedure was as followed: calculated amounts of the ethyl acrylate (cleaned using aluminum oxide) were added to the double wall reactor. All functional monomers were added to ethyl acrylate in the reactor and mixed. Afterwards, water, crosslinker and surfactant were added to the reactor. The reaction mixture was heated up to 70 °C and stirred under continuous purging of nitrogen at 700 RPM for 20 minutes. After the dispersion was build, the stirring speed was set to 220 RPM and initiator was added in order to start the reaction. In the case of the small amount of the monomers, a 25 mL flask was used as a reactor. The mixing and heating of the mixture was performed through the application of the heating plate with the stirrer. After 8 hours, the reaction was stopped and the microgel dispersion was cooled down. The product was purified by dialysis against distilled water for 3 days. After the purification process the microgel was freeze dried to remove the water. The final product was stored in dried state. The linear EA:HEMA polymers were synthesized in cooperation with the institute for organic chemistry using classical radical polymerization in THF with AIBN as initiator. The reaction conditions and mixture compositions were similar to the microgel synthesis.

Table 3.1 Reaction mixture composition for the thermo-sensitive microgels.

Name	Structure	Amount
EA		95 mol-%
HEMA (comonomer)		5 mol-%
AMPA (initiator)		1 mol-% (EA + comonomer)
BIS (crosslinker)		3 mol-% (EA + comonomer)
CTAB (stabilizer)		1 mol-% (EA + comonomer)
Water	-	90 wt-%

For the synthesis of the functionalized microgels there are three synthesis strategies possible (Figure 3.2). In a first scenario microgel synthesis is performed through direct polymerization

### 3. Microgel-Based Catalysts

of the functional monomers, which already contain the catalytic active center. Second approach is the synthesis of microgels from monomers, which have metal or metal nanoparticles sensitive ligands. For the synthesis of the catalytic active microgels, metal precursor should be added to the system by post modification. The last approach is the synthesis of pure microgel-carriers, which can be further modified with the pure ligand or with the ligand already containing the catalytic active center through the modification of the modification suitable side groups.

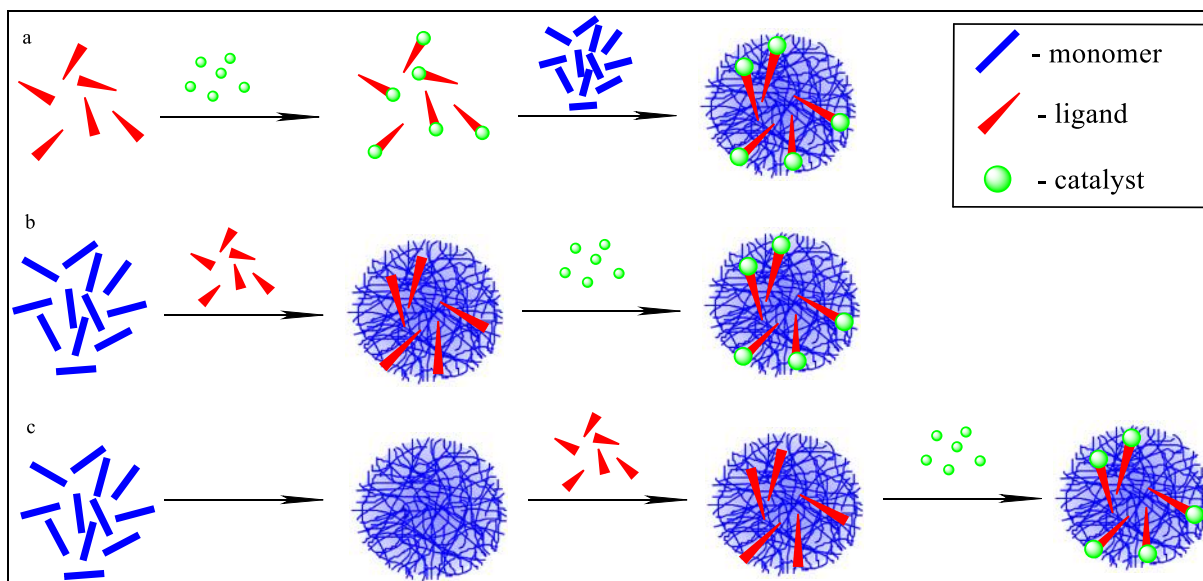


Figure 3.2 Main approaches of the catalytic active thermo-sensitive microgels synthesis. Direct modification of the microgels (a), synthesis of the functional microgels, which contain ligands for metal-complexation (b) and synthesis of the microgels with side groups for post-modification (c).

#### 3.2 Synthesis and characterization of microgels

The choice of monomers is very important for the final properties of the resulting microgel. On one hand through the right choice of the comonomer, the CAT point can be adjusted, on the other hand, comonomers should have an affinity to the catalytic centers. For the synthesis of the thermo-sensitive microgels the main monomer of the system should respond to the temperature change. Acrylate monomers were used as thermo-sensitive units in this work. As ligands or spacers a variety of organic compounds can be used (Figure 3.3). The spacer, which was used in this work, was 2-hydroxyethyl methacrylate, due to the presence of the hydroxyl group it can be used for further modification.

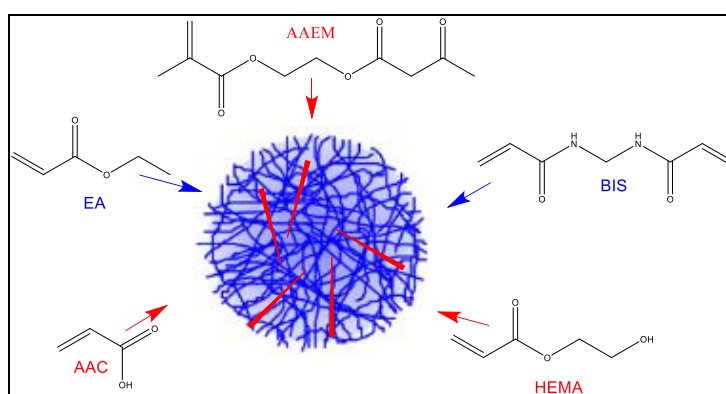


Figure 3.3 Concept of the thermo-sensitive microgel structure.

##### EA-HEMA microgels

The first model system of the thermo-sensitive microgels was a combination of ethyl acrylate (EA) and 2-hydroxyethyl methacrylate (HEMA) with different ratios. Four microgels with EA-HEMA ratios of 100:0; 95:5; 90:10 and 85:15 were synthesized. To prove the incorporation of the HEMA in the microgel, IR spectral analysis was made (Figure 3.4). From the data it can be clearly seen that the broad peak corresponding to the -OH groups from 3700 to 3200  $\text{cm}^{-1}$  increases linearly with increasing HEMA content.



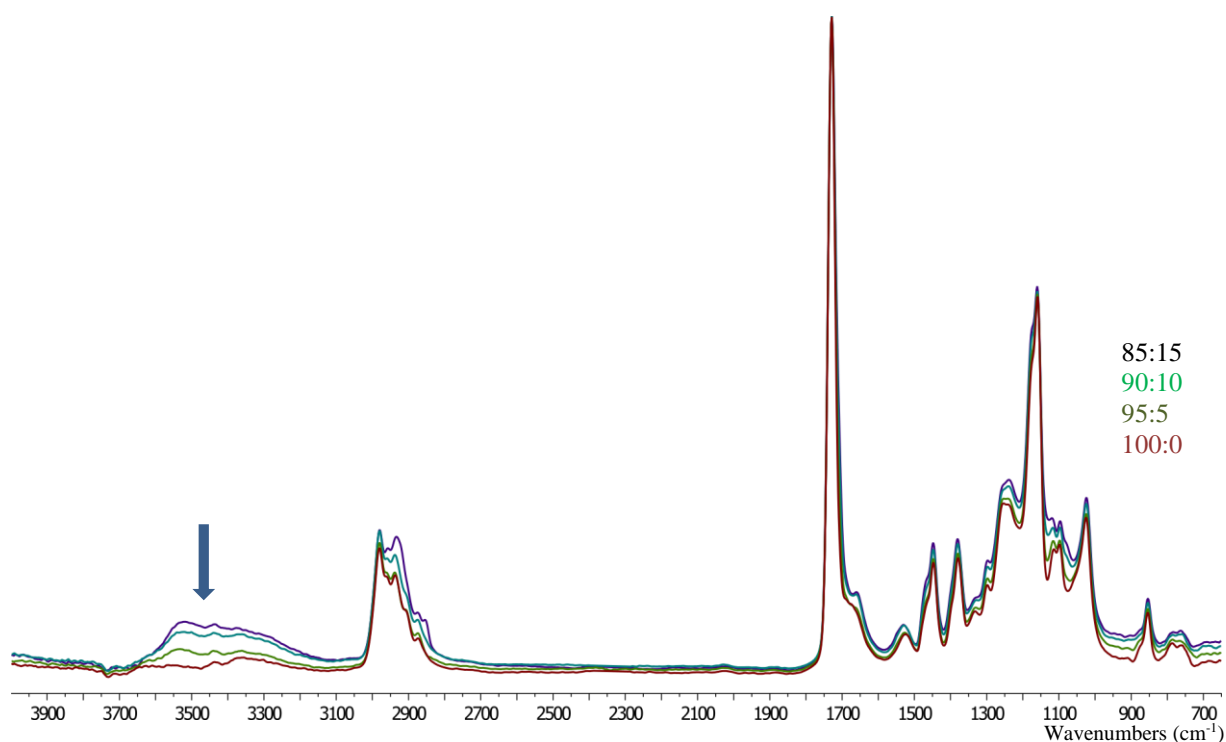


Figure 3.4 IR spectra of the EA-HEMA microgels with different monomers ratios.

To determine the sedimentation stability and optical properties of the thermo-sensitive microgels, dry samples were redispersed in an organic solvent (usually isopropanol). The concentration of these dispersions was 10 mg/mL. For the hydrodynamic diameter measurements, the samples were redispersed in isopropanol, the concentration was 1 mg/mL.

Figure 3.5 demonstrates, how the system reacts to changes of the temperature. At high temperatures, above the CAT the microgel dispersion is well dispersed and the majority of the microgels stay separated from each other (Figure 3.5 a). The dispersion is stable even under applied centrifugal force (Figure 3.5 b). At temperatures near and below the CAT microgels collapse, lose solubility and start to aggregate, the dispersion becomes turbid and the sedimentation stability decrease significantly.

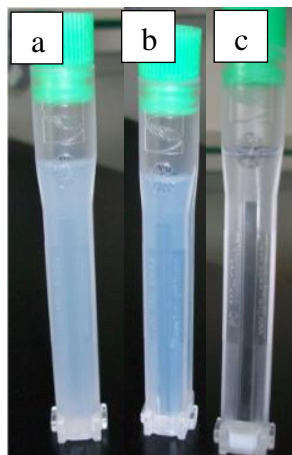


Figure 3.5 EA-organocatalyst microgels at 45°C (a), at 45°C after centrifugation (b) and after centrifugation at 5°C (c).

To investigate the optical properties of the EA-HEMA microgel systems, UV-Vis spectroscopy was performed. To make the measurements, 50 mg of the EA-HEMA microgel were redispersed in 5 mL of isopropanol. The dispersion was heated up to 60 °C and placed in a quartz cuvette. As a reference solution for the UV-Vis measurement isopropanol was used. The measurement was performed by measuring the optical density change with changing temperature. In the typical approach the temperature was changed from the 60 to 0 °C with steps of 1 °C per minute. To ensure the homogeneous temperature distribution, the cuvettes were equipped with the magnetic stirrers. The results of the UV-Vis measurements are shown in the figure 3.6. In the figure 3.6 a is shown the typical change of the transmittance in the temperature sensitive microgel dispersions. For the determination of the CAT of the microgel the use of the wavelength with the higher transmittance difference is more preferable. For EA systems it was 900 nm. Comparing the CAT points of the microgels with different content of the HEMA it is noticeable, that the CAT is linear increasing with the decrease of the HEMA content. From the diagram shown on the figure 3.6 b it is to conclude that by increasing the HEMA content to 15 mol-% the CAT temperature has changed from 34 to 18 °C. The changing in the CAT can be explained by an increase in the hydrophilicity with increase of the HEMA content in the final microgel. The changing of the CAT temperature is very important for the further application of smart microgels in catalysis.

### 3. Microgel-Based Catalysts

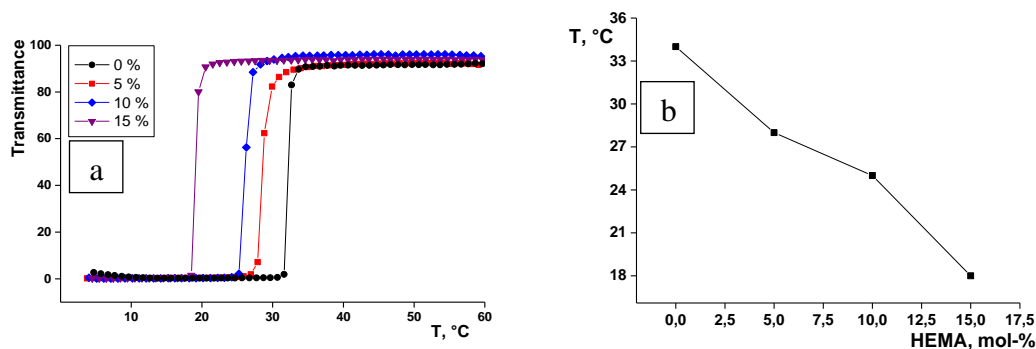
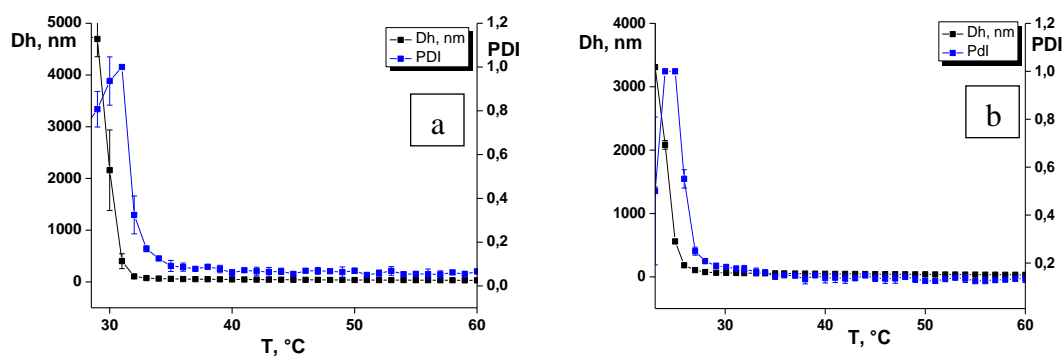


Figure 3.6 UV-Vis measurements of the EA:HEMA microgels with the different HEMA content: 0 mol-%, 5 mol-%, 10 mol-%, 15 mol-% and changes of the CAT point depending on the HEMA content (b). Dispersions of the EA:HEMA microgels in isopropanol 10 mg/mL,  $\lambda = 900$  nm.

One of the other methods to investigate the CAT properties of the microgels is the observation of the hydrodynamic size, which is changing depending on the medium temperature (Figure 3.7). For the DLS measurements, 5 mg of the microgel was redispersed in 5 mL of the isopropanol. The microgel dispersion was heated up to 60 °C in the oven. 1 mL of the dispersion was placed in the preheated quartz cuvette. The measurement was performed in the zetasizer device. The temperature trend was performed from 60 to 4 °C with steps of 1 °C. The sample was measured 3 times at each temperature.



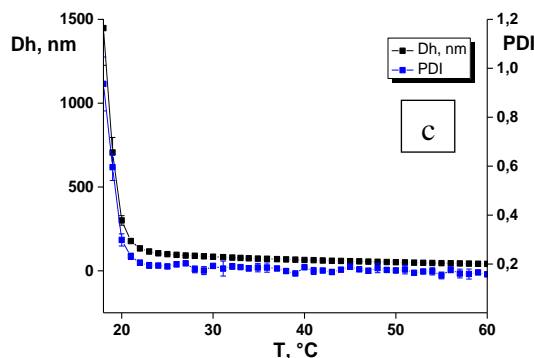


Figure 3.7 DLS measurements of the EA:HEMA microgels with different HEMA content: 5 mol-% (a), 10 mol-% (b), 15 mol-% (c). Hydrodynamic diameter black line and polydispersity index blue line. Dispersions of the EA:HEMA microgels in isopropanol 1 mg/mL.

From the zetasizer data the same trend can be observed as in case of UV-Vis measurements. In the region between 60 °C and the CAT, hydrodynamic size and the polydispersity index stay constant. At the CAT point the size of the particles and the polydispersity index increase dramatically. This change in the values can be explained by aggregation of the particles, which are no more dispersible in the solvent. In the region of the temperatures between the CAT and 4 °C the polydispersity index is very high, which indicates a big difference between the particles sizes. The constant changing of the size and error bars in this temperature region can be explained with the precipitation of the aggregated microgel particles.

#### EA-AAEM microgels

The second model system are microgels based on ethyl acrylate copolymerized with the different amounts of 2-(methacryloyloxy)ethyl acetoacetate. The presence of AAEM is needed for the incorporation, stabilization and complexation of metal ions and nanoparticles. To prove the incorporation of AAEM, IR spectra (Figure 3.8) were measured. The intensity of the typical wavenumber for enol tautomer  $\text{--CO--}$  at  $1050\text{ cm}^{-1}$  are linearly increasing with the increase of the AAEM content.

### 3. Microgel-Based Catalysts

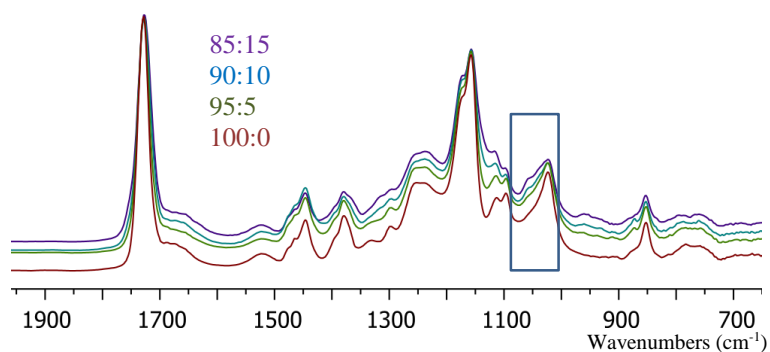


Figure 3.8 IR spectra of the EA-AAEM microgels with different monomers ratios.

From the results of the UV-Vis as in case with the EA-HEMA system, the influence of the comonomer on the CAT temperature can be observed. Due to the high hydrophilicity of the comonomer in the case with AAEM the CAT point is increasing with increasing AAEM content (Figure 3.9). The CAT point is linearly increasing from the 34 °C in case of pure EA microgel to 47 °C in case of 15 mol-% AAEM.

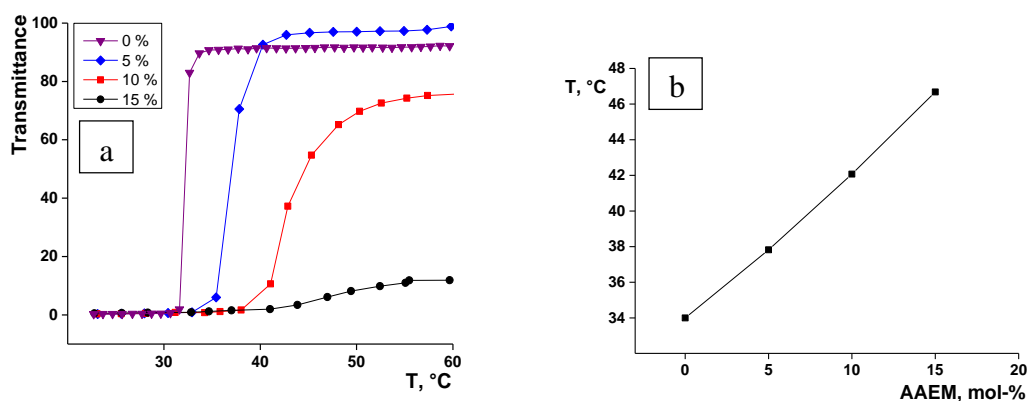


Figure 3.9 UV-Vis measurements of EA:AAEM microgels with different AAEM contents: 0 mol-%, 5 mol-%, 10 mol-%, 15 mol-% (a) and changes of the CAT point depending on the AAEM content (b). Dispersions of the EA:AAEM microgels in isopropanol 10 mg/mL,  $\lambda = 900$  nm.

The DLS measurements of the EA-AAEM microgels (Figure 3.10) confirm the presence of monodisperse microgels. The CAT points can be observed at all compositions of microgel. The polydispersity of the microgels at high temperatures stays below 0.2 which points on the presence of single not aggregated microgel particles. The size of the microgels at 60 °C does not significantly change with changing AAEM content and stays at 40-50 nm. After the CAT point the microgels start to build aggregates which are confirmed by the increasing hydrodynamic diameter and polydispersity index.

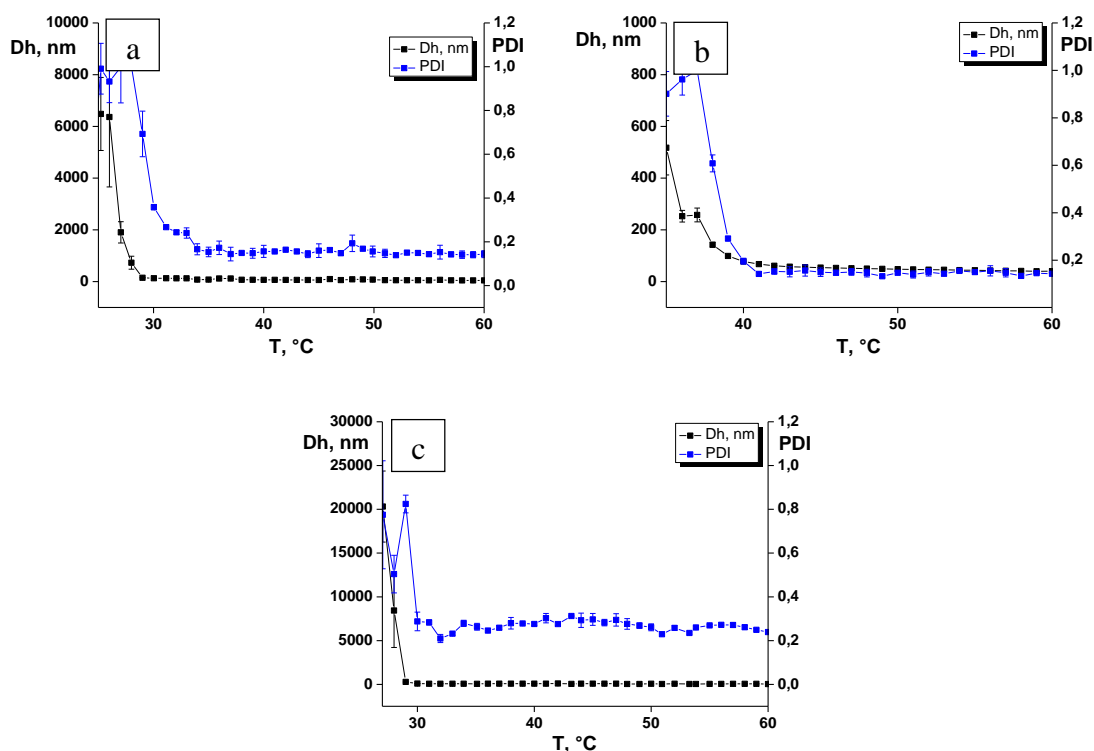


Figure 3.10 DLS measurements of the EA:AAEM microgels with the different AAEM content: 5 mol-% (a), 10 mol-% (b), 15 mol-% (c). Hydrodynamic diameter black line and polydispersity index blue line. Dispersions of the EA:AAEM microgels in isopropanol 1 mg/mL.

#### EA-HEMA-AAEM microgels

The third model system are microgels consisting of ethyl acrylate, 2-hydroxyethyl methacrylate and 2-(methacryloyloxy)ethyl acetoacetate. EA is acting as a thermo-active monomer, HEMA as a functional agent which can be further modified with other compounds due to the presence of the OH-groups. AAEM acts as a functional ligand, which can form complexes with metal ions or metal nanoparticles. In figure 3.11 the IR spectroscopy spectra of EA-HEMA-AAEM microgels with a constant content of HEMA and various contents of AAEM are shown. From the spectra the increase of the enol  $\text{--CO--}$  signal at  $1050\text{ cm}^{-1}$  can be seen, which proves the incorporation of AAEM in the microgel.

### 3. Microgel-Based Catalysts

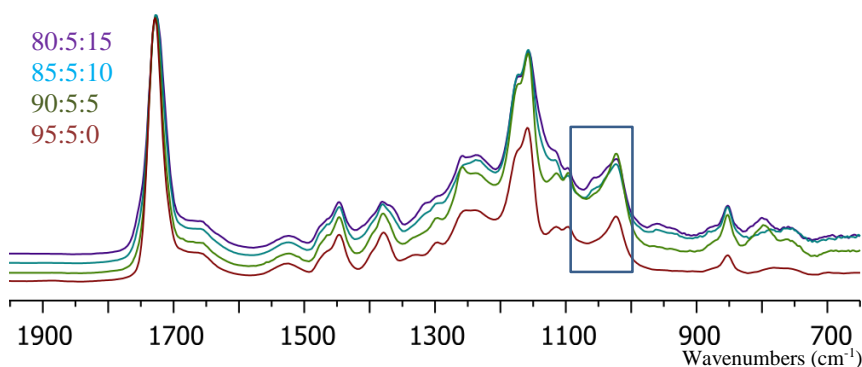


Figure 3.11 IR spectra of the EA-HEMA-AAEM microgels with different monomers ratios.

For the determination of the CAT and to investigate the influence of the AAEM and HEMA content on the CAT, UV-Vis measurements at different temperatures were made (Figure 3.12). The effect of the AAEM content on the CAT is not linear, this can be explained through the presence of HEMA which leads to a different effect as the presence of AAEM. The CAT for the EA-HEMA-AAEM microgels can be varied from 28 to 39 °C depending on the AAEM content.

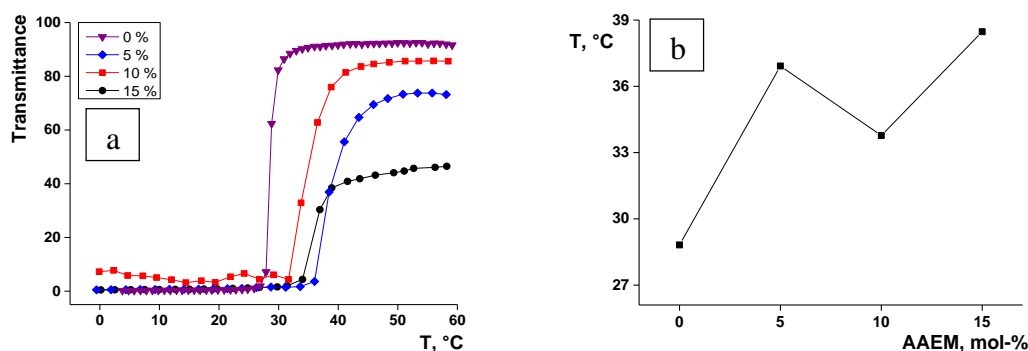


Figure 3.12 UV-Vis measurements of the EA:HEMA:AAEM microgels with a constant HEMA (5mol-%) and different AAEM content: 0 mol-%, 5 mol-%, 10 mol-%, 15 mol-% (a) and changes of the CAT point depending on the AAEM content (b). Dispersions of the EA:HEMA:AAEM microgels in isopropanol 10 mg/mL,  $\lambda = 900$  nm.

Figure 3.13 shows the aggregation of EA-HEMA-AAEM microgels under a change of temperature, measured by DLS analysis. The aggregation temperature is corresponding well to CAT, measured using UV-Vis analysis. As expected the size of the microgel particles is changing from approximately 50 nm to big microgel aggregates. The polydispersity index is dramatically increasing by a decrease of the temperature under CAT point.

### 3. Microgel-Based Catalysts

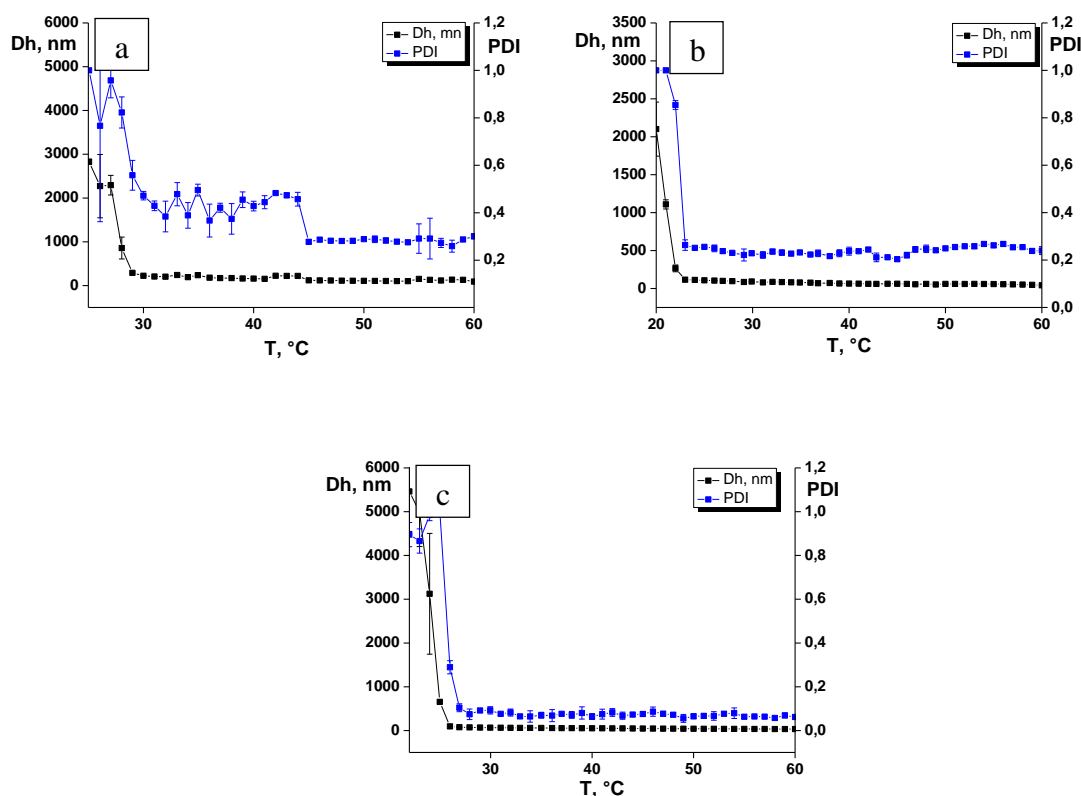


Figure 3.13 DLS measurements of the EA:HEMA:AAEM microgels with constant HEMA content the different HEMA content: 5 mol-% (a), 10 mol-% (b), 15 mol-% (c). Hydrodynamic diameter black line and polydispersity index blue line. Dispersions of the EA:HEMA:AAEM microgels in isopropanol 1 mg/mL.

#### EA-AAEM-AAC microgels

The last model system are microgels consisting of ethyl acrylate, 2-(methacryloyloxy)ethyl acetoacetate and acrylic acid. In addition to the thermo-sensitive properties of the EA and complexation ability of the AAEM, the presence of AAC brings another property. The carboxylic group of the acrylic acid is a very strong complexation agent. The presence of negative charges on one hand allows the attraction of positively charged ions, molecules and surfaces. On the other hand, it increases the hydrophilicity of the microgels in alcohol dispersions. The change of the hydrophilicity also has an influence on the CAT.

The synthesis of the EA-AAEM-AAC microgels was performed by the previously described procedure. Because of the high hydrophilicity of these microgels, in order to retain the CAT, AAC concentration in the microgels was set to 1, 2.5 and 5 mol-%. To prove the incorporation of the acrylic acid in the microgels, IR spectroscopy was performed (Figure



### 3. Microgel-Based Catalysts

3.14). The intensity of the -OH peak of the acrylic acid at  $3350\text{ cm}^{-1}$  is linear increasing with the increasing of the acrylic acid content in the microgel.

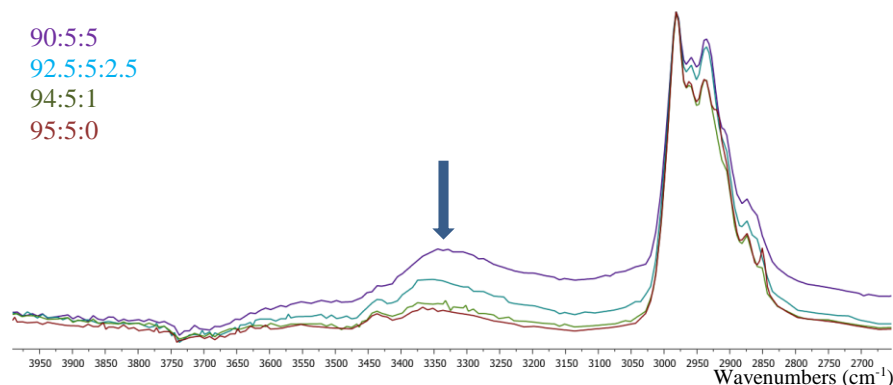


Figure 3.14 IR spectra of the EA-AAEM-AAC microgels with different monomers ratios.

UV-Vis analysis of EA-AAEM-AAC microgels was performed to investigate the change of the CAT points of the microgels with different AAC content. As mentioned before the presence of acrylic acid has a very big influence on the hydrophilicity of the final microgel. This influence can be seen in figure 3.15. According to the UV-Vis, the CAT point is decreasing linear from the  $37\text{ }^{\circ}\text{C}$  for no acrylic acid to  $13\text{ }^{\circ}\text{C}$  for 2.5 mol-% of acrylic acid. At a content of the acrylic acid of 5 mol-% due to the high hydrophilicity of the microgel the CAT point vanishes.

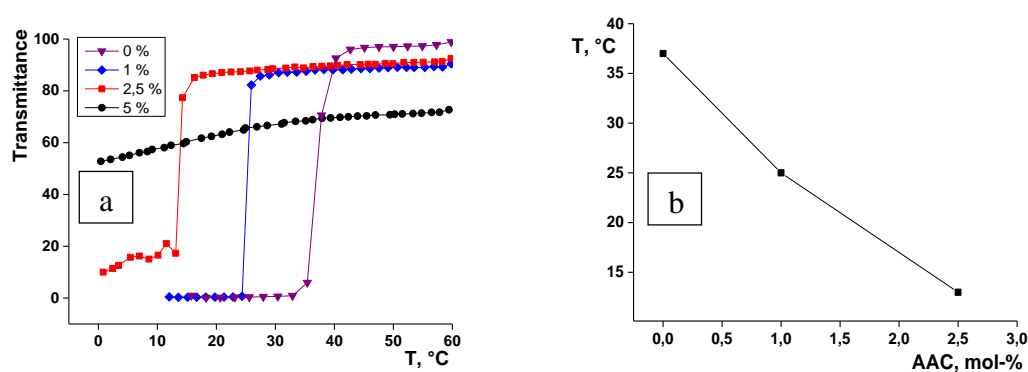


Figure 3.15 UV-Vis measurements of the EA:AAEM:AAC microgels with a constant AAEM (5 mol-%) and the different AAC content: 0 mol-%, 1 mol-%, 2.5 mol-%, 5 mol-% (a) and changes of the CAT point depending on the AAC content (b). Dispersions of the EA:AAEM:AAC microgels in isopropanol 10 mg/mL,  $\lambda = 900\text{ nm}$ .

### 3. Microgel-Based Catalysts

The fact of the high hydrophilicity of the EA-AAEM-AAC microgels is proven by dynamic light scattering analysis. The microgels with an approximate size of 40 nm start to aggregate at temperatures near to the CAT. The CAT point is decreasing with the increase of the acrylic acid content. Due to the charges on the microgel surface microgel particles cannot build the big aggregates which can be confirmed by observation of the aggregate size for different microgels at 4 °C.

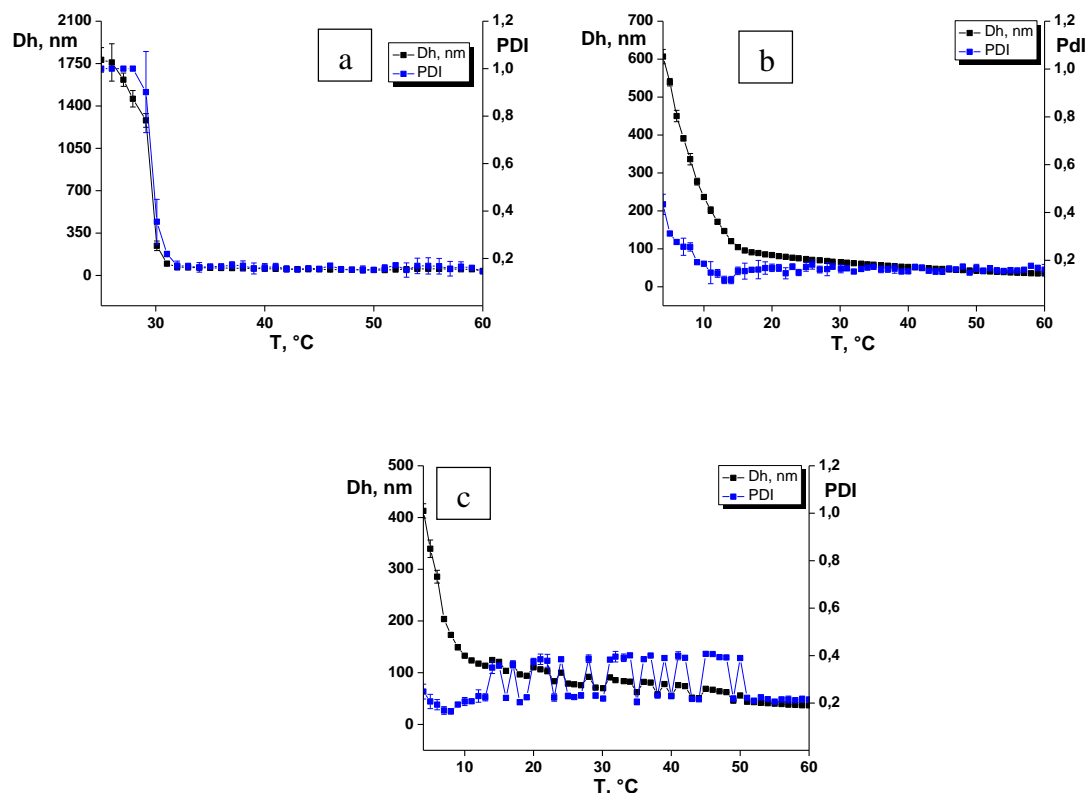


Figure 3.16 DLS measurements of the EA:AAEM:AAC microgels with constant AAEM content the different AAC content: 1 mol-% (a), 2.5 mol-% (b), 5 mol-% (c). Hydrodynamic diameter black line and polydispersity index blue line. Dispersions of the EA:AAEM:AAC microgels in isopropanol 1 mg/mL.

#### Influence of the acrylate nature and the solvent type on CAT

To investigate the influence of the acrylate nature, microgels based on isooctyl acrylate and hydroxy ethyl methacrylate were synthesized. To compare the EA and iOA microgels, UV and DLS analysis (Figure 3.17) were performed. Surprisingly, the application of the acrylates with higher molecular weight leads to the decrease of the CAT point. The CAT point

### 3. Microgel-Based Catalysts

measured by UV-Vis as well as with DLS is around 22 °C. The hydrodynamic diameter of the iOA microgels in isopropanol at 60 °C is 38 nm with a low polydispersity index of 0.07.

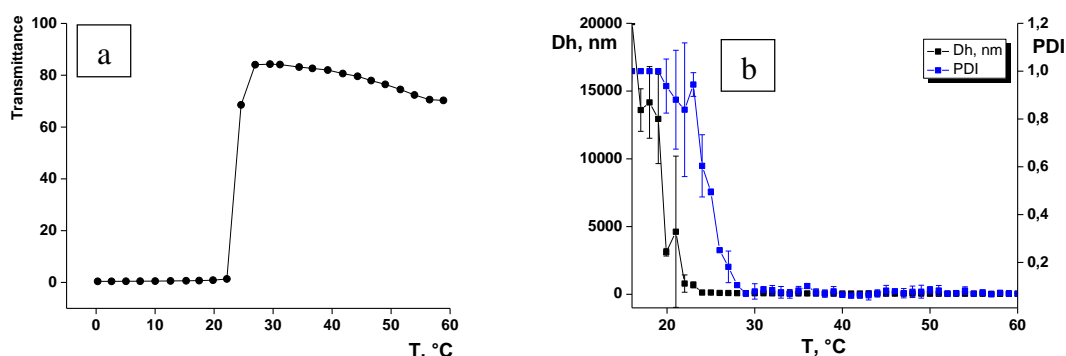


Figure 3.17 UV-Vis measurements of the iOA:HEMA microgels with a 5 mol-% HEMA content (a). Dispersions of the iOA:HEMA microgels in isopropanol 10 mg/mL and DLS measurements (b). Hydrodynamic diameter black line and polydispersity index blue line. Dispersions of the iOA:HEMA microgels in isopropanol 1 mg/mL.

The influence of the alkyl chain length of the solvent on the CAT point (Figure 3.18) was also studied. For the measurements of the CAT points UV-Vis spectroscopy was performed. For this model EA:HEMA (95:5) microgel was redispersed at 60 °C in ethanol, 1-propanol, isopropanol and 1-butanol. From the results it can be seen that the more hydrophobic the solvent, the higher the CAT point. In this case, the CAT point can be changed from 22 °C using ethanol to 39 °C using butanol.

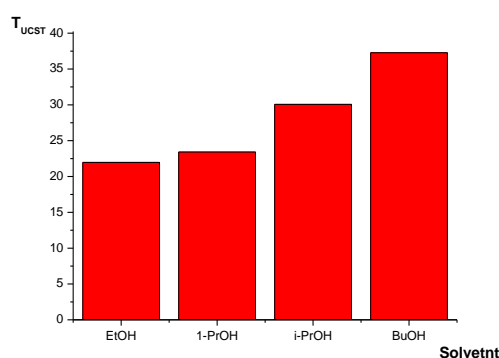


Figure 3.18 CAT points of the EA:HEMA microgel measured using UV-Vis depending on a solvent. EA:HEMA 95:5, solid content 10 mg/mL.

### 3. Microgel-Based Catalysts

#### Influence of the surfactant content on the microgel size

For the classical emulsion polymerization, surfactants are used in order to stabilize the emulsion and to prevent the aggregation of the particles. It is known from literature, that the surfactant concentration may affect the size of the microgels. To prove this, three syntheses of EA-AAEM (90:10) microgels with different surfactant concentrations were synthesized (Figure 3.19). As it is shown in figure 3.19 d, the hydrodynamic size of the microgels increase with decreasing of the surfactant content. By decreasing the surfactant content from 1 to 0.05 mol-% it was possible to increase the hydrodynamic microgel size from 40 to 80 nm (measured at 60 °C). Further decreasing of the surfactant content lead to the aggregation in the system.

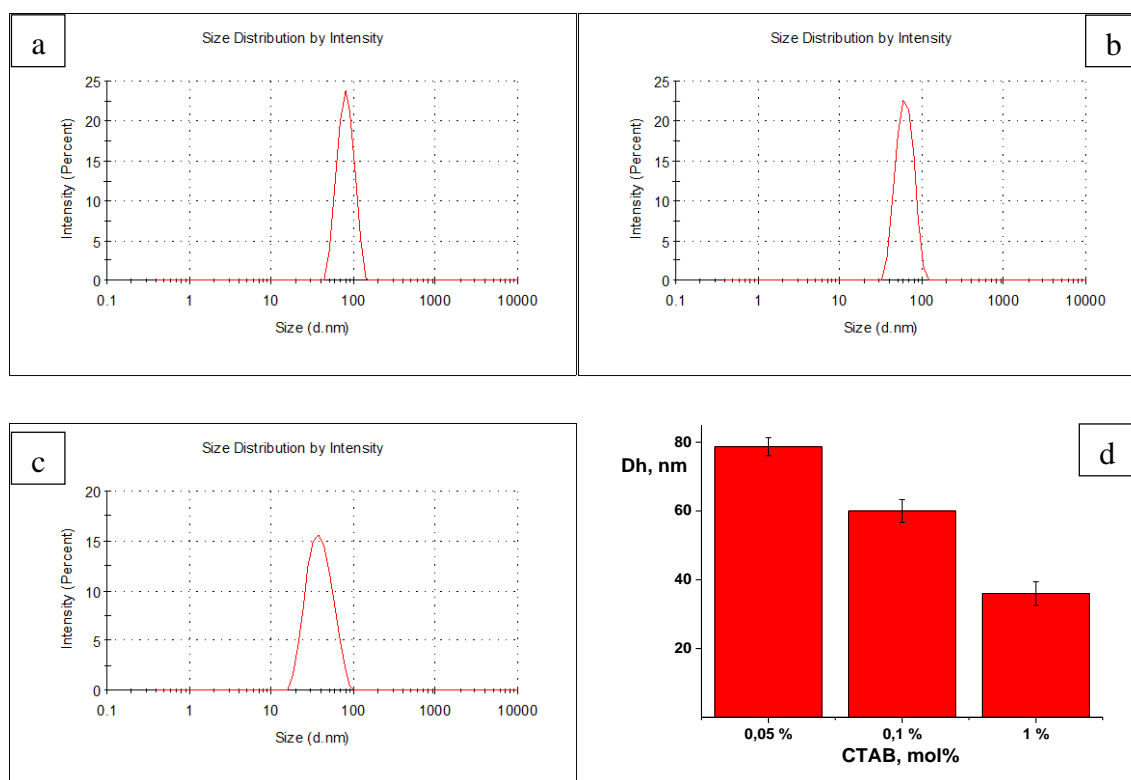


Figure 3.19 Influence of the surfactant content on the hydrodynamic microgel size. DLS measurements of the particles size (1 mg/mL in isopropanol) at surfactant concentration 0.05 mol-% (a), 0.1 mol-% (b) and 1 mol-% (c) during the synthesis. Concentration-size dependence (d).

### 3.3 Microgels with metal complexes and organocatalyst

After the successful production of model microgels, the synthesis of the catalytically active microgels was performed (Figure 3.20). The idea behind the smart, catalytically active microgels was in use of ethyl acrylate as a main monomer. The use of the ethyl acrylate ensures the temperature responsive behavior of the microgels. A functional ligand (amine, phosphine etc.) can act as a comonomer which can be further modified with a catalytically active metal or a ligand, which already includes the catalytic centrum and doesn't required a post modification.

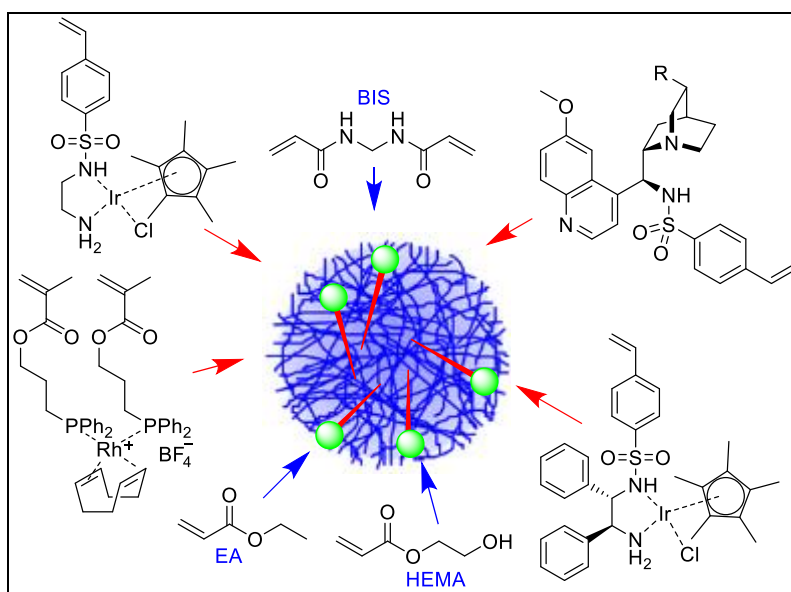


Figure 3.20 Concept of the smart thermo-responsive microgels loaded with catalytic active metal ions or organic molecules.

#### Amine-functionalized microgels

The first example are amine-functionalized microgels, which were synthesized through the copolymerization of ethyl acrylate with an amine functional ligand using emulsion polymerization (Figure 3.21). The synthesis was performed using the previously described procedure. Diamine in this case can act a chelating agent and build strong complexes with noble metal ions.

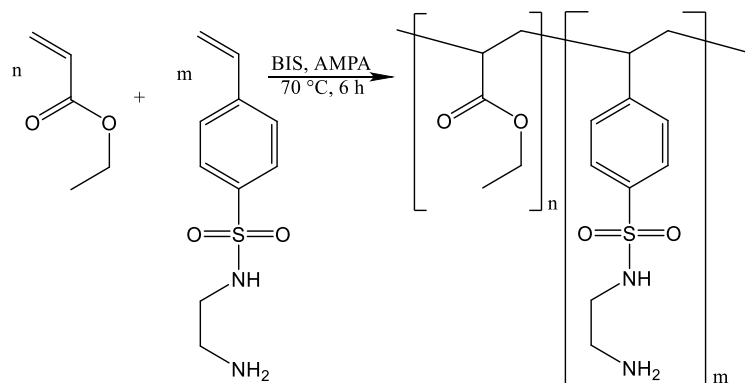


Figure 3.21 Synthesis of the amine-functionalized microgels.

To insure the incorporation of the amine functional monomer in the microgel, Raman spectroscopy was performed (Figure 3.22). The red line is the spectra of the pure ethyl acrylate microgel, the blue line is the spectra of amine-functionalized microgel. The signal of the benzene ring  $\text{-C-C-}$  at  $1600\text{ cm}^{-1}$  proves the presence of the comonomer in copolymer structure.

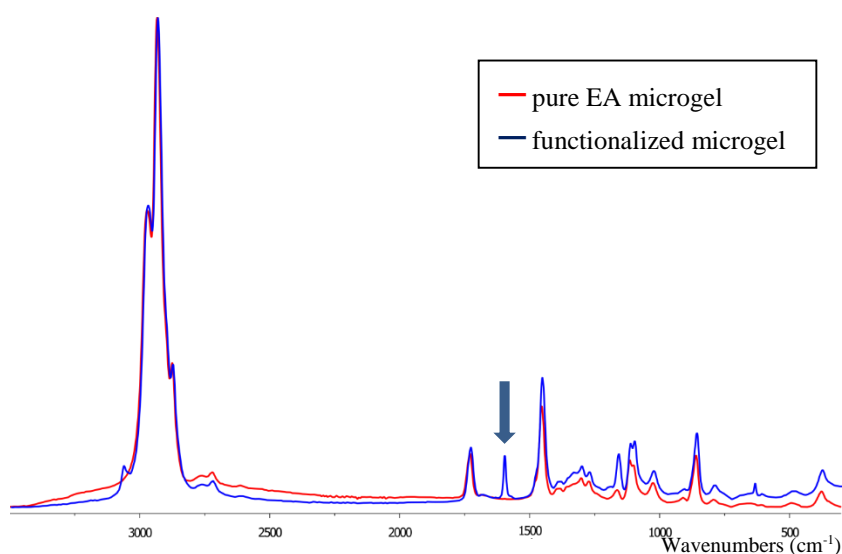


Figure 3.22 RAMAN spectra of EA-Amine microgel.

Due to the presence of the ethyl acrylate, amine-functionalized microgels are temperature sensitive and exhibit a CAT (Figure 3.23). According to the UV-Vis measurements (Figure 3.23 a) EA-Amine microgels are switchable and have the CAT point at  $37^\circ\text{C}$ . The CAT measured by UV-Vis correlates well with the CAT measured using DLS. According to DLS measurements microgels start to aggregate at  $37^\circ\text{C}$  (Figure 3.23 b). A separation analyzer was also used for the determination of the CAT (3.23 c). At high temperatures above the CAT microgels are well redispersed as single particles in isopropanol. At temperatures below the CAT, microgel particles start to aggregate. In aggregated state they are no more colloiddally

### 3. Microgel-Based Catalysts

stable and the sedimentation velocity dramatically increases with the decreasing of the temperature (Figure 3.23 c).

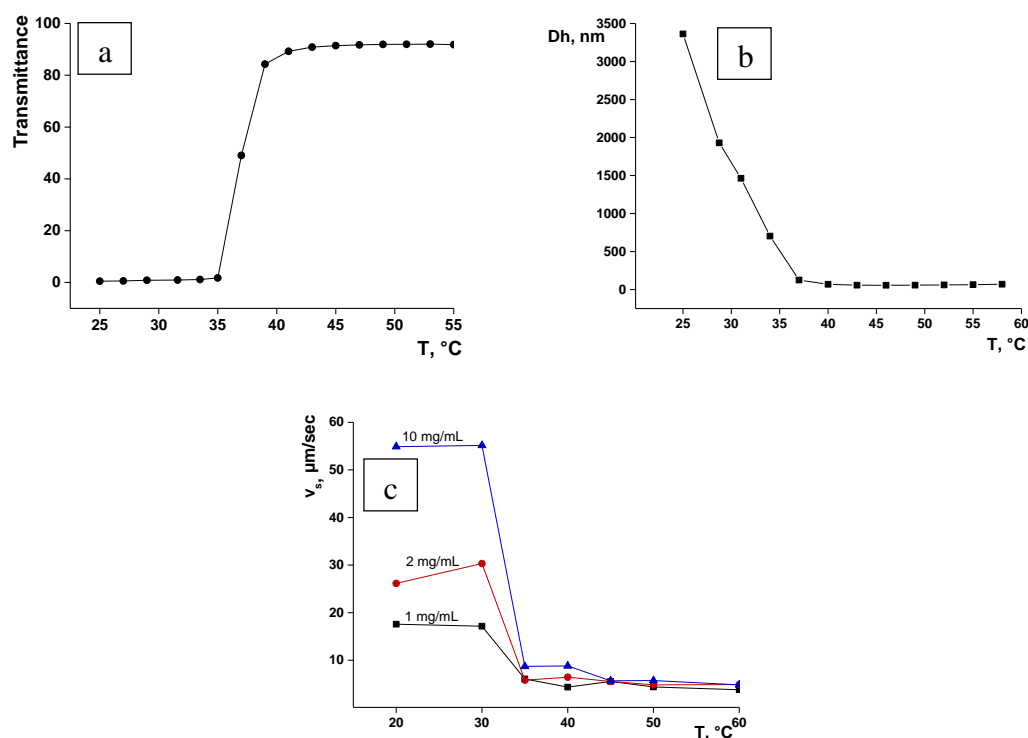


Figure 3.23 CAT point of the EA:Amine microgels measured by UV-Vis spectroscopy: 10 mg/mL in isopropanol (a), DLS: 1 mg/mL in isopropanol (b) and sedimentation velocities at 2000 rpm at different concentrations in isopropanol (c).

#### Iridium-Amine-functionalized microgels

After the successful synthesis and analysis of the amine-functionalized microgels, the direct synthesis of the functional microgels with a catalytic centrum was performed. For this, the diamine monomer was metalized with the Ir salt  $[\text{IrCp} \cdot \text{Cl}_2]_2$ . The functional monomer with an Ir complex was dissolved in a calculated amount of the ethyl acrylate co-polymerized using the standard procedure (Figure 3.24)

### 3. Microgel-Based Catalysts

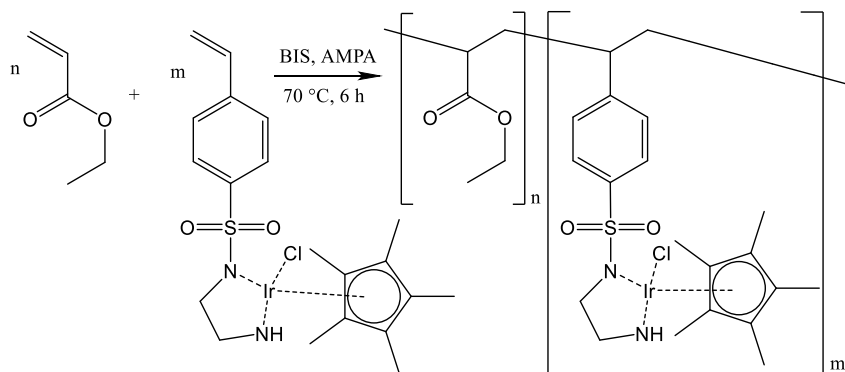


Figure 3.24 Synthesis of the Ir-Amine-functionalized microgels.

The presence of the diamine-Ir comonomer was proven using Raman spectroscopy (Figure 3.25). Red line is corresponding to the pure ethyl acrylate microgel, blue line corresponding to the EA-Amine-Ir microgel. The incorporation of the functional comonomer can be seen through the presence of the benzene ring -C-C- peak at  $1600\text{ cm}^{-1}$

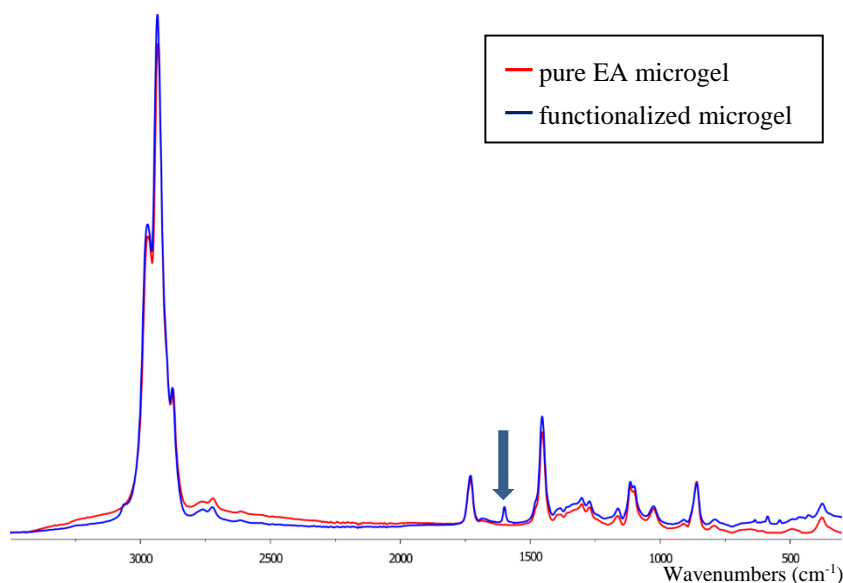


Figure 3.25 Raman spectra of EA-Amine-Ir microgel.

Due to the presence of the metal ions in the microgel, the functional microgel and microgel dispersion are intensely colored in all visible spectra. The transmittance of the microgel dispersions measured using UV-Vis is below 100 % (Figure 3.26 a). The CAT point measured using UV-Vis spectroscopy is near  $23\text{ }^{\circ}\text{C}$ . The size of the microgels at  $60\text{ }^{\circ}\text{C}$  is 34 nm with a polydispersity index of 0.142 (Figure 3.26 c). According to the temperature dependent DLS measurements (Figure 3.26 b) microgel starts to aggregate at  $25\text{ }^{\circ}\text{C}$  which is very close to the CAT measured by UV-Vis.



### 3. Microgel-Based Catalysts

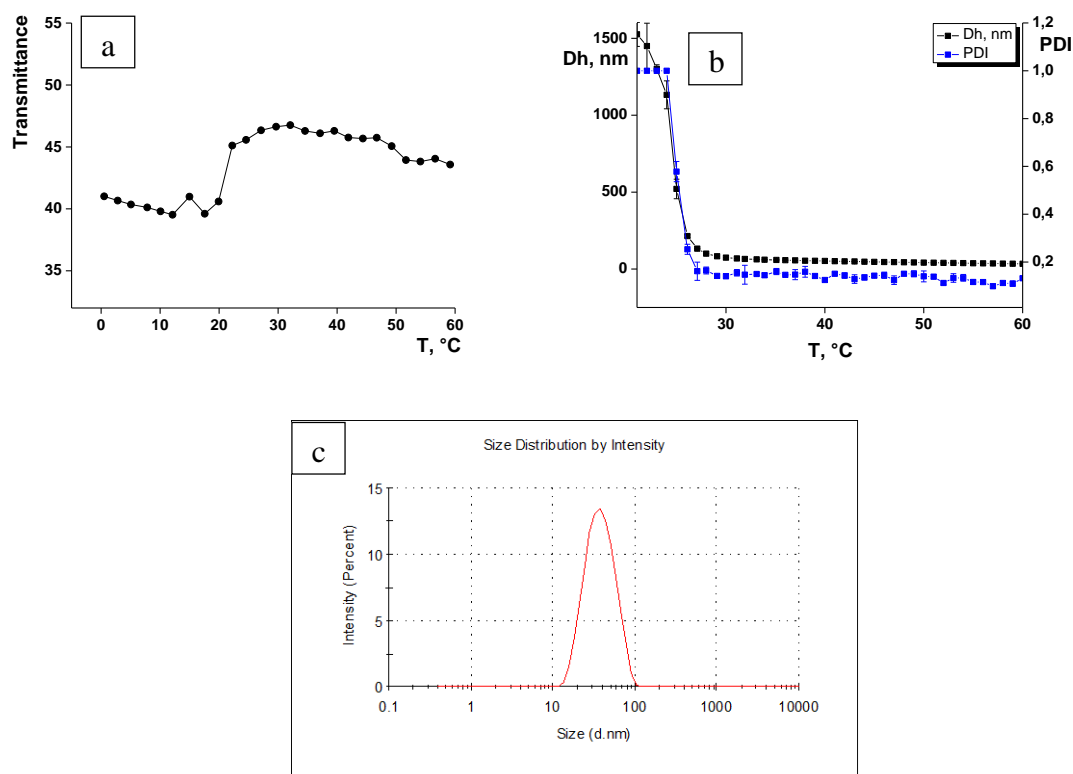


Figure 3.26 CAT point of the EA:Amin-Ir microgels measured by UV-Vis spectroscopy: 10 mg/mL in isopropanol (a), DLS: 1 mg/mL in isopropanol (b) and the size of the microgel particles at 60 °C (c).

In addition to the EA-Amine-Ir microgels, a similar microgel containing a more hydrophobic functional comonomer, was synthesized (Figure 3.27). As in the previous case, it was a direct co-polymerization of the metallized functional monomer with ethyl acrylate. The metal complex was achieved through the reaction of the ligand with an iridium salt. Before the polymerization comonomer was dissolved in the ethyl acrylate.

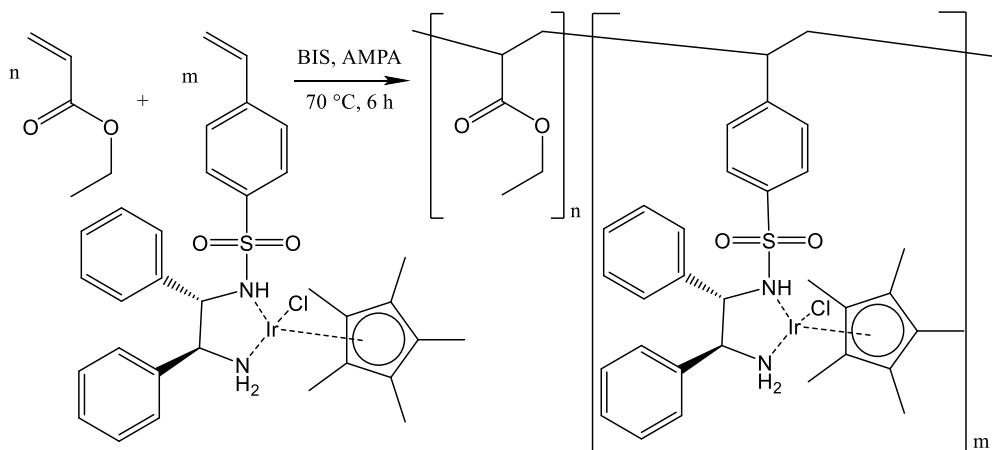


Figure 3.27 Synthesis of the Ir-Amine-functionalized microgels.

### 3. Microgel-Based Catalysts

Incorporation of the iridium complex was proven by performing Raman spectroscopy analysis of the dry functional microgel sample (Figure 3.28). As in the previous amine-iridium sample, the benzene ring -C-C- signal at  $1600\text{ cm}^{-1}$  proves the presence of the functional comonomer (blue line), compare to the pure ethyl acrylate microgel (red line)

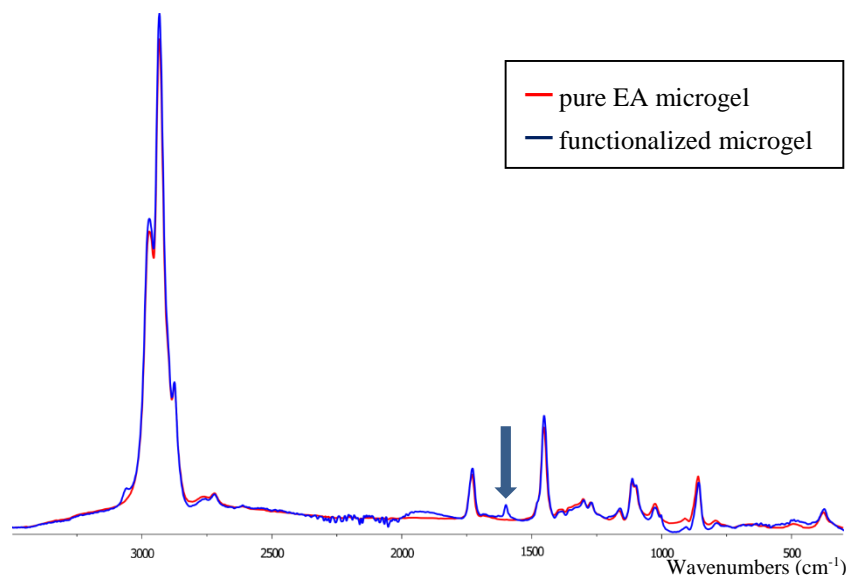


Figure 3.28 Raman spectra of EA-Amine-Ir microgel.

The intensive color of the EA-Amine-Ir microgel dispersion in isopropanol decreases the transmittance at high temperatures. The CAT point of these microgel dispersions measured using UV-Vis spectroscopy can be still recognized and is  $28\text{ }^{\circ}\text{C}$  (Figure 3.29 a). According to the DLS analysis the microgel size in isopropanol at  $60\text{ }^{\circ}\text{C}$  is  $34.5\text{ nm}$  with a polydispersity index of 0.135 (Figure 3.29 c). Microgel particles start to aggregate at  $30\text{ }^{\circ}\text{C}$  (Figure 3.29 b).

The CAT point values of these two ethyl acrylate-diamine-iridium microgels have very good correlation to their hydrophilicity. The first microgel is more hydrophilic and has CAT at  $23\text{--}25\text{ }^{\circ}\text{C}$ , the second microgel, due to the presence of the additional benzene in the comonomer structure, is more hydrophobic and has CAT at  $28\text{--}30\text{ }^{\circ}\text{C}$ .

### 3. Microgel-Based Catalysts

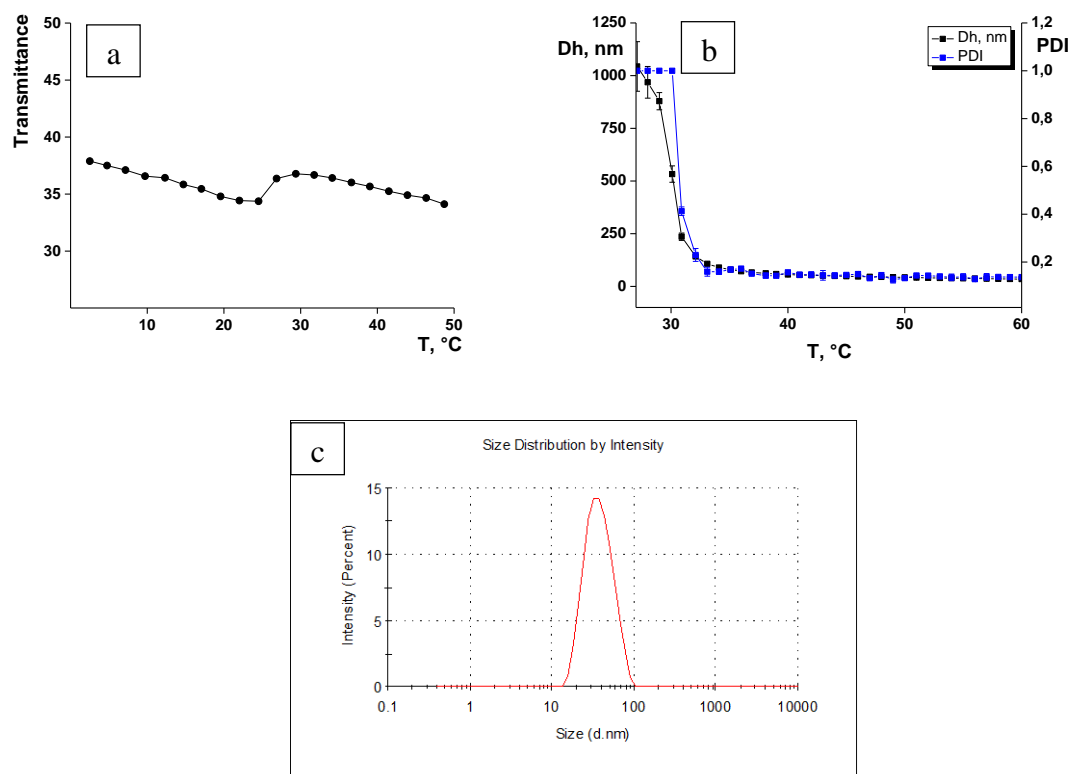


Figure 3.29 CAT point of the EA-Amin-Ir microgels measured by UV-Vis spectroscopy: 10 mg/mL in isopropanol (a), DLS: 1 mg/mL in isopropanol (b) and the size of the microgel particles at 60 °C (c).

#### EA-Phosphine-functionalized microgels and polymers

Besides amine ligands, phosphine ligands can also build strong complexes with the metal ions. In this work, phosphine-based monomers were used in order to get smart switchable microgels, which can be further modified with catalytically active metal ions. The phosphine-functionalized polymers were synthesized in two different ways (Figure 3.36). In a first approach 5 mol-% of the phosphine monomer was dissolved in a calculated amount of the ethyl acrylate and directly polymerized using emulsion polymerization (Figure 3.36 a). In the second approach phosphine-functionalized polymer was synthesized by post-modification of the linear 95:5 EA-HEMA polymer. The post-modification was possible because of the presence of –OH groups on in the polymer (Figure 3.36 b). The products synthesized in two different ways are very similar in their ability to coordinate metal ions, but due to the presence of the ester groups in the second case, they have different polarities.

### 3. Microgel-Based Catalysts

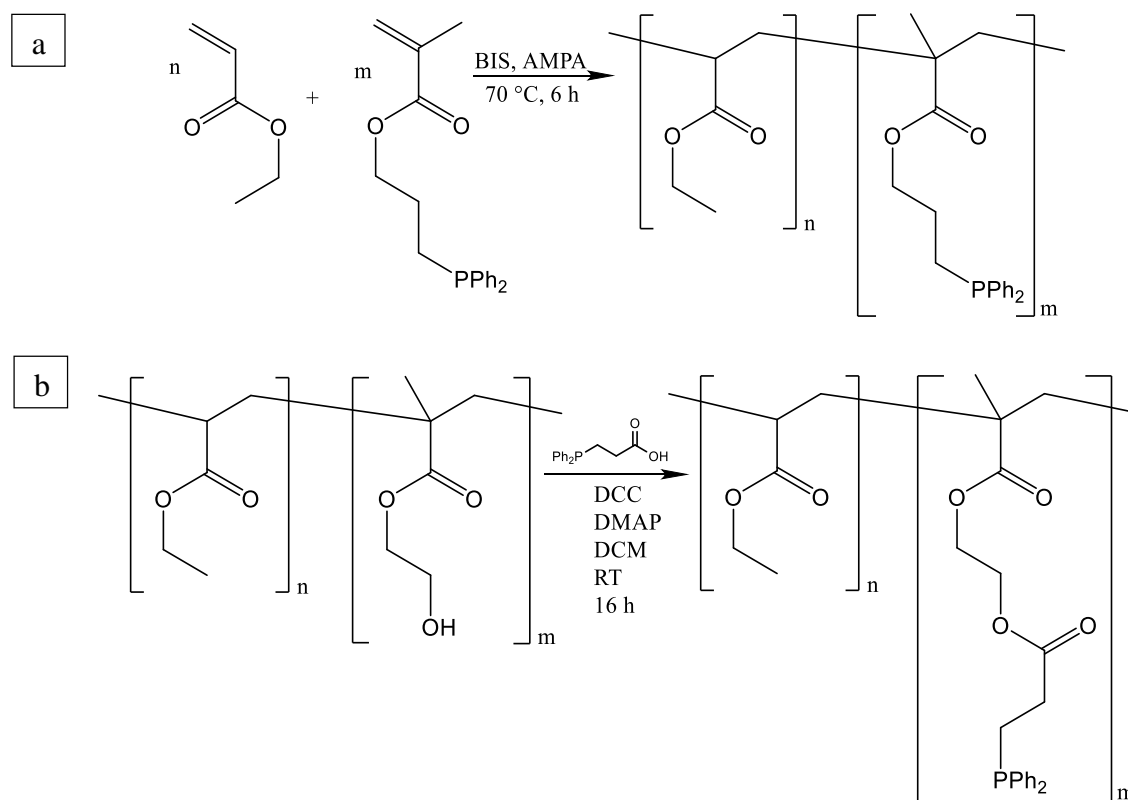


Figure 3.36 Synthesis of the Phosphine-functionalized polymers, using direct way (a) and post-modification (b).

The EA-Phosphine microgel, synthesized using direct modification was analyzed using Raman spectroscopy to prove the incorporation of the phosphine monomer (Figure 3.37). As it can be seen from the functionalized microgel spectra (blue line), the benzene rings which are attached to the phosphor atom have a -C-C- signal at  $1600\text{ cm}^{-1}$ . As a comparison, pure ethyl acrylate microgel was used (red line).

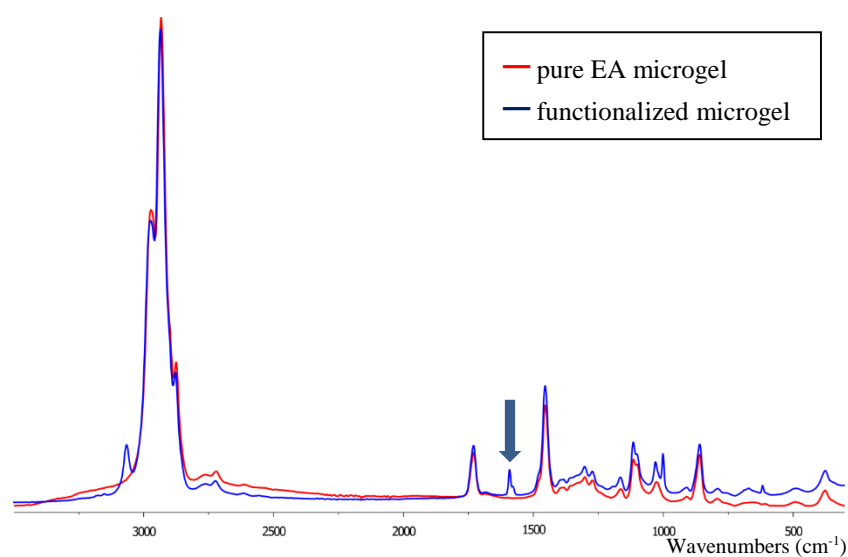


Figure 3.37 Raman spectra of EA-Phosphine microgel.

### 3. Microgel-Based Catalysts

The size and CAT properties of the EA-Phosphine microgels were measured using DLS and UV-Vis spectroscopy. The EA-Phosphine microgel particles at 60 °C have a size of 50.7 nm and narrow size distribution. The polydispersity index is 0.15. The CAT point measured with UV-Vis spectroscopy is 45 °C. The aggregation point of the EA-Phosphine microgel measured by DLS is 45 °C. The high CAT point can be explained with the high hydrophobicity of the co-monomer.

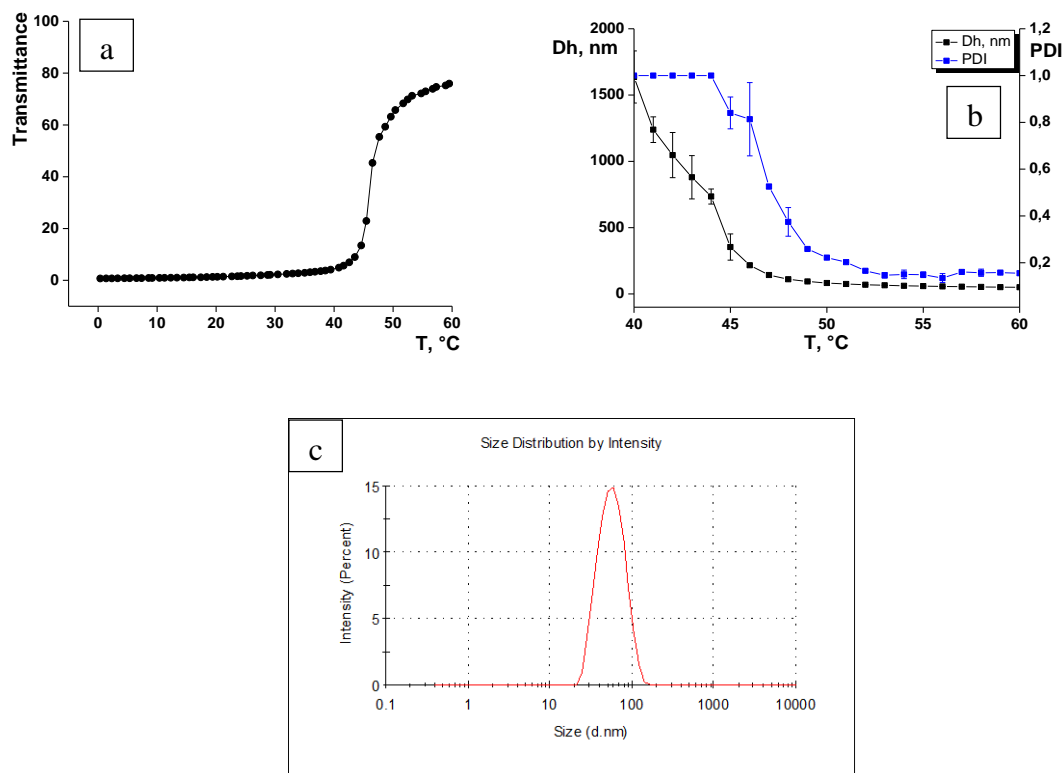


Figure 3.38 CAT point of the EA-Phosphine microgels measured by UV-Vis spectroscopy: 10 mg/mL in isopropanol (a), DLS: 1 mg/mL in isopropanol (b) and the size of the microgel particles at 60 °C (c).

To make the polymer catalytically active the EA-Phosphine polymer, synthesized by post-modification of the EA-HEMA co-polymer, was loaded with rhodium ions using two different rhodium salts  $\text{Rh}(\text{cod})_2\text{BF}_4$  and  $\text{Rh}(\text{cod})\text{acac}$  (Figure 3.39). The anion of the noble metal salt can have an influence on the catalytic activity of the final product. For metalation, the dry functional polymer was redispersed in the DCM/THF mixture. The solution of the rhodium salts was added under continuous stirring. After 1 hour of reaction the product was dried and redispersed in isopropanol for further analysis and catalysis tests.

### 3. Microgel-Based Catalysts

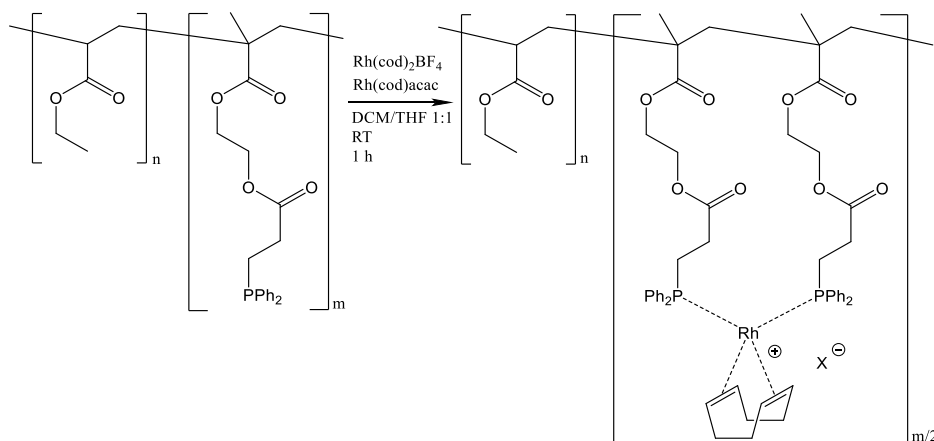


Figure 3.39 Functionalization of the EA-Phosphine polymers with rhodium.

The isopropanol dispersions of the final catalytically active EA-Phosphine-Rh polymers were analyzed using UV-Vis spectroscopy (Figure 3.40). Both polymers show CAT properties, in case of more hydrophilic BF<sub>4</sub><sup>-</sup> anion the CAT point is lower and is 15 °C, in case of more hydrophobic acac<sup>-</sup> anion the CAT is 17 °C. The difference in CAT of this product to the EA-Phosphine microgel synthesized in direct way can be explained by the presence of the hydrophilic ester groups.

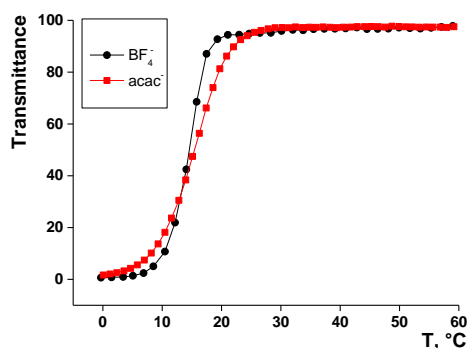


Figure 3.40 UV-Vis spectra of the EA-Phosphine-Rh polymers.

#### EA-organocat-functionalized microgels

A new and promising approach is the copolymerization of temperature sensitive microgels with organic-catalyst (Figure 3.41). The main advantage of the EA-organocatalyst microgels compared to the metal-ions or metal nanoparticles catalysts is that the organocatalyst is chemically bonded to the ethyl acrylate chains of the microgel and cannot be washed out from the microgel with a solvent. The ethyl acrylate acts in this case as temperature sensitive agent and helps to remove the catalyst by centrifugation after the reaction for further use. The organocatalyst is used as a catalyst. For the synthesis 1, 5 and 10 mol-% of the organocatalyst

### 3. Microgel-Based Catalysts

monomer were dissolved in the calculated amount of the ethyl acrylate. Further synthesis was performed using the above described procedure.

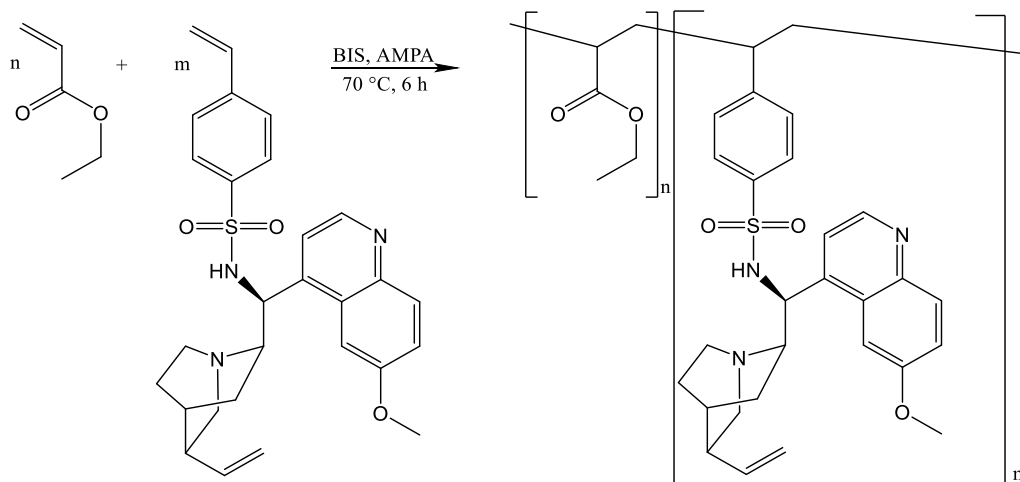


Figure 3.41 Synthesis of the organocatalyst-functionalized microgels.

To prove the incorporation of the organocatalyst, IR spectroscopy measurements were performed (Figure 3.42). For the analysis, five samples were chosen. The first sample was pure ethyl acrylate microgel it has  $\text{C=O}$  signal at  $1730\text{ cm}^{-1}$ . Samples 2, 3 and 4 have 1, 5 and 10 mol-% of the organocatalyst and show two signature signals at  $1625\text{ cm}^{-1}$  and  $1595\text{ cm}^{-1}$  which are corresponding to the  $\text{C=C}$  and  $\text{C=N}$  signals of the aromatic ring in the organocatalyst molecule. The fifth system was pure organocatalyst monomer, which does not have the absorbance at  $1730\text{ cm}^{-1}$ , but has very strong signals at  $1625\text{ cm}^{-1}$  and  $1595\text{ cm}^{-1}$ . It is also noticeable that with the increasing of the organocatalyst content in the functional microgel signals of the organocatalyst were also increasing.

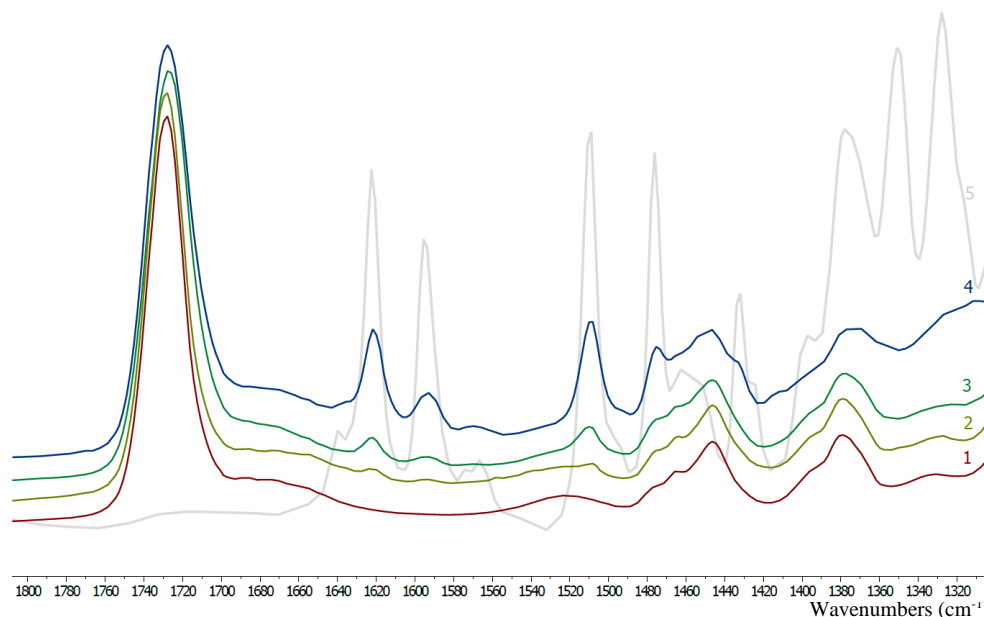
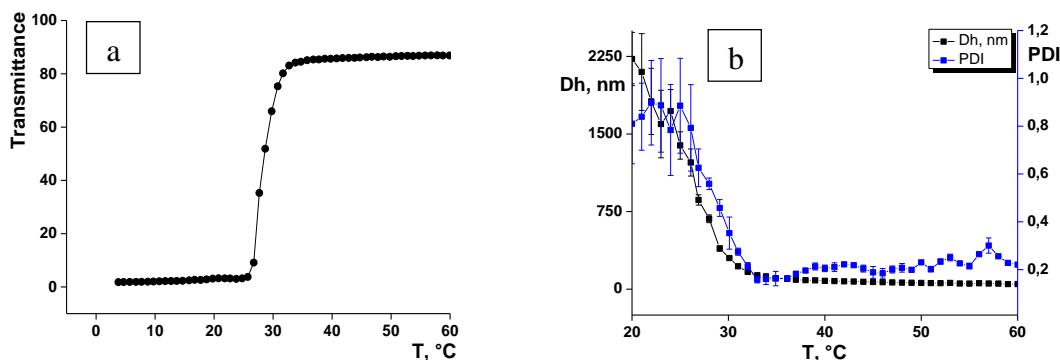


Figure 3.42 FT-IR spectra of pure EA microgel (1); microgels with variable organocatalyst amounts: EA-OC (99:1) (2), EA-OC (95:5) (3), EA-OC (90:10) (4); and organocatalyst (5).

To investigate the microgel properties solid EA-organocatalyst 95:5 microgel was redispersed in isopropanol at 60 °C. According to the UV-Vis measurements, the CAT point of the microgel is at 31 °C. At high wavelength, the microgel dispersion is transparent (Figure 3.43 a). According to the DLS measurements at 60°C, the size of the microgels is 50 nm. The microgel is starting to aggregate at 30 °C (Figure 3.43 b). The CAT point and aggregation temperature correlate with the data of the analytical centrifuge, LUMiFuge (Figure 3.43 c). According to the sedimentation velocity measurements at different temperatures, the sedimentation velocity of microgel dispersions at 2000 rpm increases dramatically at temperatures below 30 °C.





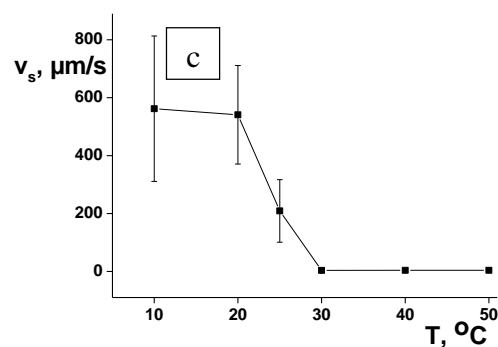


Figure 3.43 CAT point of the EA-organocatalyst microgels measured by UV-Vis spectroscopy: 10 mg/mL in isopropanol (a), DLS: 1 mg/mL in isopropanol (b) and LUMiFuge at 2000 rpm 10 mg/mL in isopropanol (c).

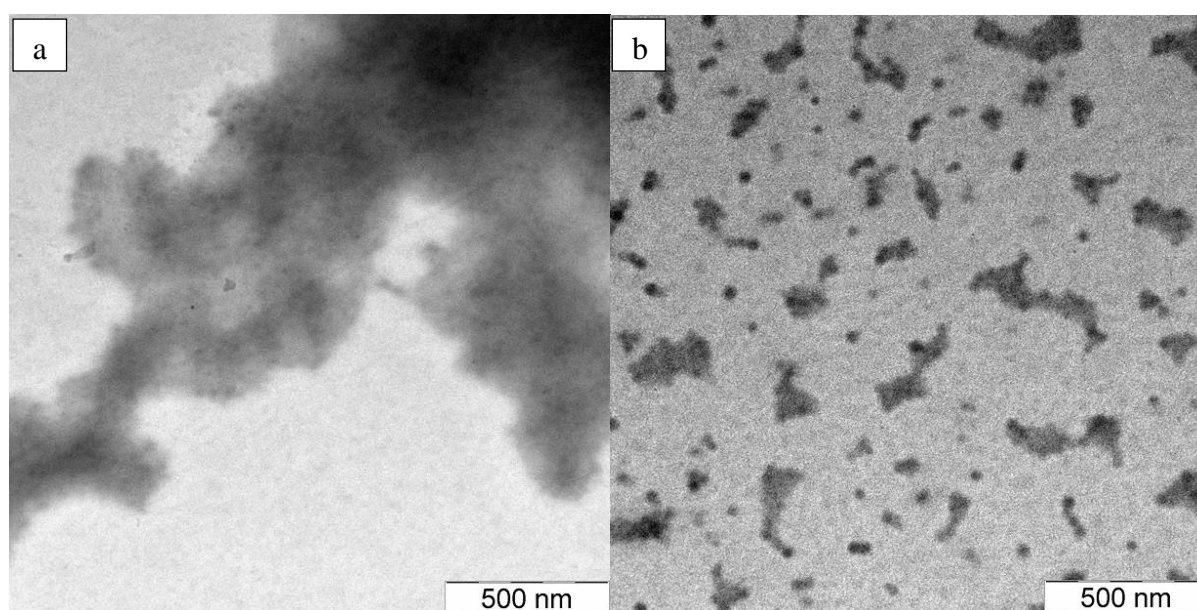


Figure 3.44 TEM images of the EA-organocatalyst microgels 95:5 measured at 5 (a) and 45 °C (b).

The aggregation of the microgel particles at low temperatures was also studied using TEM microscopy (Figure 3.44). The samples were prepared at two different temperatures: 5 and 45 °C. For the preparation of the low temperature sample, isopropanol microgel dispersion, containing 1 mg/mL of microgel, was dropped on a cold TEM grid and dried in the fridge at 5 °C. For the preparation of the 45 °C sample, warm microgel dispersion with the same concentration was dropped on a hot TEM grid from the oven and dried in the oven at 45 °C. By measuring of the 5 °C sample big grid areas were covered with microgel aggregates. By

### 3. Microgel-Based Catalysts

---

measurements of the 45 °C samples of the microgels, no big aggregates of the microgel dispersions were detected. Small aggregates of the microgel on a 45 °C microgel samples occurring by microgel drying and cannot be avoided.

Because of the low glass transition temperature, small size and high softness of the microgels, taking a clear TEM image is difficult. Glass transition temperatures and softness issues can be minimized by using of the Cryo-TEM microscopy (Figure 3.45). The difference between cryo and standard TEM microscopy is in the sample preparation. For the cryo TEM microscopy the TEM grid will be immersed in the sample dispersion and rapidly cooled down with liquid nitrogen. According to the Cryo-TEM images, the microgel consists of round particles with a size of 50 nm (grey lines are grid meshes).

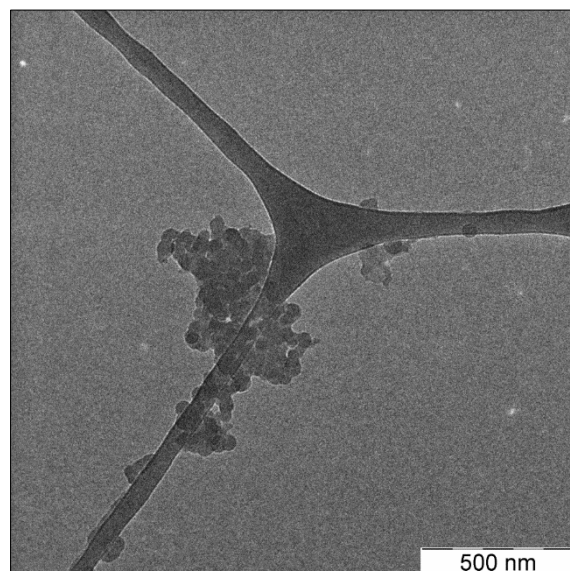


Figure 3.45 Cryo-TEM images of EA-AAEM microgel 90:10.

### 3.4 Microgels loaded with metal nanoparticles

As an alternative to metal ions or organocatalysts, microgels can be loaded with metal nanoparticles. Because of the big surface area, noble metal nanoparticles find a big field of applications in catalysis. The main problem in the application of the metal nanoparticles in catalysis is the difficulty in separation after the catalysis process. In this work, this problem was solved by using microgels as a thermo-sensitive carrier for metal nanoparticles. At the catalytic reaction temperatures, metal-loaded microgel particles are swollen and well dispersed in the solvent. After cooling the reaction mixture to the temperatures below the CAT, microgel particles start to aggregate and can easily be removed from the reaction mixture and reused again. To insure the incorporation and holding of the nanoparticles inside the microgels, functional comonomers, which can build metal complexes, were incorporated in the microgel. Besides thermo-active ethyl acrylate, metal bonding ligands such as 2-(methacryloyloxy)ethyl acetoacetate, 2-hydroxyethyl methacrylate or acrylic acid were co-polymerized in the microgel (Figure 3.46).

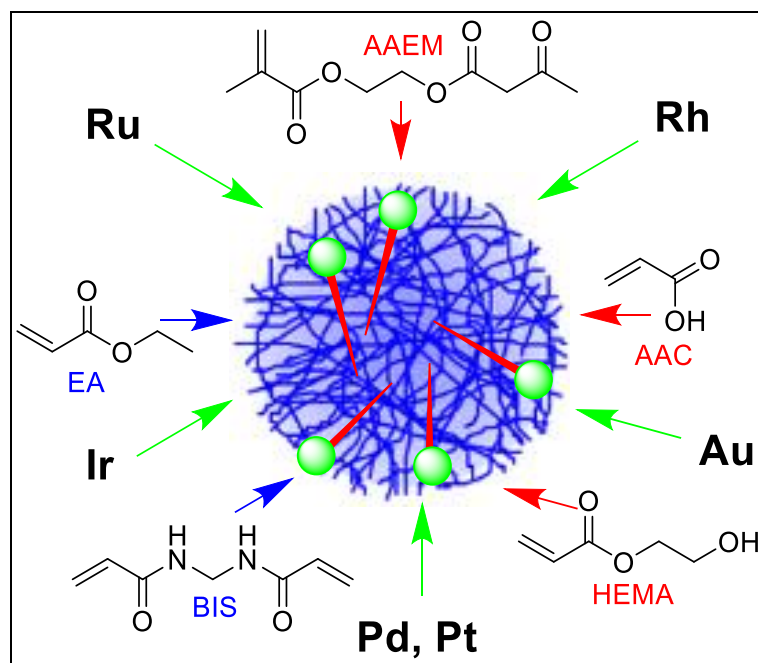


Figure 3.46 Concept of the smart thermo-responsive microgels loaded with catalytic-active metal nanoparticles.

For the incorporation of metal nanoparticles in the microgel, dry microgels were redispersed in isopropanol at 60°C; the concentration of the microgel was 10 mg/mL. An isopropanol solution of the noble metal salt was added to the microgel dispersion under continuous

### 3. Microgel-Based Catalysts

stirring. In a general case, the concentration of the metal in the microgel was 1.0 wt. %. The reduction of the metal ions in this work was performed in two different ways (Figure 3.47). The presence of the  $\beta$ -diketones from the functional co-polymers insure the coordination of the metal and metal nanoparticles. Using the first approach a hot mixture of microgel and metal salt in isopropanol was stirred for 1 hour to insure the complete complexation of the metal ions within the microgel. Finally 5-time excess of the hydrazine (related to metal concentration) was added to perform the reduction. After 2 hours reaction time the mixture was cooled down and purified by centrifugation in order to remove the hydrazine excess.

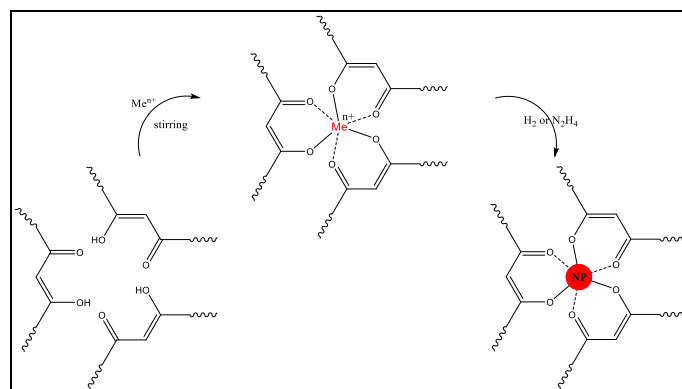


Figure 3.47 In-situ incorporation of the metal nanoparticles in microgel.

The second way to synthesize the hybrid microgel@MeNPs was the in-situ reduction of metal ions by hydrogen at high pressure. The main advantage of using the hydrogen as a reducing agent is the absence of side products and there is no need to clean the product from the rest of non-reacted reducing agent. For the reduction of metal ions using the hydrogen approach, a hot mixture of microgels and metal salt was placed in the autoclave. The temperature of the reactor was held at 60 °C to insure the absence of microgel aggregates. After loading the samples, the reactor was sealed up and the hydrogen was purged inside. The reduction process was performed over night at 150 bar hydrogen pressure. After 16 hours reaction time the heating and the hydrogen supply were switched off, the reaction mixture was cooled down to room temperature and removed from reactor. The final product (Figure 3.48 b) was heated to 60 °C. After this the microgel@MeNPs were redispersed (Figure 3.48 c) and stored in the oven at 60 °C for next analysis and catalytic tests.

### 3. Microgel-Based Catalysts

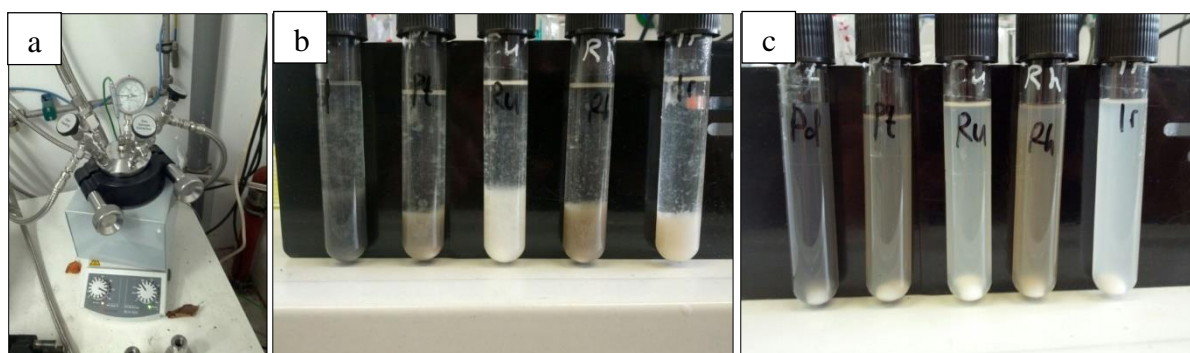
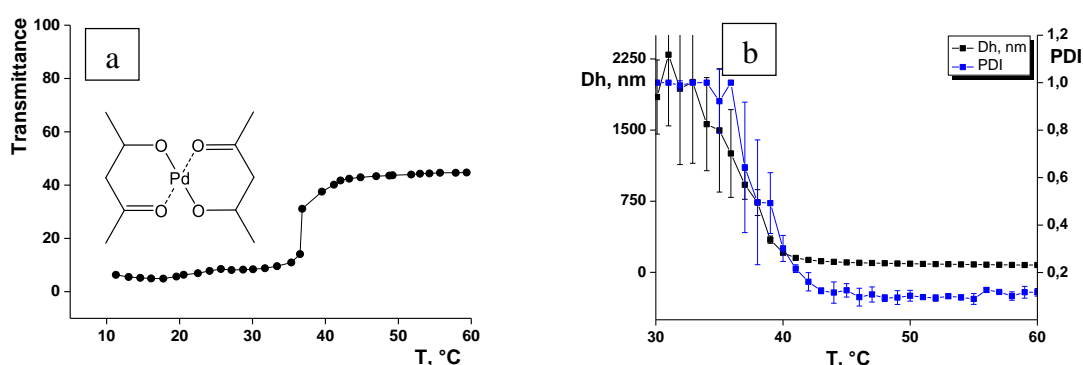


Figure 3.48 Autoclave for in-situ hydrogen reduction of the metal ions in the microgel dispersion (a), microgel@MeNPs after the synthesis cooled to room temperature (b), microgel@MeNPs after heating to 60 °C (c).

After the synthesis for all hybrid microgels, a qualitative metal analysis using IPC-AES was made. To prove the incorporation of the metal nanoparticles into microgel, a small amount of hybrid microgel was purified through the centrifugation. The pure hybrid microgel dispersion was dried in the oven. In order to measure the IPC-AES all metal nanoparticles must be transformed into the ion state. Due to the high stability of the noble metal to the chemicals, all samples were dissolved in an HCl:HNO<sub>3</sub> 3:1 acid mixture. All qualitative tests show the presence of metals.

#### EA-AAEM microgels loaded with palladium nanoparticles

The first test hybrid microgel system was EA-AAEM microgel loaded with 1 wt-% of palladium nanoparticles. As precursors for the nanoparticle synthesis Pd(acac)<sub>2</sub>, Pd(cod)Br<sub>2</sub> and PdCl<sub>2</sub> were used. The EA-AAEM-PdNPs microgel is switchable and has a grey color (Figure 3.49 c). The color of the hybrid microgel prevent 100 % of transmittance, but the CAT can be detected around 38 °C (Figure 3.49 a). The hybrid microgel has a low polydispersity index at high temperatures and starts to aggregate at 39 °C (Figure 3.49 b).



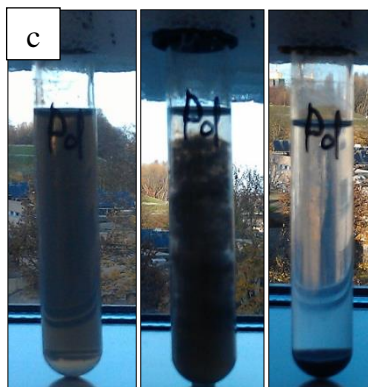


Figure 3.49 CAT point of the EA-AAEM-Pd microgels measured by UV-Vis spectroscopy: 10 mg/mL in isopropanol (a), DLS: 1 mg/mL in isopropanol (b) and the photo of the hybrid microgel at 60 °C, 20 °C, and 20 °C after centrifugation at 2000 rpm (c).

To investigate the morphology of the hybrid microgel loaded with the palladium nanoparticles and the size of the palladium nanoparticles itself, STEM microscopy of the EA-AAEM-PdNPs microgels was performed (Figure 3.50). The palladium nanoparticles are located only in small microgel aggregates. No nanoparticles were detected outside of the microgel. The palladium nanoparticles do not build aggregates and are 20 nm in diameter.

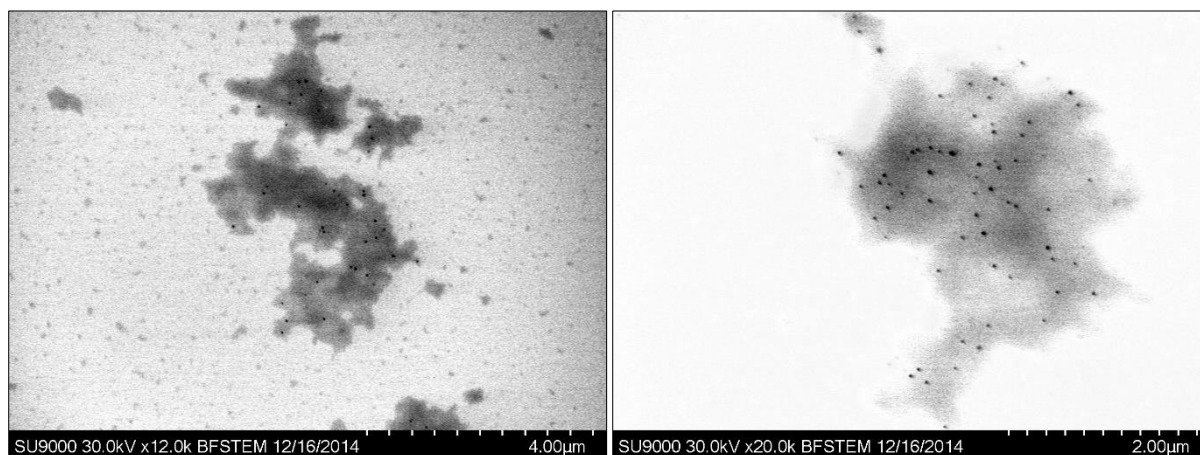


Figure 3.50 STEM images of the EA-AAEM-Pd microgels.

#### **EA-AAEM microgels loaded with rhodium nanoparticles**

Another noble metal hybrid microgel, which is interesting for the catalytic application was EA-AAEM-RhNPs microgel (Figure 3.51). The hybrid microgel was made with a Rh(cod)acac precursor. The slightly brown color of the microgel dispersion strongly absorbs the light at 400-500 nm. The CAT point measured by UV-Vis spectroscopy is around 30 °C. Because of the broad application field of the rhodium nanoparticles in catalysis, besides 1 wt-



### 3. Microgel-Based Catalysts

% of RhNPs loading for this system, hybrid microgels with 2.5 and 5 wt-% of RhNPs were also synthesized. Interestingly the increase of the rhodium nanoparticles loading leads to the decrease of the aggregation temperature; this can be explained with an increase in the surface charge of the hybrid microgels. In this case, the aggregating-temperature decreases from 25 to 16 °C (Figure 3.51 b, c, d).

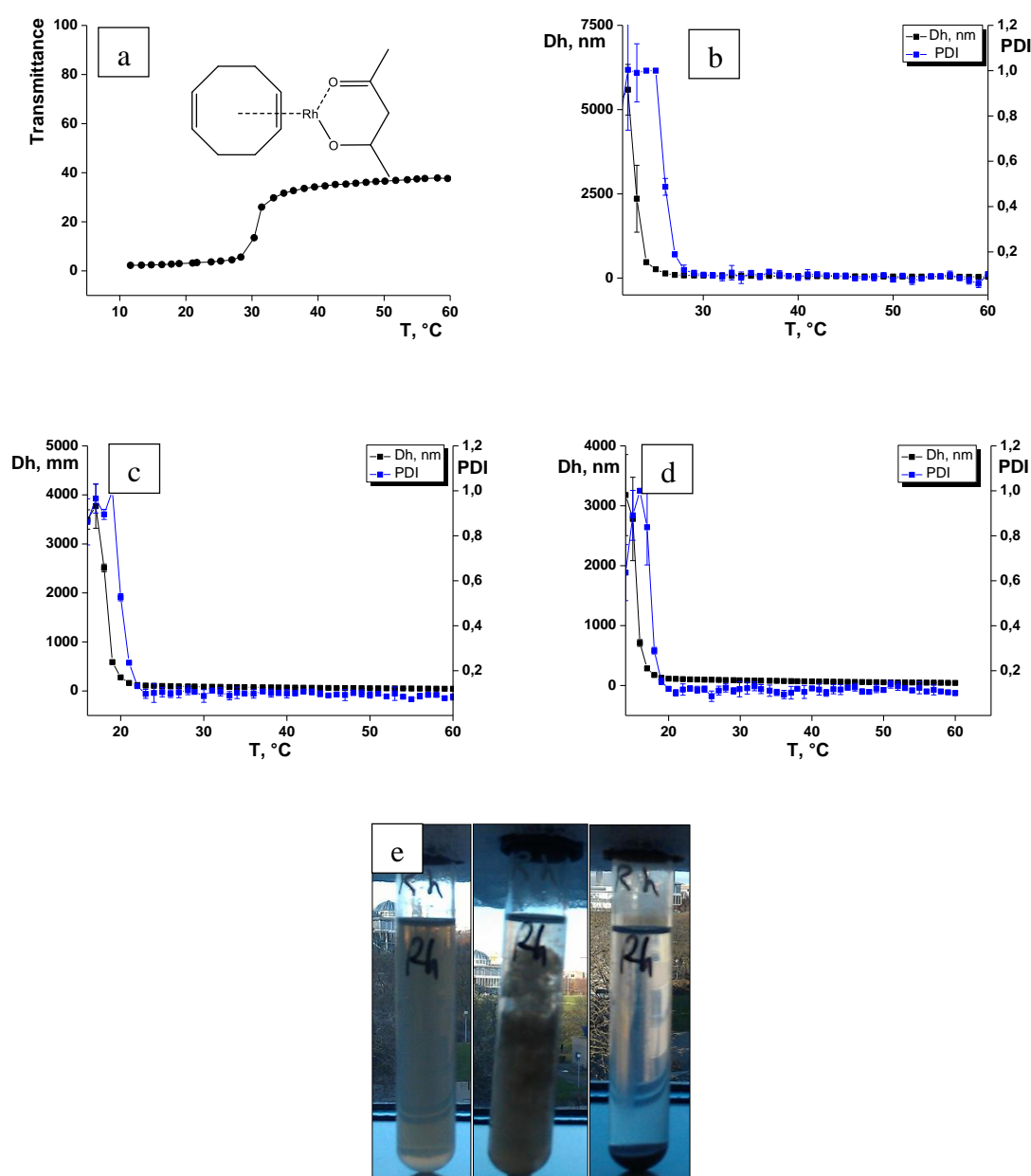


Figure 3.51 CAT point of the EA-AAEM-Rh microgels measured by UV-Vis spectroscopy: 10 mg/mL in isopropanol (a), DLS: 1 mg/mL in isopropanol with different metal loading (b, c, d) and a photo of the hybrid microgel at 60 °C, 20 °C, and 20 °C after centrifugation at 2000 rpm (e).

### 3. Microgel-Based Catalysts

The STEM images prove the building and incorporation of the RhNPs in functional EA-AAEM microgels. The size of the rhodium nanoparticles is 2-3 nm, the particles are good redispersed and located only inside of the microgels (Figure 3.52). Small nanoparticles size and large surface area will increase the catalytic activity of EA-AAEM-RhNPs hybrid microgels.

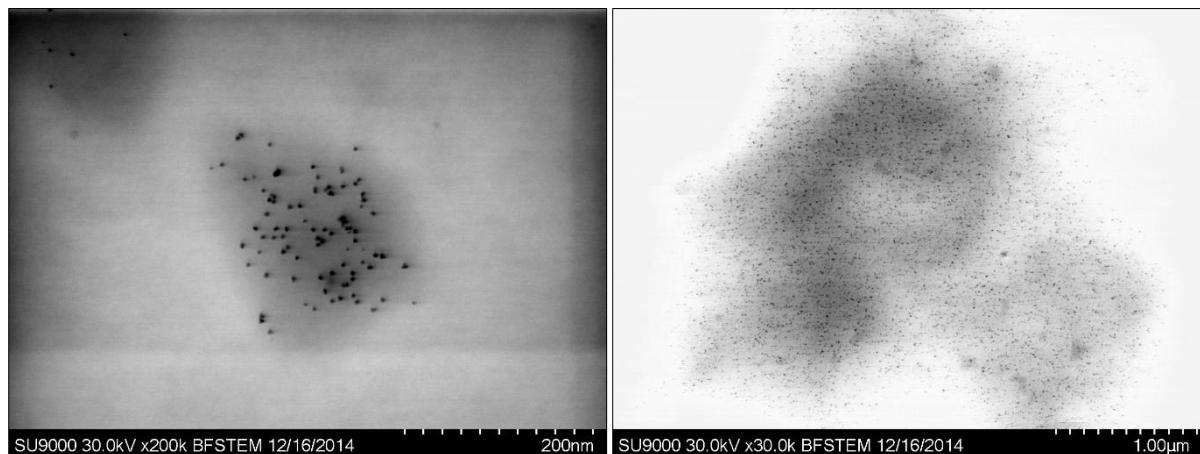


Figure 3.52 STEM image of the EA-AAEM-Rh microgels.

The high loading of the EA-AAEM microgels with 5 wt-% of rhodium nanoparticles allowed to make EDX spectroscopy to insure that the metal nanoparticles consist of rhodium atoms (Figure 5.53). The normal STEM image can be seen in figure 3.53 a, for the purpose of the EDX measurements the most densely loaded microgel aggregate was chosen. In figure 3.53 b rhodium atoms are marked with the red dots. The dots outside of the microgel can be explained with the analysis noise. The rhodium element mapping can be better seen on a black background (Figure 3.53 c). The shape of the densest location of the red dots corresponds to the location of the rhodium nanoparticles. The overview of the elements viewed in table (Figure 3.53 d) can be used only for quantitative evaluation of the element composition of the rhodium-loaded hybrid microgels. According to the EDX analysis, metal nanoparticles consist of rhodium.



### 3. Microgel-Based Catalysts

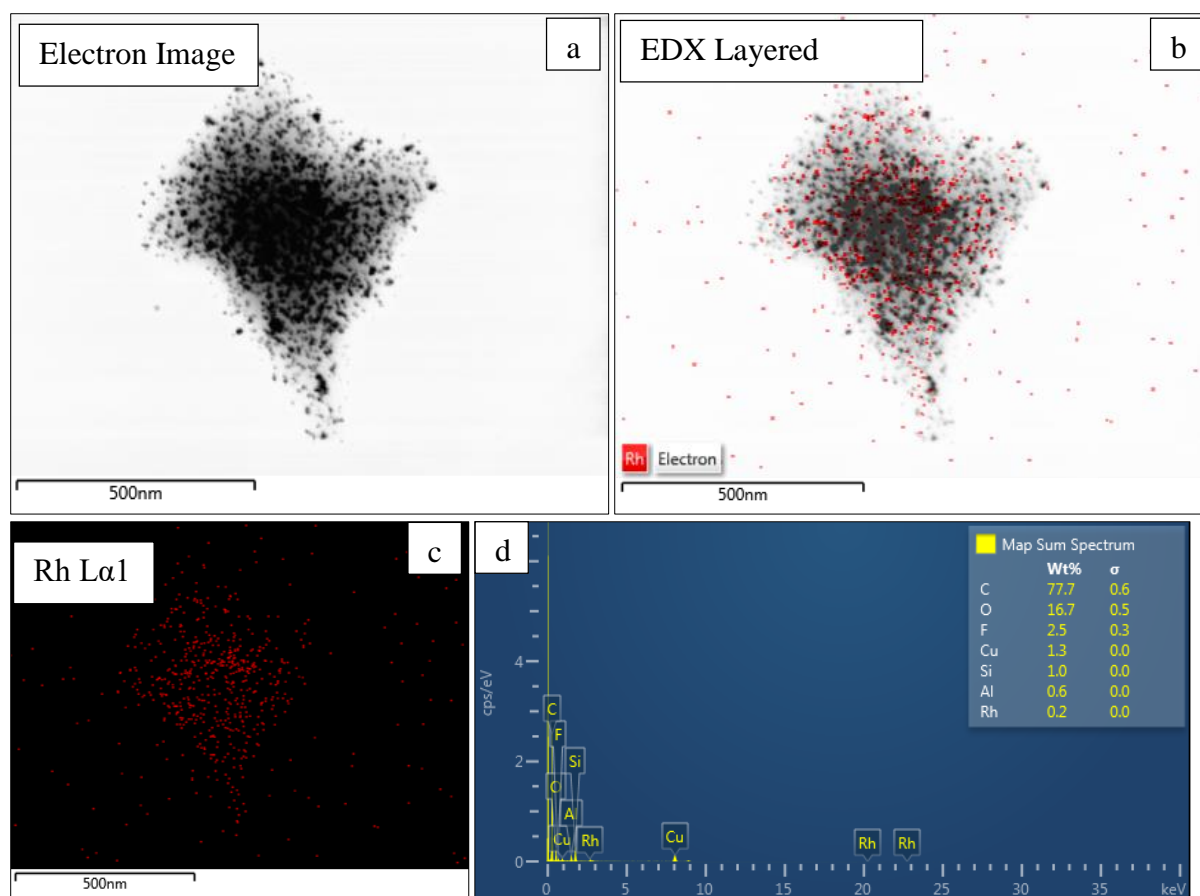


Figure 3.53 EDX spectroscopy of the EA-AAEM-Rh hybrid microgels.

### 3.5 Application of hybrid microgels in catalysis

#### EA-Phosphine-Rh catalyst

The first system as a proof of concept was linear ethyl acrylate polymer co-polymerized with 5 mol-% of phosphine monomer loaded with rhodium salt (Figure 3.54). This system was used for the catalytic hydrogenation of different organic compounds in methanol or isopropanol as a reaction media. The catalysis was performed at different hydrogen pressures and temperatures below and above the CAT points.

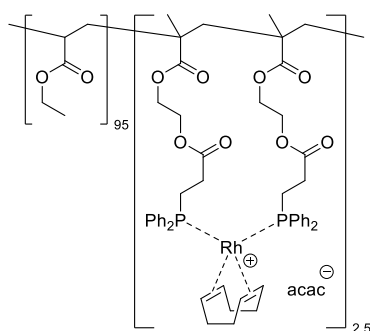
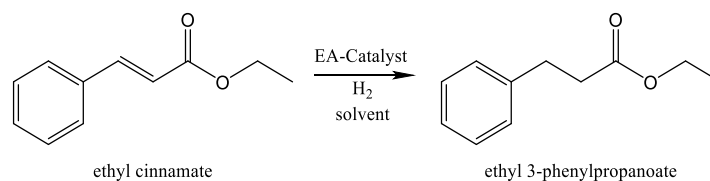


Figure 3.54 EA-Phosphine-Rh thermo-sensitive catalyst.

The EA-Phosphine-Rh was used as a catalyst in the hydrogenation of ethyl cinnamate in methanol (Scheme 3.1). The reaction was performed with 1 mol-% of the catalyst in relation to the educts. The yield of the reaction was determined using gas chromatography. As it can be seen from the result (Table 3.2) the reaction of the hydrogenation happens at room temperature and 20 bar of hydrogen only with a low yield of 1.5%. This can be explained with the aggregated state of the catalyst, which leads to a reduction of the surface area. Interestingly by increasing the hydrogen pressure to 50 bar, the reaction can be completed with a yield of 99%, which indicate the catalytic activity of the catalyst even in aggregated state. By increasing the temperature to 50 °C the catalyst will be found only in single particles form. The bigger surface area makes it possible to use lower hydrogen pressures. In this case, the hydrogen pressure of 20 bar was enough for 99 % hydrogenation of ethyl cinnamate. The catalysis at 50 bar was also successfully performed with a yield of 99%. Similar to hydrogenation of ethyl cinnamate in methanol, this reaction was performed using isopropanol as a solvent. From the previous results, it is known that the alcohol polarity has an influence on the CAT point. The CAT point in isopropanol is more shifted to higher temperatures. Analyzing the results of the hydrogenation in isopropanol, only 0.5 % of the ethyl cinnamate was reduced at room temperature and 20 bar hydrogen pressure. By increasing of the

### 3. Microgel-Based Catalysts

temperature to 50 °C, it was possible to reduce up to 99 % of ethyl cinnamate at hydrogen pressure of 20 bar.

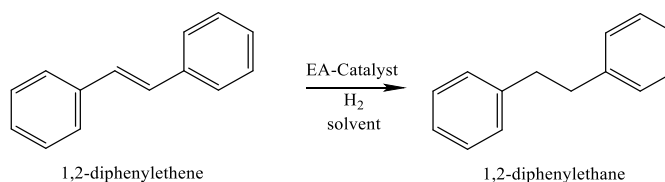


Scheme 3.1 Catalytic hydrogenation of the ethyl cinnamate.

Table 3.2 Reaction conditions and results of the catalytic ethyl cinnamate hydrogenation.

Solvent	T [°C]	p [bar] H <sub>2</sub>	% reactant	% product
MeOH	RT	20	98.5	1.5
MeOH	RT	50	0	99
MeOH	50	20	0	99
MeOH	50	50	0	99
i-PrOH	RT	20	99	0.5
i-PrOH	50	20	0	99

Another catalytic test reaction was hydrogenation of the 1,2-diphenylethene in methanol (Scheme 3.2). The results (Table 3.3) show that at room temperature and 20 bar hydrogen pressure, the reaction yield is only 4 %, increasing the hydrogen pressure to 50 bar leads to 99 % yield. On the other hand, increasing the temperature and at the same time increasing the surface area of the catalyst lead to almost full hydrogenation of 1,2-diphenylethehe at both 20 and 50 bar hydrogen pressure. The same results were achieved using isopropanol as a solvent. At room temperature and 50 bar of the hydrogen pressure it was possible to hydrogenate 98 % of the 1,2-diphenylethehe in isopropanol. At 50 °C almost full hydrogenation was found.



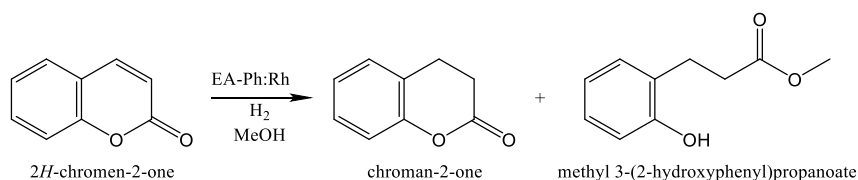
Scheme 3.2 Catalytic hydrogenation of the 1,2-diphenylethene.

### 3. Microgel-Based Catalysts

Table 3.3 Reaction conditions and results of the catalytic 1,2-diphenylethene hydrogenation.

Solvent	T [°C]	p [bar] H <sub>2</sub>	% reactant	% product
MeOH	RT	20	96	4
MeOH	RT	50	0.5	99
MeOH	50	20	2.5	97.5
MeOH	50	50	1	99
i-PrOH	RT	50	2	98
i-PrOH	50	20	1	99

The third catalysis test reaction for the EA-Phosphine-Rh catalyst was the hydrogenation of coumarin (Scheme 3.3). The reaction may happen in the presence of a side product methyl (3-(2-hydroxyphenyl)propanoate). The results of the catalytic hydrogenation of coumarin in methanol are listed in table 3.4. At room temperature and a hydrogen pressure of 20 bar the reaction does not happen, while increasing the hydrogen pressure to 50 bar leads to a yield of the main product of 73.5 % and 7 % of the side product. An increase of the reaction temperature leads to an increase of the product yield, but at the same time to an increase of the side product. At 50 °C and 20 bar the reaction takes place producing 3.5 % of the main product and 44.5 % of the side product. Increasing the hydrogen pressure to 50 bar at 50 °C leads an increase of the products concentration but the ratio main product to side product is almost 50:50.



Scheme 3.3 Hydrogenation of the 2H-chromen-2-one in methanol.

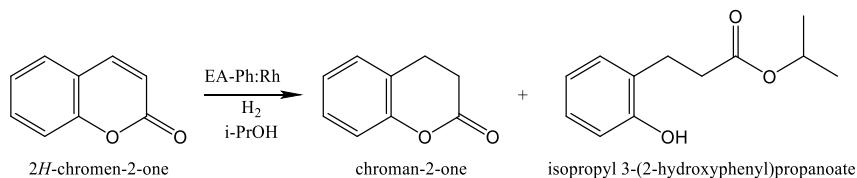
Table 3.4 Reaction conditions and results of the 2H-chromen-2-one hydrogenation in methanol.

T [°C]	p [bar] H <sub>2</sub>	% reactant	% product	% side product
RT	20	99	0	0
RT	50	19.5	73.5	7
50	20	52	3.5	44.5
50	50	7	47	46

The usage of isopropanol as a solvent (Scheme 3.4, Table 3.5) for this reaction at room temperature leads to a complete aggregation of the catalyst and minimization of the surface

### 3. Microgel-Based Catalysts

area. In this case the hydrogenation happens only for 1 %. The increase of the temperature to 50 °C leads to an almost complete hydrogenation with a concentration of the main product of 72 %.



Scheme 3.4 Hydrogenation of the 2H-chromen-2-one in isopropanol.

Table 3.5 Reaction conditions and results of the 2H-chromen-2-one hydrogenation in isopropanol.

T [°C]	p [bar] H <sub>2</sub>	% reactant	% product	% side product
RT	50	99	1	0
50	50	0.5	72	27.5

#### EA-Amine-Ir catalyst

Next a microgel based on ethyl acrylate functionalized with amine and loaded with iridium was used as a thermo-sensitive catalyst (Figure 3.55). The catalyst was used for the hydrogenation of ethyl cinnamate and 1,2-diphenylethene. The catalysis reaction was performed at two different temperatures: room temperature and 40 °C. The hydrogen pressure was set to 50 bar in both cases, toluene was used as a solvent.

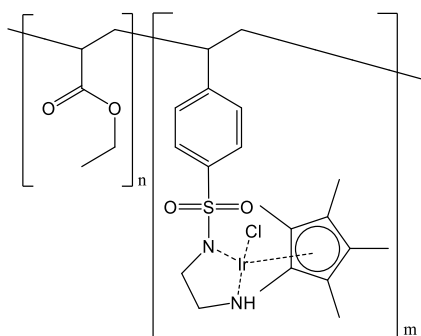


Figure 3.55 EA-Amine-Ir thermo-sensitive catalyst.

The EA-AMIN-Ir microgel catalyst was tested in a number of runs. After the reaction the mixture was cooled down in order to aggregate the catalyst particles. After the centrifugation and removing of the fluids, the solid catalyst was redispersed in a new portion of solvent with educts in order to do the next catalysis cycle. The first test reaction was hydrogenation of the

### 3. Microgel-Based Catalysts

ethyl cinnamate (Scheme 3.1). As it can be seen from the results (Table 3.6), the catalyst at room temperature doesn't show significant activity due to the aggregates, the yield of the first run is 48%. By increasing the temperature to 40 °C the yield of the first run increased to 99 %. The next runs show significant decrease in catalyst activity and can be explained with the leaching of the metal ions from the microgel particles at high temperatures. The leaching can be prevented by using stronger ligands compared to amines as a comonomer in the microgel synthesis.

Table 3.6 Reaction conditions and results of the ethyl cinnamate hydrogenation.

# run	T [°C]	p [bar] H <sub>2</sub>	% reactant	% product
1	RT	50	52	48
2	RT	50	49	51
3	RT	50	59	41
4	RT	50	79	21
1	40	50	1	99
2	40	50	42	58
3	40	50	88	12

The second catalytic test reaction was the hydrogenation of 1,2-diphenylethene (Scheme 3.2, Table 3.7) as in a case with ethyl cinnamate the reaction was run over a few cycles at two different temperatures at a hydrogen pressure of 50 bar. At low temperature the content of the product after the catalytic hydrogenation was in a range of 26-43 %. At 40 °C, the first run shows a yield of 96 %. The next cycles were not so successful due to the leaching of the catalyst ions from the microgel.

Table 3.7 Reaction conditions and results of the 1,2-diphenylethene hydrogenation.

# run	T [°C]	p [bar] H <sub>2</sub>	% reactant	% product
1	RT	50	74	26
2	RT	50	57	43
3	RT	50	69	31
4	RT	50	83	17
1	40	50	4	96
2	40	50	41	59
3	40	50	77	23

### 3. Microgel-Based Catalysts

#### EA-organocatalyst

Microgels, which contain organocatalyst (Figure 3.56), were also tested in catalytic reactions. The main advantage of these microgels is the covalent bonding of the catalyst to the microgel. Covalent bonding insures a strong bonding and compared to the noble ion complexes no leaching occurs in the system.

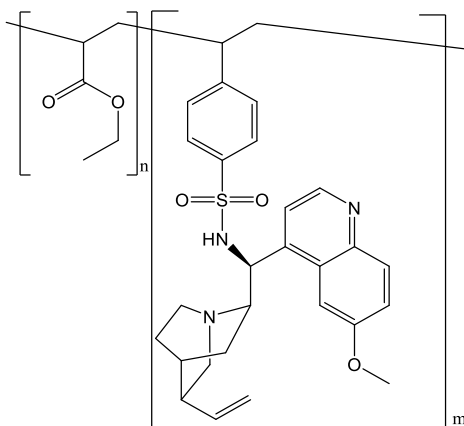
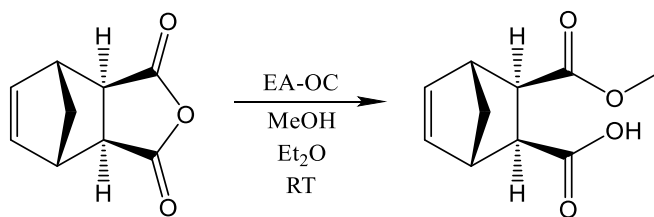


Figure 3.56 EA-organocatalyst thermo-sensitive microgel.

As a test reaction, asymmetric alcoholysis of cis-tetrahydrophthalic anhydride derivate was chosen (Scheme 3.5). The reaction was performed using diethyl ether as a solvent, methanol was used as a nucleophile. The concentration of the catalyst was kept at 5 mol-% in relation to the educt. The concentration of the nucleophile was kept at five equivalents to the educt.



Scheme 3.5 Alcoholysis of cis-tetrahydrophthalic anhydride derivate.

The alcoholysis of the cis-tetrahydrophthalic anhydride derivate was performed for 8 runs. After each run the reaction mixture was cooled down in order to remove the catalyst, to use it again in the next run. From the result (Table 3.8) can be seen that the reaction has relatively high yields over 8 runs and has a high enantiomeric ratio.

### 3. Microgel-Based Catalysts

Table 3.8 Reaction conditions and results of the cis-tetrahydrophthalic anhydride derivate alcoholysis.

# run	T [°C]	% reactant	% product	e:r
1	RT	33	67	75:25
2	RT	26	74	81:19
3	RT	23	77	81:19
4	RT	33	67	85:15
5	RT	28	72	83:17
6	RT	30	70	79:21
7	RT	29	71	80:20
8	RT	29	71	81:19

#### EA-AAEM- RhNPs catalyst

In addition to the noble metal complexes, noble metal nanoparticles find broad application in catalysis. Compared to the metal ions, metal nanoparticles have a bigger size and can have a stronger hold in the microgel structure. The first hybrid microgel studied on its catalytic activity in this work was a microgel based on 90 mol-% ethyl acrylate and 10 mol-% 2-(methacryloyloxy)ethyl acetoacetate, loaded with 0.01 to 1 wt-% rhodium nanoparticles (Figure 3.57).

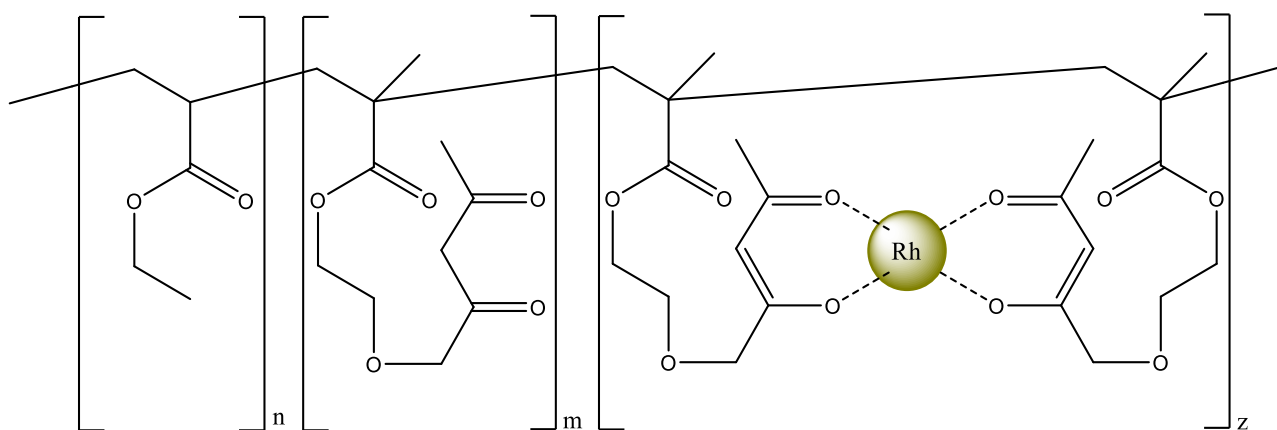
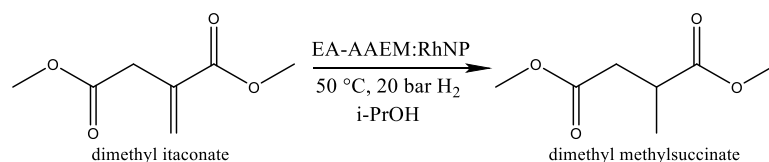


Figure 3.57 EA-AAEM-RhNPs catalyst.

The catalyst was used in catalytic hydrogenation of dimethyl itaconate (Scheme 3.6, Table 3.9). The catalyst was used 10 times in a row. After each run, the mixture was cooled down and the catalyst was centrifuged and reused in the next run. The catalyst exhibits a high activity even after 6 runs and has a high resistance to leaching. Even at low catalyst loading it was possible to achieve high yields.



### 3. Microgel-Based Catalysts



Scheme 3.6 Catalytic hydrogenation of the dimethyl itaconate.

Table 3.9 Reaction conditions and results of the dimethyl itaconate hydrogenation.

# run	T [°C]	p [bar] H <sub>2</sub>	Loading 1 wt-%		Loading 0.1 wt-%		Loading 0.01 wt-%	
			% reactant	% product	% reactant	% product	% reactant	% product
1	50	20	1	99	1	99	10	90
2	50	20	1	99	1	99	17	83
3	50	20	1	99	23	77	19	81
4	50	20	1	99	43	57	23	77
5	50	20	1	99	51	49	25	75
6	50	20	1	99	58	42	51	49
7	50	20	14	86	68	32	78	22
8	50	20	33	67	89	11	85	15
9	50	20	63	37	100	0	100	0
10	50	20	67	33	100	0	100	0

#### EA-AAEM-PdNPs catalyst

In the next hybrid microgel system, palladium nanoparticles were used, as noble metal (Figure 3.58). The influence of the metal precursor of the nanoparticles on the catalytic activity was also studied.

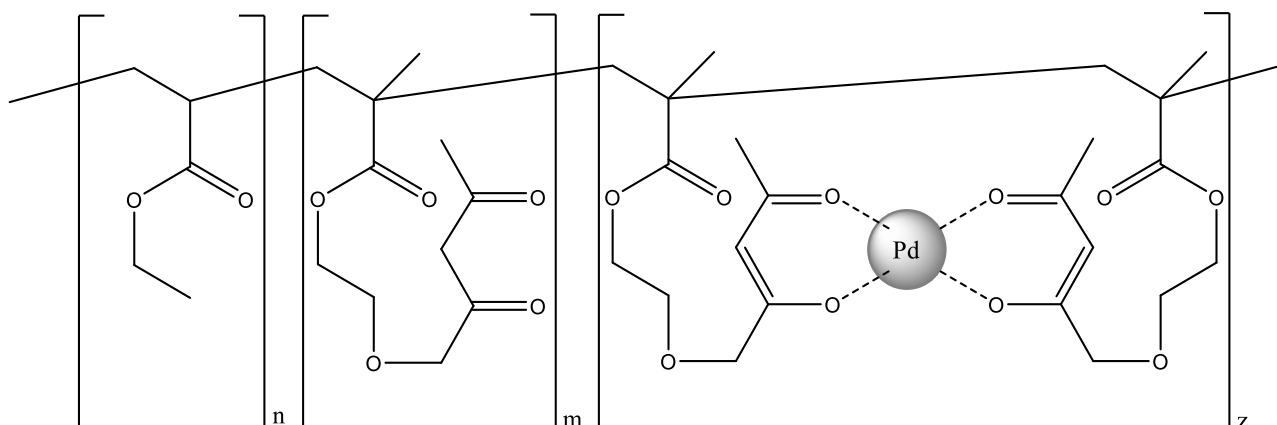


Figure 3.58 EA-AAEM-PdNPs catalyst.

### 3. Microgel-Based Catalysts

Hydrogenation of the ethyl cinnamate was used as a catalytic test reaction (Scheme 3.1, Table 3.10). The catalyst was used for ten runs. Compared to the RhNPs catalyst, the PdNPs based catalyst is less active and prone a loss of activity because of the leaching of metal nanoparticles. The precursor for the nanoparticles synthesis does not show any significant changes in catalytic activity. Catalytic activity measurements were performed in cooperation with Prof. Rueping group members R. Borrmann and M. Fernandes.

Table 3.10 Reaction conditions and results of the ethyl cinnamate hydrogenation.

# run	T [°C]	p [bar] H <sub>2</sub>	Precursor PdCl <sub>2</sub>		Precursor Pd(cod)Br <sub>2</sub>	
			% reactant	% product	% reactant	% product
1	50	20	1	99	23	77
2	50	20	12	88	28	72
3	50	20	28	72	28	72
4	50	20	57	43	31	69
5	50	20	58	42	34	66
6	50	20	62	38	75	25
7	50	20	63	37	98	2
8	50	20	75	25	100	0
9	50	20	88	12	100	0
10	50	20	93	7	100	0

## 4 Microgel-based conductive films

### 4.1 Experimental part

#### Materials

The following chemicals were purified by distillation at reduced pressure in order to remove the inhibitors and stored by 4 °C:

- *N*-Vinylcaprolactam, 98% (Sigma-Aldrich)
- Acrylic acid, 99% (Sigma-Aldrich)

Purified by passing through the syringe filled with Al<sub>2</sub>O<sub>3</sub> powder were:

- 2-(Methacryloyloxy)ethyl acetoacetate, 95% (Sigma-Aldrich)
- 1-Vinyl-2-pyrrolidone, 99% (Sigma-Aldrich)
- [2-(Methacryloyloxy)ethyl]trimethylammonium chloride (MEAK)

All other reagents were used as received:

- Aluminum oxide, purum p.a. (Fluka)
- Hydrazine monohydrate, 98% (Sigma-Aldrich)
- 2,2'-Azobis[*N*-(2-carboxyethyl)-2-methylpropionamidine]hydrate, 99% (Wako)
- Acetaldehyde, 99.5% (Sigma-Aldrich)
- Hexadecyltrimethylammonium bromide, 98% (Sigma-Aldrich)
- Copper (II) sulfate pentahydrate, 99% (Sigma-Aldrich)
- *N,N'*-Methylenebisacrylamide, 99% (Sigma-Aldrich)
- Silber nitrate, 99% (Sigma-Aldrich)

Distilled water was used for all polymerization and purification processes.

## 4.2 Synthesis and characterization of microgels

From the literature and previous works in Pich's group, the possibility was shown to synthesize microgel particles with variable dimensions and crosslinking density, as well as the incorporation of desired active groups. Based on these results two different poly(*N*-vinylcaprolactam)-based microgels with different comonomers were synthesized. The monomers were chosen due to their ability to immobilize Me-nanoparticles during synthesis. The UV induced reduction of Me-ions, the reduction with hydrazine and the influence of the microgel on the reduction process were studied in this work.

### Synthesis of VCL-VP-AAEM-MEAK Microgels

The first microgel is based on *N*-vinylcaprolactam crosslinked with *N,N'*-methylenebisacrylamide (BIS). 2-(Methacryloyloxy)ethyl acetoacetate (AAEM), 1-vinyl-2-pyrrolidone (VP) and [2-(methacryloyloxy)ethyl]trimethylammonium chloride (MEAK), were used as functional comonomers. MEAK on one hand is used to stabilize the microgel dispersion, and on the another hand to bind the metal nanoparticles. Figure 4.1 shows schematically this microgel.

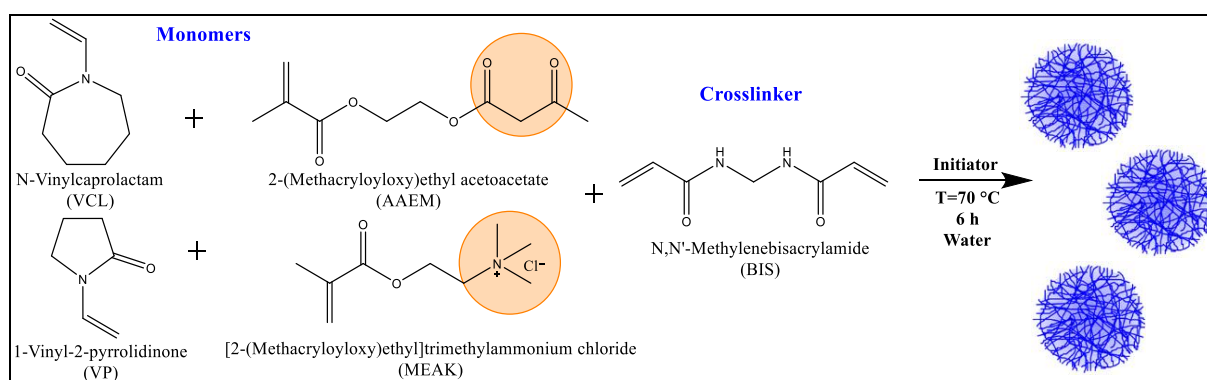


Figure 4.1 Synthesis schema of VCL-VP-AAEM-MEAK Microgels

Microgels particles were synthesized by precipitation polymerization using recipes given in table 4.1. The reaction was carried out in double wall thermostated glass reactor, equipped with stirrer.

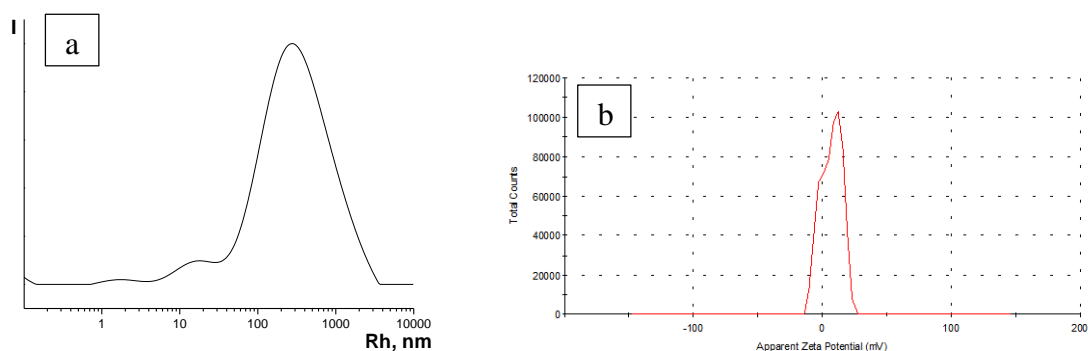
#### 4. Microgel Based Conductive Films

Table 4.1 VCL-VP-AAEM-MEAK microgel composition

Educt	n [mmol]	m [g]
VCL	12.75	1.7746
VP	0.75	0.083
AAEM	0.75	0.1606
MEAK	0.75	0.1946
BIS	0.389	0.0600
AMPA	0.184	0.0500
Water		100

The required amount of water, monomers and crosslinker were inserted into the reactor which was purged for 20 min with nitrogen. The mixture was homogenized with stirrer at 220 rpm and heated up to 70 °C. The reaction was started by adding the initiator in water solution. The synthesis was carried out for 6 hours at a stirring velocity of 220 rpm. After the synthesis, the microgel was slowly cooled down to room temperature. The final microgel was placed in dialysis tubes to get rid of unreacted monomers and initiator. The system was dialyzed for 5 days against water in 12000 MWCO regenerated cellulose tube (Carl ROTH). The water was changed every day.

This microgel was analyzed and characterized by dynamic light scattering (DLS), zeta-potential measurements (ZP) and transmissions electron microscopy (TEM) (Figure 4.2).



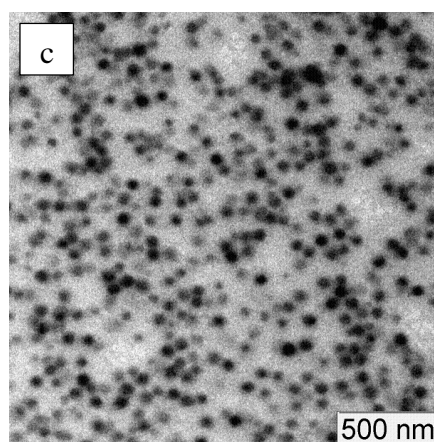


Figure 4.2 Analysis of VCL-VP-AAEM-MEAK Microgel. a – dynamic light scattering, b –  $\zeta$ -potential measurement and c – TEM image.

The DLS measurement of the water dispersion of the microgel in swollen state gives an average hydrodynamic diameter of 340 nm. At the same time the diameter of the dried microgels measured by TEM gives an average size of 80 nm. The size difference can be explained through shrinking and drying of the microgel. These properties of the microgel can be useful for further conductivity and film building properties of hybrid microgels.

Zeta potential measurements at pH 7 showed that the microgel is positively charged (+7.17 mV). A positive microgel charge proves the incorporation of the MEAK to the microgel. The positive charge also prevents the aggregation of the microgel particles. The stability of the emulsions can be also seen from the TEM images (Figure 4.2 c). The microgel particles (black dots) are homogeneously distributed on the TEM-grid and are isolated from each other.

Therefore, the synthesis of the VCL-VP-AAEM-MEAK can be successfully performed. Because of the presence of functional groups and the ability to change size this system is suitable for loading with MeNPs and for the production of the conductive films.

##### **Synthesis of VCL-AAEM-AAC microgels**

The second microgel type was based, besides *N*-vinylcaprolactam and crosslinker *N,N'*-methylenebisacrylamide (BIS), on functional comonomers 2-(methacryloyloxy)ethyl acetoacetate (AAEM) and acrylic acid (AAC). These comonomers make the complexation of metal ions and metal nanoparticles possible. This microgel was prepared for the reduction of the metals with hydrazine. That's why the copolymerization of the photo reducing agent as in previous system was not needed.

#### 4. Microgel Based Conductive Films

The synthesis of the microgel (Figure 4.3) was performed in glass reactor as in the previous case. The composition of the microgel is shown in table 4.2.

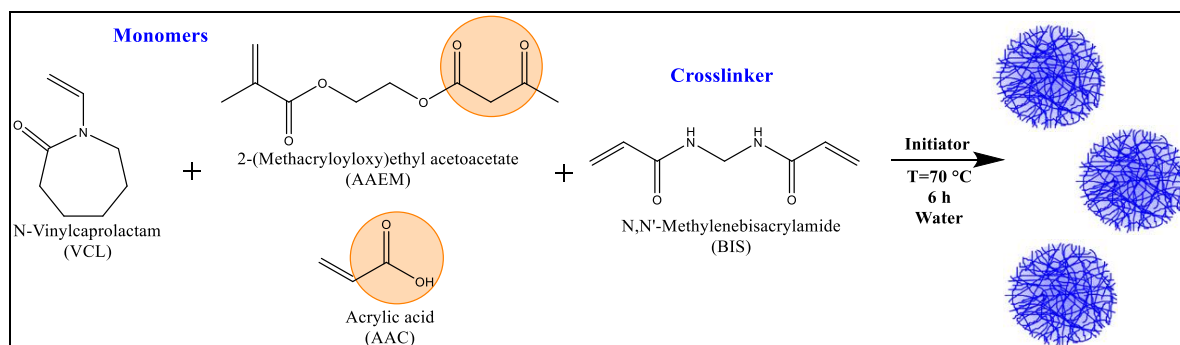


Figure 4.3 Synthesis schema of VCL-AAEM-AAC Microgels

Table 4.2 VCL-AAEM-AAC Microgel composition

Educt	n [mmol]	m [g]
VCL	38.43	5.3490
AAEM	4.50	0.9630
BIS	1.17	0.1800
ACMA	0.53	0.1800
ACC	9.74	0.7020
SDS	0.97	0.1800
Water		450

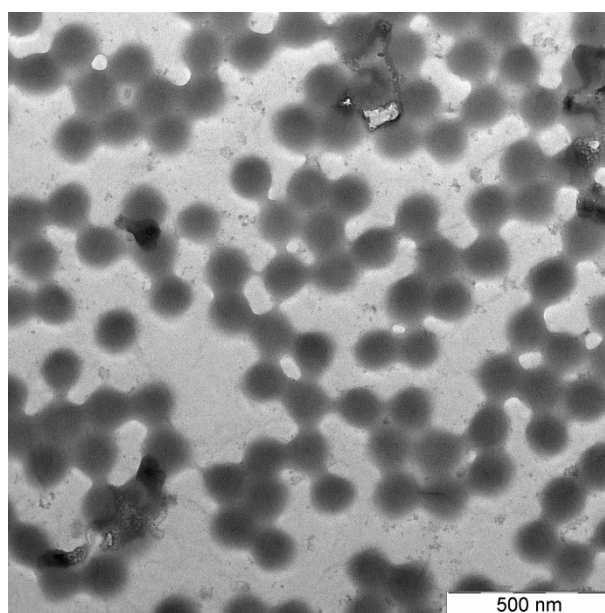


Figure 4.4. TEM image of VCL-AAEM-AAC Microgel

#### 4. Microgel Based Conductive Films

The analysis and characterization of VCL-AAEM-AAC microgels were performed using dynamic light scattering (DLS), transmissions electron microscopy (TEM) and zeta-potential measurements (ZP).

The presence of VCL in the microgel make it temperature sensitive on one hand and on another hand the high amount of acrylic acid makes the microgel pH sensitive. The hydrodynamic diameter of the microgel dispersion in swollen state measured by DLS is approx. 450 nm. The size change from 450 nm to 150 nm after collapsing and drying of the microgel can be observed in TEM (Figure 4.4). Analog to the VCL-VP-AAEM-MEAK system this system has also swelling-shrinking properties. The slightly higher difference between swollen and dried microgel in the first system (3,4) can be explained by the different hydrophobicity of the used monomers. 1-Vinyl-2-pyrrolidone is more hydrophilic in comparison to *N*-vinylcaprolactam. This leads to a higher swelling degree of the VCL-VP-AAEM-MEAK microgels.

VCL based microgels are thermo sensitive, which means that they collapse and aggregate above a certain (Volume-Phase-Transition-Temperature, VPTT) temperature. It is important to study the swelling-collapsing (aggregation) properties and their temperature range for further loading with metal nanoparticles. For this, at different temperatures between 5 und 60 °C DLS measurements were made. The temperature dependent changes of the hydrodynamic diameter at pH 5 are shown in the Figure 4.5.

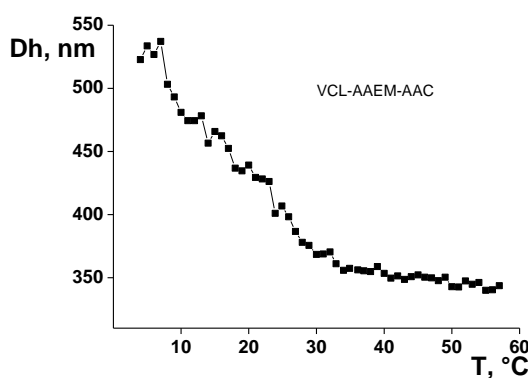


Figure 4.5 Hydrodynamic diameter of the VCL-AAEM-AAC Microgel depending on temperature

The results of these measurements indicate that the microgel starts to swell at the temperatures below 32 °C. Based on these results loading of the microgels should be



#### 4. Microgel Based Conductive Films

performed at a temperature lower than 32°C to ensure the optimal distribution of the metal nanoparticles inside of the microgel shell.

The usage of acrylic acid as a copolymer leads also to the pH sensitivity of the obtained microgels. Zeta potential measurements show that at pH 7 the microgel is strongly negatively charged (-41 mv). This ensures electrostatic stabilization of the microgel dispersions. To prove the pH sensitivity, zeta potential as well as DLS in relation to the pH were performed (Figure 4.6).

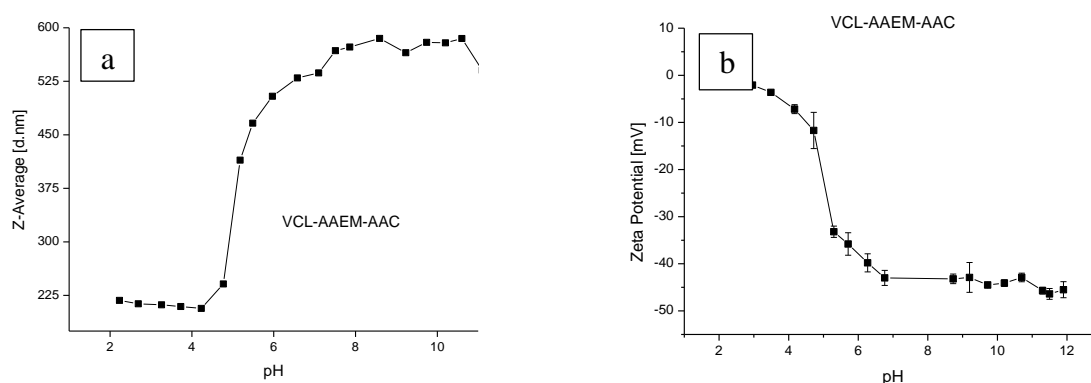


Figure 4.6 Dependence of hydrodynamic diameter (a) and Zeta potential of the VCL-AAEM-AAC Microgel on the pH (b)

From Figure 4.6 a, it can be seen that with the rise of pH value, the amount of non-protonated carboxylic group of the microgel increases. As a result, carboxyl groups become more negatively charged and begin to repel each other making the microgel particles bigger in diameter. This data correlated well with the zeta potential measurement of the colloid and looks like an upside down picture (Figure 4.6 b). The zeta potential is slightly going to the negative values in the range of pH 2-4, rapid increase from 4 to 6 and stays unchangeable from pH 6. Zeta potential size measurements dependent on pH can prove the incorporation of the acrylic acid in the microgel.

### 4.3 Post modification of microgels

#### Selection of suitable metal nanoparticles

The conductivity of the metal depends on the presence and velocity of the movable charge carrier. In table 4.3 a few of the most conductive metals are listed. It is known that silver is the most conductive metal, followed by copper, gold and aluminum. To get the highest conductivity for hybrid films, silver and copper in form of metal nanoparticles were chosen. The usage of copper is of big interest because of the good conductivity/price combination, but the possibility of applications compared to silver is limited because of the high oxidation instability of copper nanoparticles.

Table 4.3 Comparison of metal conductivities and prices. (London metal exchange 2016, <https://lme.com>)

Metal	$\sigma$ in S/m	Price in USD/ounce
Silver	$61.39 \cdot 10^6$	19.70
Copper	$\geq 58.0 \cdot 10^6$	0.14
Gold	$44.0 \cdot 10^6$	1323.20
Aluminum	$36.59 \cdot 10^6$	0.0453

#### Synthesis of copper nanoparticles

Copper nanoparticles were synthesized using two approaches. Using these methods efficiency and production costs were compared. Also two different syntheses allowed to obtain different dimensions of the nanoparticles. Besides the reduction of the metals with UV-Light in the presence of photo initiator a reduction with hydrazine was performed. By common synthesis using the UV method presented in table 4.4, copper sulfate pentahydrate was dissolved in distilled water. For the stabilization of the copper nanoparticles surfactant polyvinylpyrrolidone (PVP) with molecular weight 40000 was used. Finally, an ethanol solution of photo initiator benzophenone BP was added to the reaction mixture. To start the synthesis, the mixture was irradiated in the reactor with UV-light at  $\lambda_{\text{max}}=250\text{-}350$  nm (Figure 4.7). To avoid the oxidation of the copper nanoparticles, the reaction was performed under continuous purging of nitrogen through the solution.

#### 4. Microgel Based Conductive Films

Table 4.4 Reaction mixture composition for CuNPs synthesis.

	n [mmol]	V [mL]	m [mg]
H <sub>2</sub> O		300	-
PVP	13.49*	-	1500
CuSO <sub>4</sub> · 5H <sub>2</sub> O	0.3	-	74.9
Cu <sup>2+</sup>	0.3	-	19.2
BP	0.03	-	5.4

\* related to monomer molecular weight



Figure 4.7 UV reactor. Heraeus Noble UV-RS-4 700 W

To find out the reaction time the kinetic of the reduction process was investigated. For this after the certain amount of time 1 mL of the reaction mixture was removed with the syringe from the reactor. The sample was measured with UV-Vis spectroscopy. As it shown in figure 4.8, the presence of copper nanoparticles is indicated by the plasmon band at 575 nm. Following the changing of the peak intensity with time at this wave-length, the kinetic of the reaction can be observed, shown in figure 4.8 b. From the graphic it can be seen that the reduction time is 20 min.

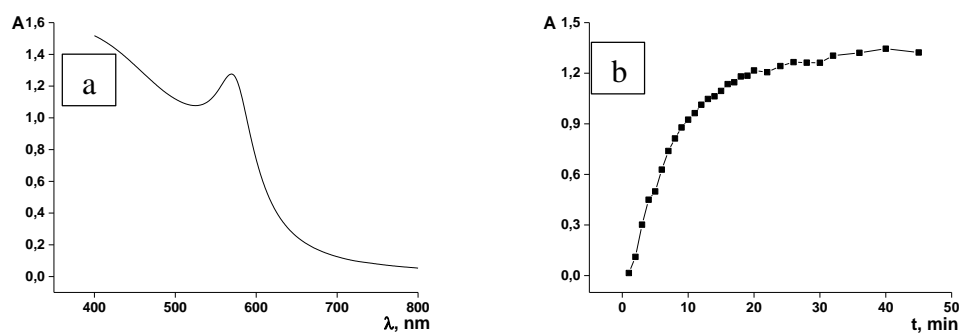


Figure 4.8 Absorption spectra of the CuNPs (a) and the kinetic of the CuNPs synthesis (b)

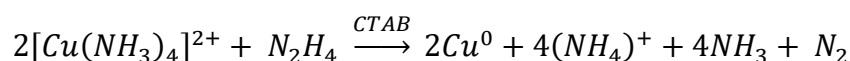
#### 4. Microgel Based Conductive Films

Another way to synthesize the copper nanoparticles in this work was the use of hydrazine as a reduction agent. The nanoparticles in this method were obtained by the reduction of the copper ammonium complex with hydrazine. Hexadecyltrimethyl-ammonium bromide CTAB was used as a stabilizing agent. Due to the amphiphilic structure of the CTAB, CuNPs can be stabilized and also usage of the stabilizer prevents the aggregation and sedimentation of the particles in the system. By common synthesis using the hydrazine method (Table 4.5) copper sulfate and CTAB were dissolved in water. Ammonia solution was added drop wise to obtain a clear violet solution. Finally, by continuous stirring the hydrazine solution was added to the reaction. After adding the reduction agent, the color of the system changed from violet to clear and after 20 min the solution became red color, because of the copper nanoparticles.

Table 4.5 Reaction mixture composition for CuNPs synthesis.

	n [mol]	V [mL]	m [g]
H <sub>2</sub> O		500	
CTAB	5.00E-3	-	1.8223
CuSO <sub>4</sub> · 5H <sub>2</sub> O	5.00E-4	-	0.1248
Cu <sup>2+</sup>	5.00E-4	-	0.0318
N <sub>2</sub> H <sub>4</sub> · H <sub>2</sub> O	0.04	2.06	-

Scheme 4.1 shows the reduction of the copper ammonium complex ions to the copper nanoparticles.



Scheme 4.1 Chemical reduction of the Cu<sup>2+</sup> to Cu<sup>0</sup> with hydrazine.

Similar to the case of photo-chemical reduction, the kinetic of the chemical reduction was studied using UV-Vis spectroscopy. Because of the different sizes of the nanoparticles obtained in the different way, the plasmon band of the copper nanoparticles obtained by hydrazine reduction is shifted to 602 nm, (Figure 4.9 a). The kinetic curve, figure 4.9 b, indicates that the reaction has an induction period of 20 min. The induction period shows the presence of dissolved oxygen in the reaction mixture. After 60 min the reaction is completely finished.

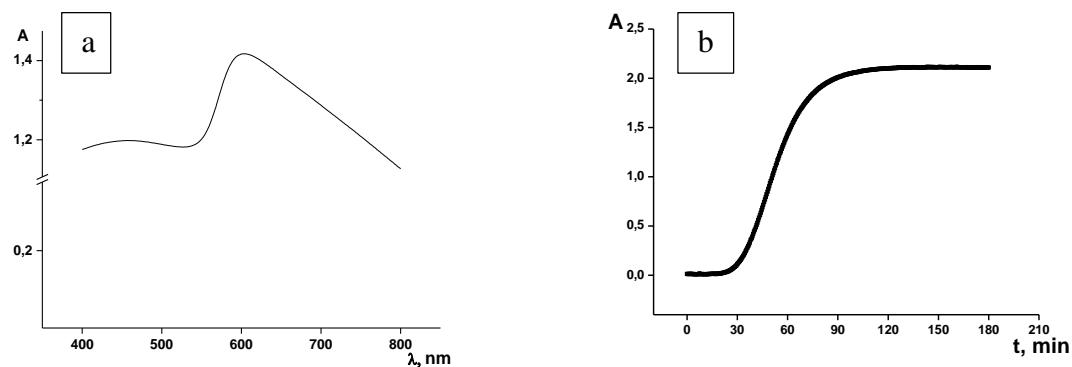


Figure 4.9 Absorption spectra of the CuNPs (a) and the Kinetic of the CuNPs synthesis (b)

Copper nanoparticles obtained in both ways are relatively small, reactive and can be completely oxidized by the oxygen present in the air within one hour, (Figure 4.10). Through the oxidation process, the color of the mixture changed from red to transparent. That's why the application of the pure copper nanoparticles for the loading of the microgels is not possible. To prevent the oxidation of the particles, the upper layer of the copper should be covered with an oxidation stable layer. At the same time, the protective layer should be conductive and relatively cheap.

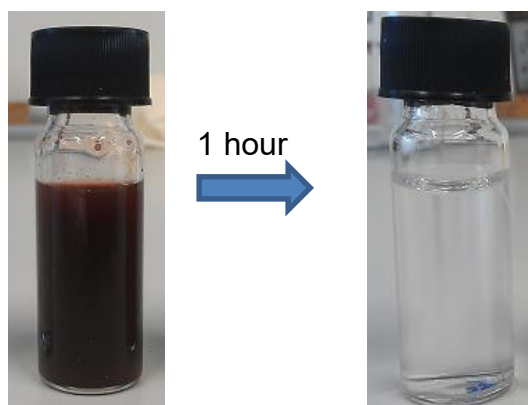


Figure 4.10 Photo of the CuNPs directly after synthesis (left) and after 1 hour exposed to air.

#### Synthesis of copper@silver core-shell nanoparticles

For the conductive layer only a metal that is more stable against oxidation than copper can be used. In this work we have chosen silver because of the good combination of price, oxidation stability and conductivity. Figure 4.11 shows schematically the process of the copper nanoparticles synthesis, followed by forming an oxidation stable silver layer, performed by adding the silver nitrate solution.

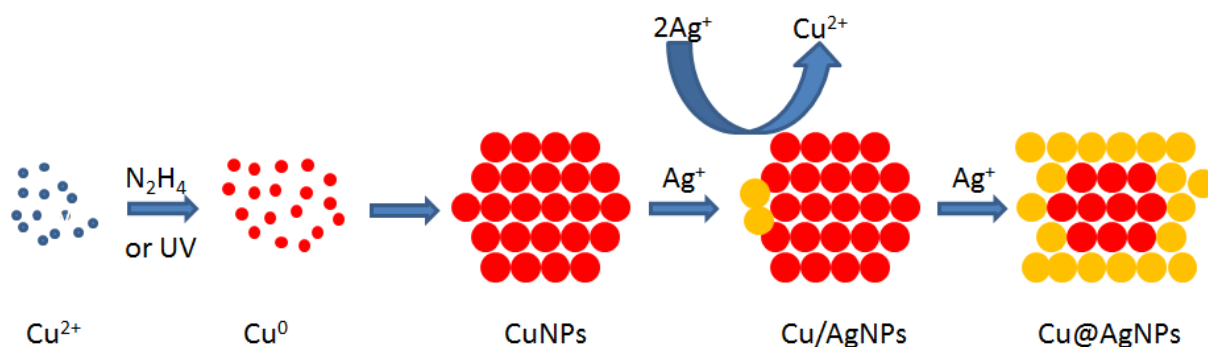
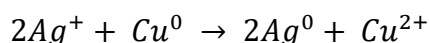


Figure 4.11 Synthesis of copper nanoparticles with additional covering with silver shell <sup>[153]</sup>

According to the Figure 4.11 the synthesis of Cu@Ag was performed in the following four steps:

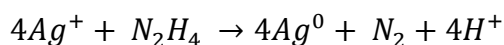
1. Reduction of the copper ions with hydrazine or UV light
2. Growth of the copper nanoparticles
3. Settling of the  $\text{Ag}^0$  on the copper surface through the reduction of silver ions with  $\text{Cu}^0$
4. Growth of the silver shell

The building of the silver shell is possible because of the different electronegativity between copper and silver. Copper is more active than silver which is why the covering procedure is performed electrochemically. Scheme 4.2



Scheme 4.2 Electrochemical reduction of silver ions on CuNPs surface.

Depending on the synthesis route of the copper nanoparticles the process of achieving the coating process is different. In the case of photochemical reduction of copper, the system doesn't have extra reducing agent and the silver nitrate solution can be directly added to the copper nanoparticles dispersion to build a silver shell. In the case of hydrazine reduction, we have an excess of reducing agent in the nanoparticle dispersion which leads to the direct reduction of silver nitrate not on the copper surface, but directly in the solution (Scheme 4.3). This is happening because of the higher reduction activity of the hydrazine compared to the metallic copper.



Scheme 4.3 Reduction of silver ions in solution by excess of hydrazine.

#### 4. Microgel Based Conductive Films

Therefore, when applying the hydrazine method, it is necessary to remove the excess of hydrazine before adding of the silver salt. The challenge here is that the reagent, which is used for the neutralization of hydrazine does not react by any means with copper nanoparticles. For example, all oxidation agents will destroy the hydrazine, but at the same time they will oxidize the copper nanoparticles, which will lead on one hand to the loss of conductivity, and on the other hand to building of an oxide layer, thus the silver will not be able to make a shell on it. In this work we decided to use the acetaldehyde to neutralize the excess of hydrazine (Scheme 4.4).



Scheme 4.4 Neutralizing of hydrazine by excess of acetaldehyde.

The silver shell on the copper nanoparticles can be built only when the remaining hydrazine is neutralized. The composition of the Cu@Ag nanoparticles and the thickness of the silver shell can be easily tuned through the Cu-Ag ratio. The real ratio of the copper and silver can be found by using the IPC-AES. In figure 4.12 it is shown theoretical and practical, investigated with the IPC-AES, composition of the particles that were made using the hydrazine method. The good correspondence between the theoretical and measured values in the system can be observed. These results show principal feasibility of the covering process and possibility to achieve the desired thickness of the shell. This creates a good possibility for development of new cost efficient alternatives to nanoparticles made from pure silver.

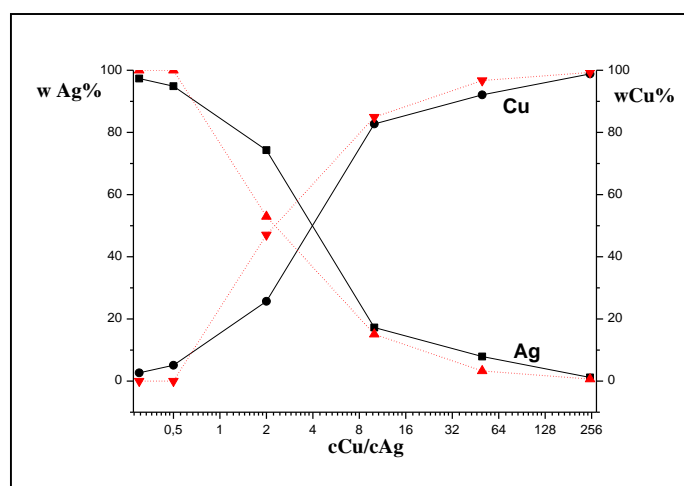


Figure 4.12 Composition of the Cu@AgNPs in relation to Cu/Ag ratio used. Black: IPC-AES measured values, red: theoretical values.

#### 4. Microgel Based Conductive Films

After the preparation of the copper nanoparticles dispersion, calculated amount of the silver nitrate was added to the dispersion by continuous purging of nitrogen. After adding of silver nitrate the color of the dispersion was changed from red to yellow. This proves that copper nanoparticles are completely covered with silver. To find the amount of silver needed to build a stable shell around the copper nanoparticles, UV-Vis measurements for different Cu/Ag ratios were performed (Figure 4.13).

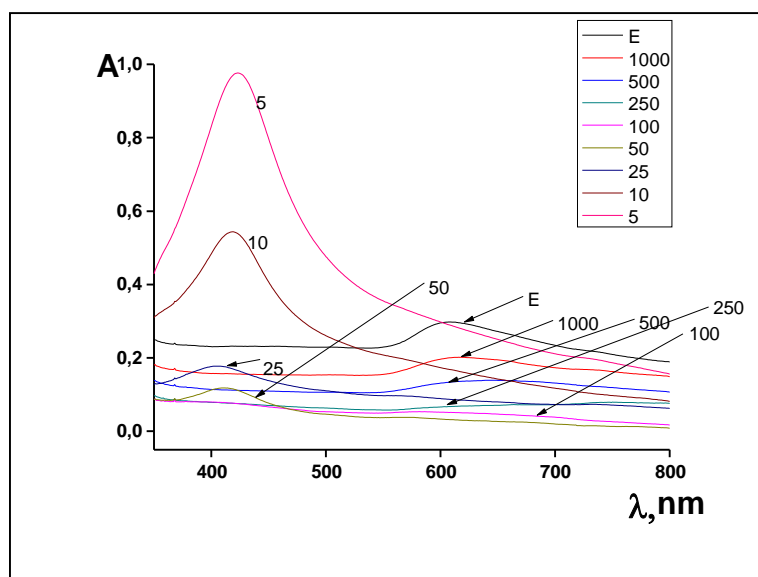


Figure 4.13 UV-Vis absorption spectra of Cu@AgNPs by different Cu/Ag molar ratios (E- pure copper nanoparticles dispersion)

In figure 4.13 the copper plasmon band at 602 nm can be observed for pure CuNPs. With the increase of silver nitrate concentration, the copper plasmon band disappeared and starting from the ratio Cu:Ag 50:1, the silver plasmon band at 430 nm appears in the system. By further adding of silver salt, a growth of the silver signal can be observed. This can be explained by the growth of the silver shell. The growth of the silver shell leads to the increase of the corrosion stability, but at the same time increases the production costs. To ensure the oxidation stability, the Cu/Ag ratio should be hold at 50:1 level.

In order to additionally investigate the core@shell structure of the system, certain samples were analyzed with XRD (Figure 4.14). For this, 50 mL of Cu@Ag nanoparticles dispersion with starting copper concentration of  $10^{-3}$  M was centrifuged in order to remove the solvent. In addition, wet samples were dried on the air. Because of the small amount of nanoparticles, all samples were additionally mixed with Vaseline, which leads to the noises in the basis lines of some samples. For the evaluation of results, a comparison of the measurement data and



#### 4. Microgel Based Conductive Films

diffractogram of elemental copper (COD ID: 5000216) and silver (COD ID: 1100136) was used. This allows finding out whether elements are present in the form of alloy or simple metals.

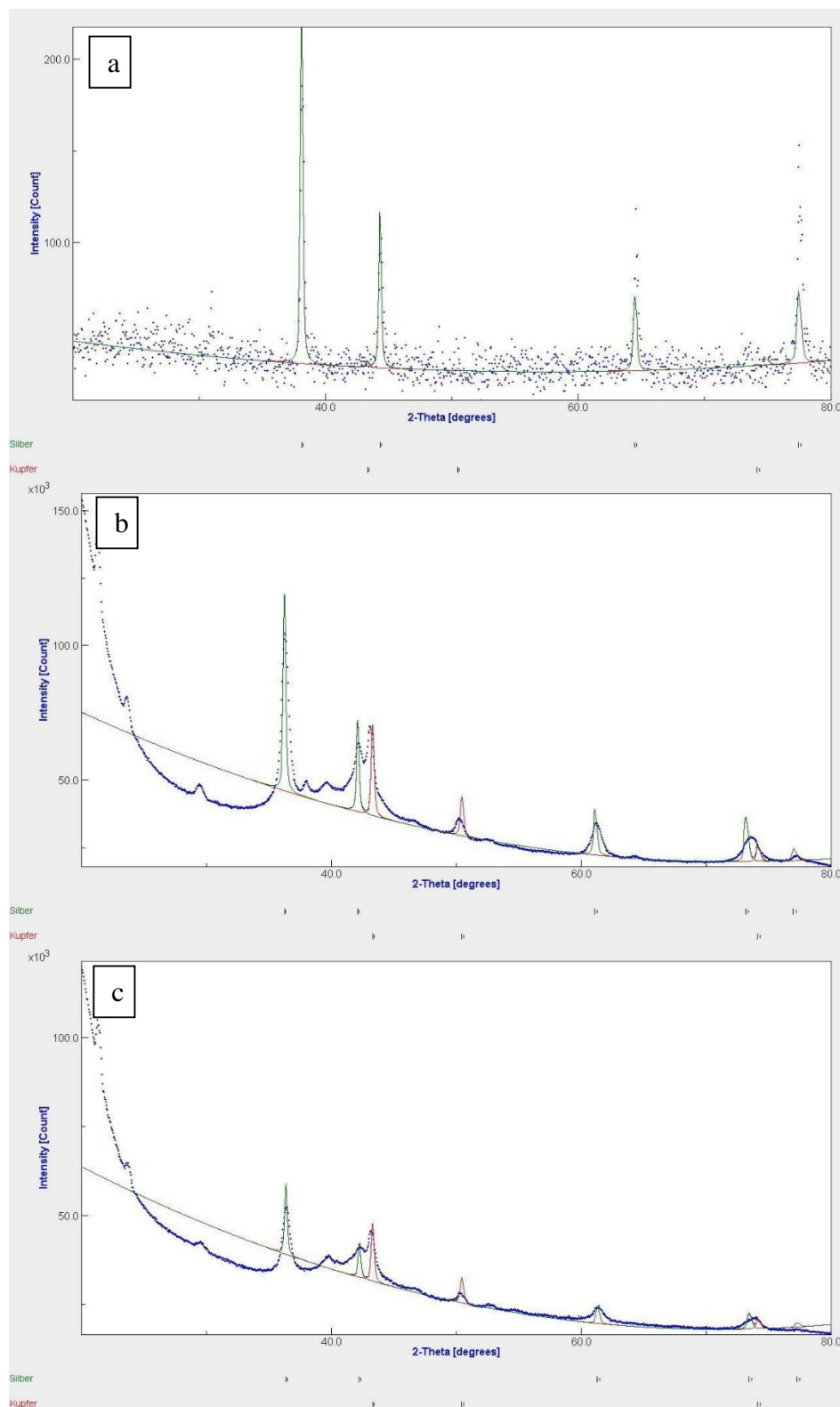


Figure 4.14 XRD for nanoparticles with high silver content  $c_{Ag}/c_{Cu}=5$  (a), moderate silver content  $c_{Ag}/c_{Cu}=0.02$  (b) and low silver content  $c_{Ag}/c_{Cu}=0.004$  (c)

#### 4. Microgel Based Conductive Films

From this data it is noticeable the relation between signal intensities and metals ratios. By comparison of this graphics, the fall of the silver peak intensity with the decrease of silver content is remarkable. Also, all signals are related only to elementary silver and copper, which proves the core@shell structure of the Cu@Ag nanoparticles. For further investigation of the core@shell structure and to discover the elements composition on the surface of the particles, the samples were analyzed with XPS (Figure 4.15). For this, the wet samples after the centrifugation were cast on a silicium wafer and dried at room temperature. As in the case with XRD analysis, the intensity of the signals directly corresponds to the copper/silver ratio. With decrease of the Ag/Cu ratio, there is also a noticeable decrease of the silver peak intensity at 365 eV. That means that the number of the silver atoms on the surface is decreasing with the decrease of Ag/Cu ratio. After the ratio Ag/Cu 0.004 there is no more silver signal detectable. In opposite, the copper signal (930 eV) is growing, because more and more copper atoms are located near the particle surface where the photon beam can reach them. By the sample with the ratio Ag/Cu = 5 no more copper signal can be seen. That indicates that the shell of the particles consists completely of the silver atoms and the shell is entirely closed, which proves the success in the core@shell particles synthesis. XPS and XRD measurements were performed within the bachelor thesis of David Schroeter.

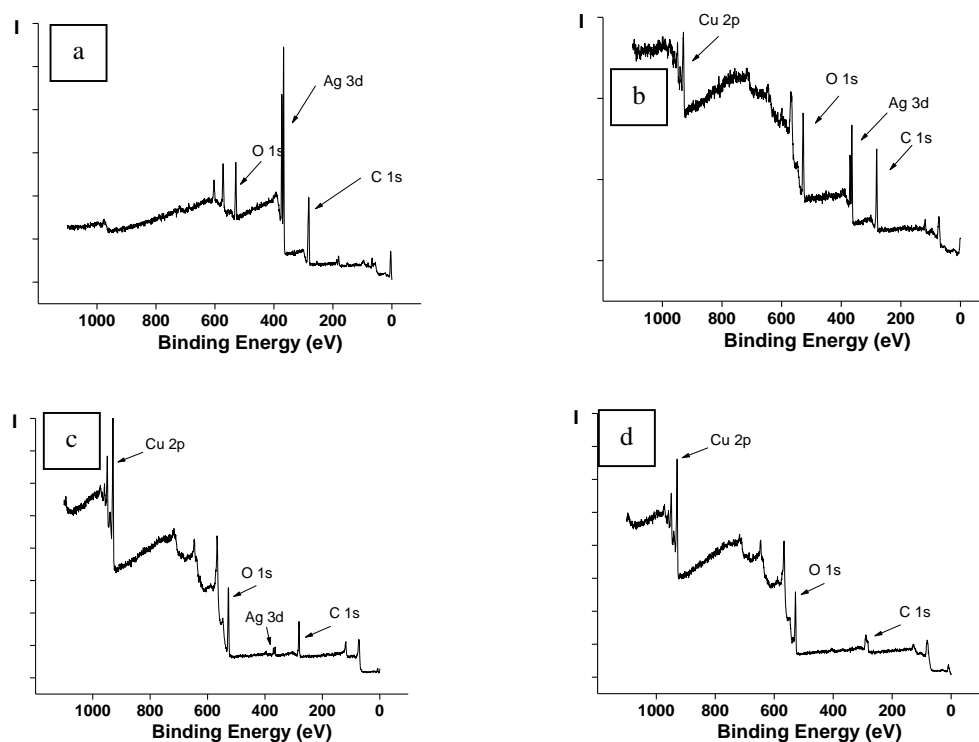


Figure 4.15 XPS spectra of the Cu@Ag nanoparticles with Ag/Cu ratio 5 (a), 0.5 (b), 0.02 (c) and 0.004 (d)

#### 4. Microgel Based Conductive Films

In this work the kinetic of the silver deposition process onto copper nanoparticle was also studied. The covering reaction times are different and relate to the copper nanoparticles synthesis. The covering of copper nanoparticles, which were synthesized using the hydrazine method, with silver, was performed within few seconds. The reaction can be seen by simple observation, after the addition of the silver nitrate to the red copper nanoparticles dispersion the color of the suspension turns yellow rapidly. The building of the silver layer on the copper particles synthesized by UV method happens significantly slower and is completed only after 120 min (Figure 4.16).

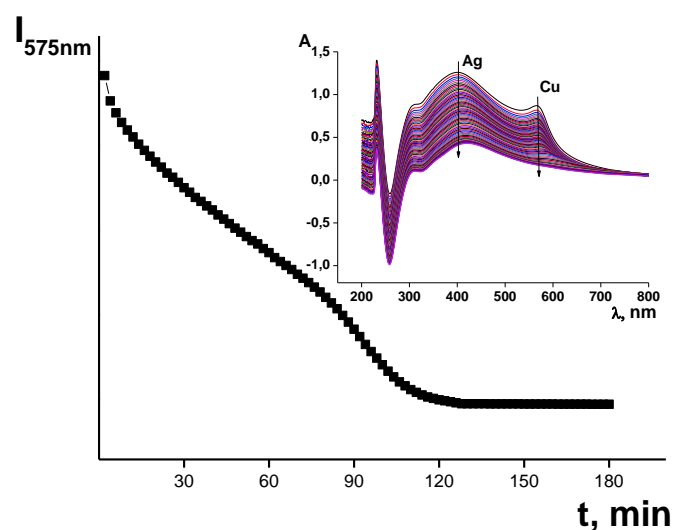


Figure 4.16 Time dependent change of the copper plasmon band intensity.

Figure 4.16 shows that the copper plasmon band intensity at 575 nm is decreasing with increasing of the exposure time. At the same time, the intensity of the silver plasmon band at 423 nm is rising with the time. (Figure 4.16 right above). Also this is the proof of the core@shell structure of the particles.

The synthesized copper@silver nanoparticles exhibit noticeable colloidal stability in water dispersions. Besides of the oxidation stability this is also a very important feature of the conductive inks. Figure 4.17, shows that even after one month of the dispersion storage all particles are dispersed in the solvent and no sedimentation occurs in the system.



Figure 4.17 Cu@AgNPs after the synthesis (left) and after the one-month storage on the air (right)

A possible reason for the difference of the covering time of the copper nanoparticles synthesized accordingly using the hydrazine and UV methods may be the difference of the particles diameters and respectively their surface area. To prove this suggestion and to investigate the particles morphology, diameter as well as polydispersity of the Cu@Ag nanoparticles synthesized with different methods, TEM measurements were performed (Figure 4.18)

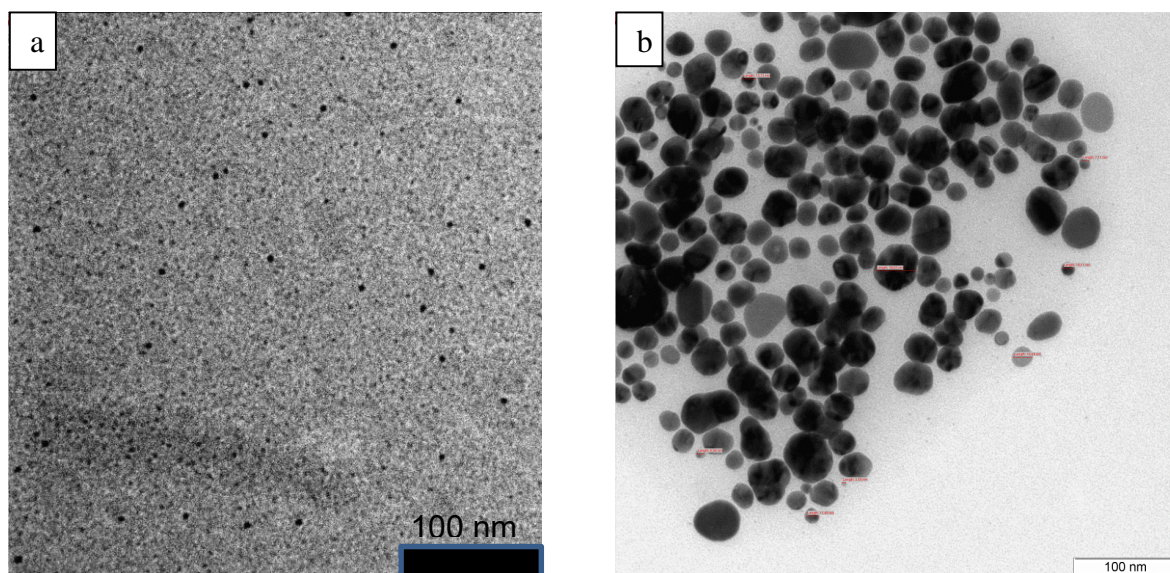


Figure 4.18 TEM images of the Cu@AgNPs synthesized accordingly to the hydrazine method (a) and accordingly UV method (b).

From the TEM images a difference is clearly noticeable between the nanoparticles sizes, morphologies and polydispersities, in relation to the synthesis method used. The core@shell

#### 4. Microgel Based Conductive Films

particles synthesized with the hydrazine method (Figure 4.18 a) are 6-7 nm in diameter and exhibit high monodispersity and equal shape. The particles, which were synthesized using the UV method show big differences in particle sizes and have the average size of 30 nm, which is 5 times bigger than the particles synthesized using the hydrazine method. In addition to the diameter differences, particles achieved by the UV method are polydisperse and have different shapes (Figure 4.18 b). The big diameter and fluctuation in the size of the particles make the covering time much longer than in the case of small, active, monodisperse particles synthesized with the hydrazine method. Another disadvantage of the big and not homogeneous particles is that the pores of the microgels have certain dimensions and not all particles will enter the microgel.

According to this, the synthesis of Cu@Ag nanoparticles is preferable using the hydrazine method than by using the UV method. Even if the copper nanoparticles synthesis is faster by UV method, the hydrazine method allows synthesis of small monodisperse particles. The short covering time and cheap technique does not require UV lamps and does not require work under inert gas atmosphere. In table 4.6. all parameters of both UV and hydrazine methods are compared.

Table 4.6 Comparison of the UV and hydrazine methods.

Method	Synthesis time	Preparation before covering	Covering time	Inert gas	Middle Cu@AgNPs size	Particle size distribution
UV	20 min	-	95 min	+	30 nm	broad
Hydrazine	90 min	+	< 1 min	-	6 nm	narrow

To sum up, the results and analysis of the core@shell nanoparticles shows that the synthesis was successfully done. Accordingly to the XPS and UV-Vis spectroscopy copper nanoparticles were completely covered with the silver shell. According to the one-month observation, the silver shell is able to protect the copper core from oxidation. All this creates a good possibility to use these particles as a charge carrier in low-price hybrid microgels.

#### 4.4 Loading of the microgels with metal nanoparticles

The synthesis of the hybrid microgels was performed through the incorporation and immobilization of the metal nanoparticles in the pores of the hydrophilic polymer colloids. The microgels that were synthesized in this work have special functional groups (amino-,

#### 4. Microgel Based Conductive Films

carboxyl-), which are able to immobilize metal ions and metal nanoparticles (Figure 4.19). In this case, the metal nanoparticles were directly synthesized inside of the microgel.

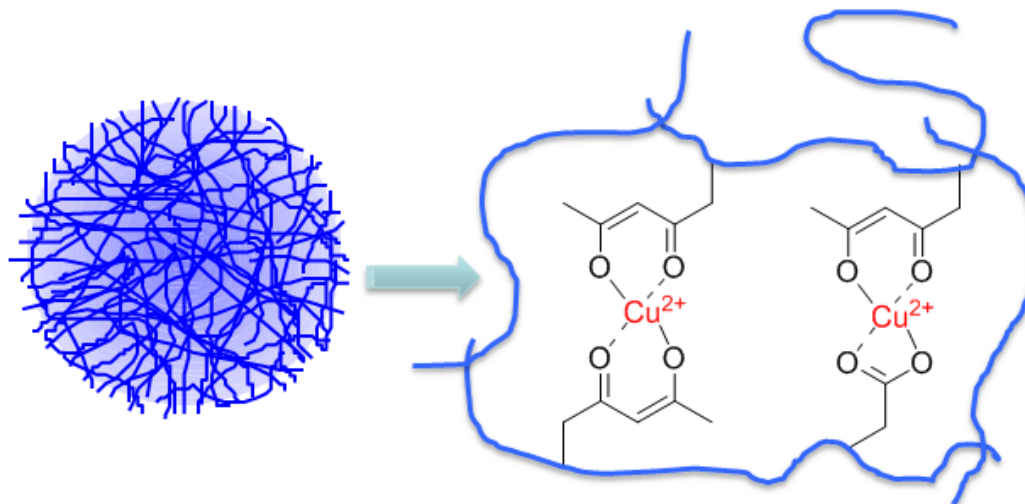


Figure 4.19 Schematic demonstration of copper complex building in the microgel pores.

For the synthesis of the hybrid microgels, using the hydrazine method (Table 4.7), microgel-dispersions were placed in a 50 mL centrifuge tubes. Under continuous stirring, the calculated amount of copper sulphate solution was added to the mixtures. The total volume of the mixtures was set to 25 ml with distilled water. After 5 min hydrazine solution was added. The color of the solution turned from blue to red and the nitrogen bubbles started to appear on the top of the mixture. The reaction was stopped and the excess of hydrazine was removed after 8 hours by adding acetaldehyde. Due to the low boiling point of acetaldehyde, the neutralization of hydrazine was performed in an ice bath. After 15 min of reaction time, silver nitrate solution was added to the mixture, in order to get the silver shell around the copper nanoparticles. Finally, the hybrid microgels were dialyzed against distilled water for three days. Schematically this process can be seen in figure 4.20.

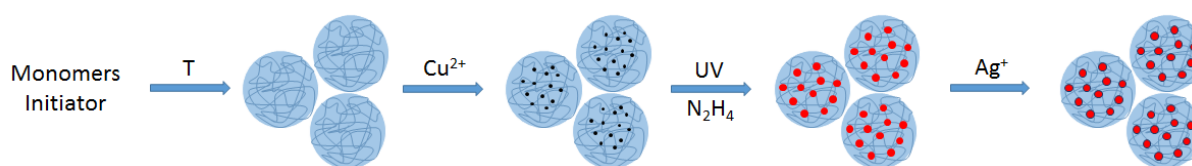


Figure 4.20 Schematic demonstration of hybrid microgel synthesis.

#### 4. Microgel Based Conductive Films

Table 4.7 Reaction mixture composition for Cu@Ag hybrid microgel synthesis

Sample	$\omega_{\text{Metall}}$	$n_{\text{CuSO}_4 \cdot 5\text{H}_2\text{O}}$ [mmol]	$m_{\text{CuSO}_4 \cdot 5\text{H}_2\text{O}}$ [mg]	$n_{\text{N}_2\text{H}_4}$ [mmol]	$V_{\text{N}_2\text{H}_4}$ [mL]	$n_{\text{CH}_3\text{CHO}}$ [mmol]	$V_{\text{CH}_3\text{CHO}}$ [mL]	$n_{\text{AgNO}_3}$ [mmol]	$m_{\text{AgNO}_3}$ [mg]
1	0.23	0.098	24.6	2.46	0.12	12.3	0.69	0.01	1.7
2	0.33	0.169	42.1	4.22	0.20	21.1	1.19	0.017	2.9
3	0.44	0.262	65.5	6.56	0.32	32.8	1.84	0.026	4.5
4	0.54	0.393	98.2	9.84	0.48	49.2	2.77	0.039	6.7
5	0.64	0.590	147.3	14.8	0.72	73.8	4.15	0.059	10.0
6	0.73	0.918	229.2	22.9	1.12	115	6.45	0.092	15.6

To investigate the real concentration of copper and silver, which were loaded in the VCL-AAEM-AAC microgel and its relation to the theoretical values, 5 mL of the hybrid microgel dispersion was dried. The mass of the dried microgel was measured. Dry hybrid microgel was dissolved in 5 mL of concentrated nitric acid. The total volume was set to 25 mL with distilled water. All samples were measured with ICP-AES in order to get the silver and copper concentration. From these results and the initial hybrid microgel mass, the content of the silver and copper in the hybrid microgel can be calculated (Table 4.8).

Tab. 4.8 Copper and silver content in the hybrid PVCL-AAEM-AAC microgel measured with IPC-AES

Theoretical Cu-content, %	Experimental Cu-content, %	Yield, %	Theoretical Ag-content, %	Experimental Ag-content, %	Yield, %
5.7	3.8	67.4	1.0	1.0	103
11.9	9.5	80.3	2.0	2.4	110
18.8	12.1	64.3	3.3	3.6	108
26.5	18.2	68.7	4.8	5.6	109
35.1	25.6	73.0	6.3	7.4	108
44.8	34.1	76.2	8.0	8.8	109
55.8	41.5	74.4	10.3	9.6	94
82.9	71.1	85.7	14.4	14.1	98

From the data it can be seen that with the increase of copper ions concentration in the start of the synthesis we can see the increase of the copper nanoparticles in microgels. The same can

#### 4. Microgel Based Conductive Films

be seen in the case with the silver ions. According to these data, the ratio between microgel and metal nanoparticles can be adjusted.

For further investigation TGA analysis of the loading of the metal nanoparticles in microgel was performed. For this 5 mL of hybrid microgel was placed in the round bottom flask and frozen in liquid nitrogen. After the microgel was frozen, the flask was put on the lyophilizer in order to dry the hybrid microgel. After a few days of drying 10 mg of the hybrid microgel was placed in the ceramic crucible and put in the TGA device. The temperature program from 25 to 950 °C was run over 5 hours. At the temperature of 250 °C the microgel starts to sublimate. At the same time copper and silver stay in the crucible. From the difference of the starting mass of the hybrid microgel and the rest in the crucible, the total metal content can be calculated. The results of the solid content measurements can be seen in figure 4.21.

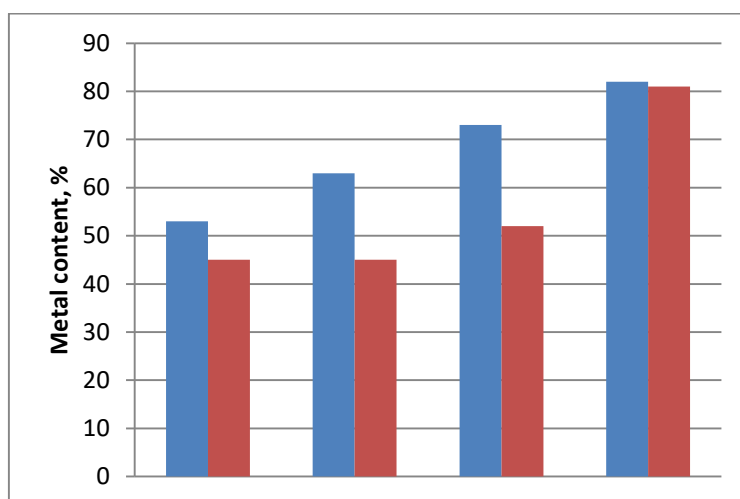


Figure 4.21 Experimental (red) and theoretical (blue) metal content in the hybrid microgel, measured using TGA analysis.

To investigate the influence of the metal nanoparticles content on the hydrodynamic radius and the sedimentation stability of the hybrid microgel, samples were analyzed using DLS and LUMiFuge methods. For this microgels with different starting concentration of copper and silver ions were converted into hybrid microgels.

To study the change of the size of the hybrid microgels with a changing metal content, DLS measurements of the diluted hybrid microgels dispersions were performed (Figure 4.22). From these data it can be seen that up to a metal nanoparticles content of 50 % the hydrodynamic radius of the hybrid microgels stays relatively constant at approx. 210 nm, and



#### 4. Microgel Based Conductive Films

with further increase of the metal nanoparticles content the radius increases. In addition, a high increase of the polydispersity of the hybrid microgel radius with the metal nanoparticles content higher than 50 % can be seen. The deviation of the particles sizes of 100 nm for particles with an average radius of 200 nm tells about the large polydispersity in the system.

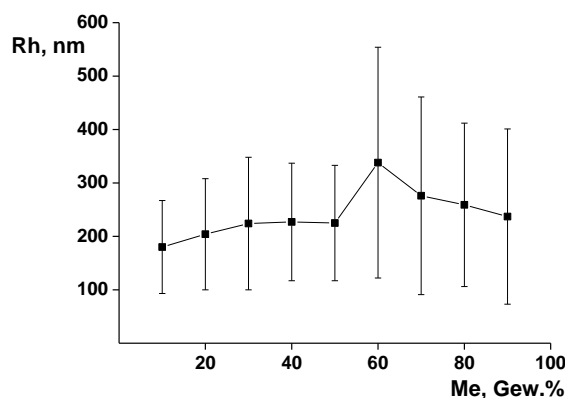


Figure 4.22 Dependence of the hybrid microgel radius on the metal nanoparticles content. VCL-AAEM-AAC microgel loaded with Cu/Ag nanoparticles.

Like the pure VCL-AAEM-AAC microgel, the hybrid microgel loaded with Cu/Ag nanoparticles shows a temperature sensitivity. At high temperatures the hydrogen bonds between water and C=O groups of poly(*N*-vinylcaprolactam) break, water gets ejected of the microgel pores and the microgel shrinks. This leads to the changing of the microgel size. To investigate the change of the hybrid microgel size, temperature trends using ALV were performed (Figure 4.23).

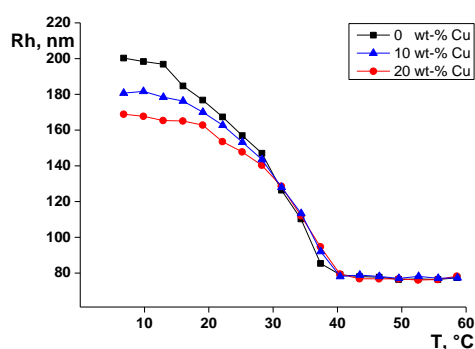


Figure 4.23 Changing of the hydrodynamic radius of pure and loaded VCL-AAEM-AAC microgel depending on temperature.

The interesting result here is that the VPTT stays constant (40 °C) and is not dependent on the metal nanoparticle content. With the increase of the nanoparticle content, the hydrodynamic

#### 4. Microgel Based Conductive Films

radius at low temperatures becomes smaller. This can be explained with the complexation of the microgel end groups with metal nanoparticles. In swollen state the end groups of the pure microgel are far away from each other, at the same time the end groups of the hybrid microgel are bound to the metal nanoparticles.

The metal nanoparticles also have an influence on the colloidal stability of the resulting hybrid microgel (Figure 4.24). For the sedimentation stability analysis, water dispersions of the hybrid microgels with a metal nanoparticle content from 10 to 80 % were placed in the LUMiFuge cuvettes and rotated in the device at 4000 rpm. From the results it can be seen that till 50 wt-% of metal nanoparticles the hybrid microgel is stable. At higher concentrations the system becomes instable, which leads to an increase in the sedimentation velocity. With the increase of temperature, it is also noticeable that the decrease of the sedimentation stability, due to the fact, that the microgel is in a collapse state above VPTT.

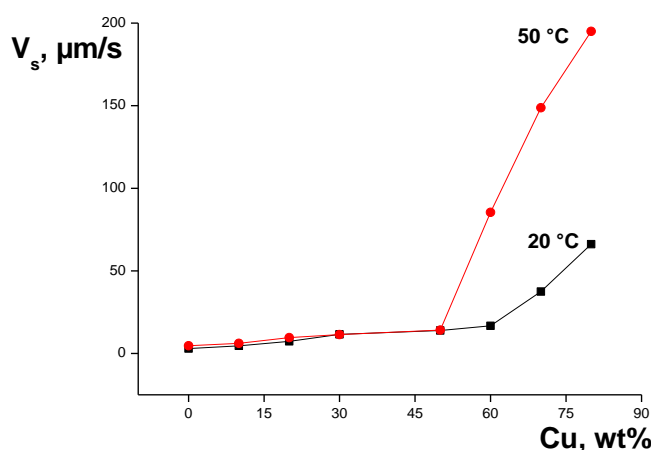


Figure 4.24 Sedimentation stability of the hybrid microgel samples with different metal nanoparticles content at different temperatures.

For visual proof of the metal nanoparticles incorporation in the microgel, an analysis of the hybrid microgel by transmission electron microscopy was made. In figure 4.25 TEM images of the hybrid microgels with different metal content are shown. For this, a diluted solution of the hybrid microgel was dropped on the TEM grid and dried at room temperature. The results are showing that in all cases the metal nanoparticles are incorporated or situated on the surface of the microgel, no metal nanoparticles can be found separately of the microgel. Noticeable is that the metal nanoparticles are building spherical structures around the microgel particles. This is the proof of principal of the possibility to synthesize the hybrid

#### 4. Microgel Based Conductive Films

microgels. The size of the metal nanoparticles is around 40 nm, which is more than what was expected from the hydrazine method. A possible reason for this is that the stabilizing agent in the case with pure metal nanoparticles synthesis was CTAB, while in the case of the hybrid microgel synthesis the microgel itself acts as a stabilizing agent and no additional surfactant is required.

As expected the metal concentration has a proportional influence on the loading density of the microgels.

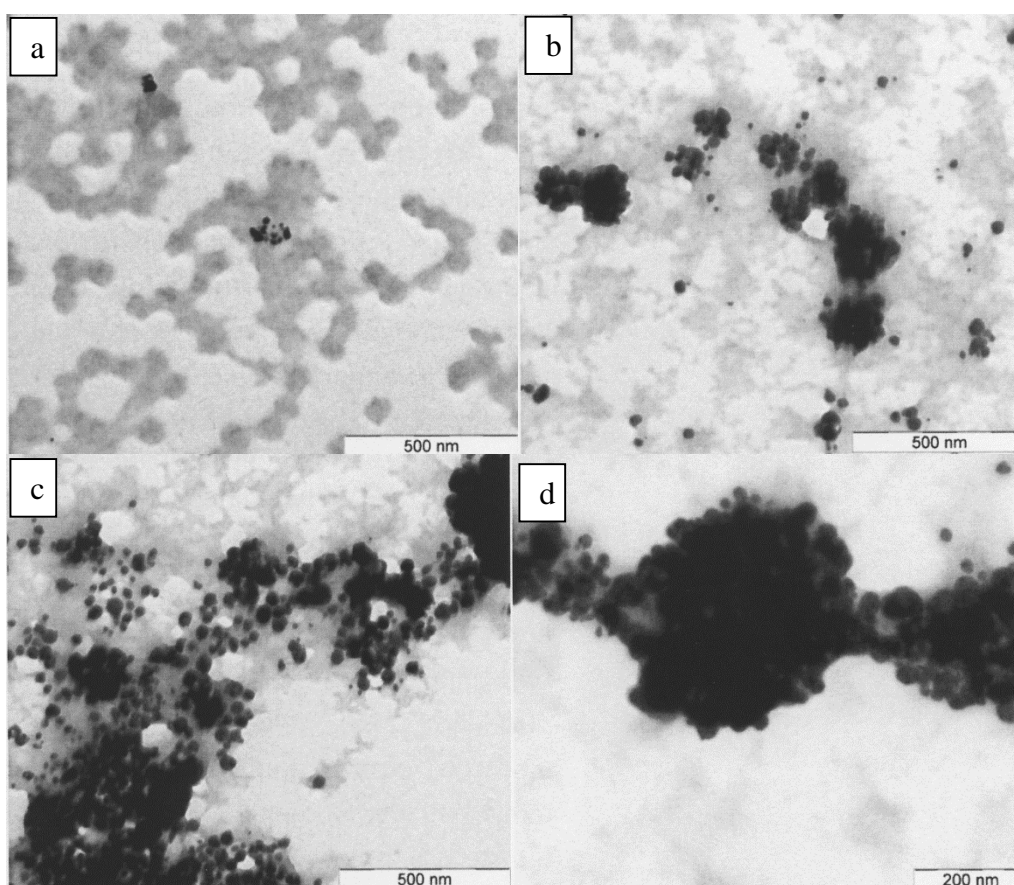


Figure 4.25 TEM images of the hybrid microgels with a different content of metal nanoparticles 12 wt-% (a), 33 wt-% (b), 54 wt-% (c) as well as detailed TEM image of the hybrid microgel sample with 73 wt-% of metal nanoparticles.

For the microgel loaded with nanoparticles, a concentration of metal nanoparticles of more than 50% was not achieved. In order to optimize the loading and distribution of the metal nanoparticles in the microgel, the reaction conditions such as reagents concentrations, stirring velocity, and reduction agent adding velocity were varied. Through the variation of these parameters, it was possible to get a colloidal stable hybrid microgel with a homogeneous distribution of metal nanoparticles. Moreover, all microgel particles were completely covered

#### 4. Microgel Based Conductive Films

---

with metal nanoparticles, which were in continuous contact to each other. This creates a good conditions for high conductivity of the hybrid microgels. Figure 4.26 shows the results of the successful optimization of the synthesis parameters.

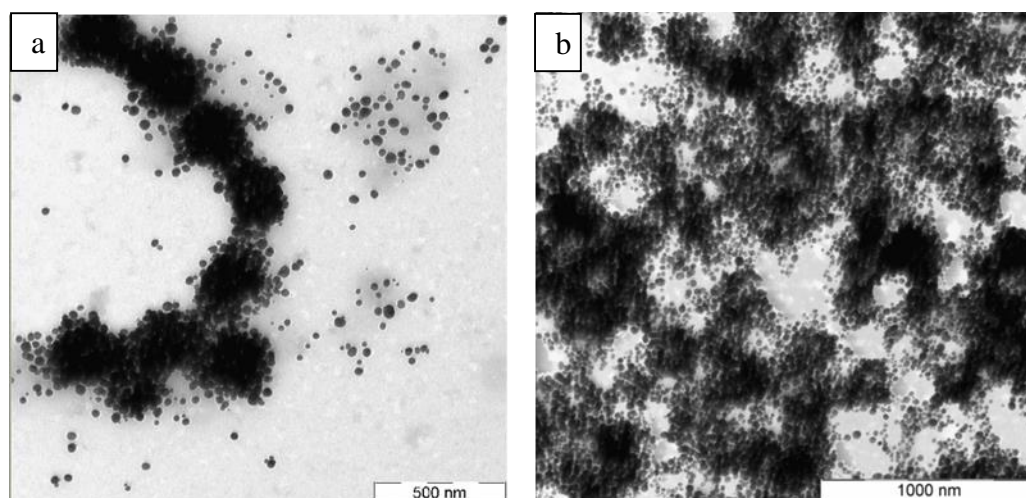


Figure 4.26 TEM image of the hybrid microgel samples with the 50 wt-% metal content after optimization of the synthesis conditions.

The hybrid microgels were also synthesized using the UV-method. But using this method, the microgel based on VCL-AAC-AAEM cannot be used due to that fact that it does not have the VP in their structure, which is acting as photo initiator for the reduction of the metal ions.

Therefore, the UV synthesis of the hybrid microgels, a microgel based on VCL-VP-AAEM-MEAK was used. For this the microgel dispersion was mixed with the copper salt and irradiated in the UV-reactor for 1 hour. After the synthesis of the copper nanoparticles under continuous purging of nitrogen, silver salt solution was added in order to make a silver shell around the copper nanoparticles. After dialysis of this microgel the total copper concentration was measured with the IPC-AES. From the result it was determined that the real copper concentration was only 20 % of the theoretical value. The reason for it is the sedimentation of the copper on the reactor and UV lamp walls (Figure 4.27).

#### 4. Microgel Based Conductive Films

---

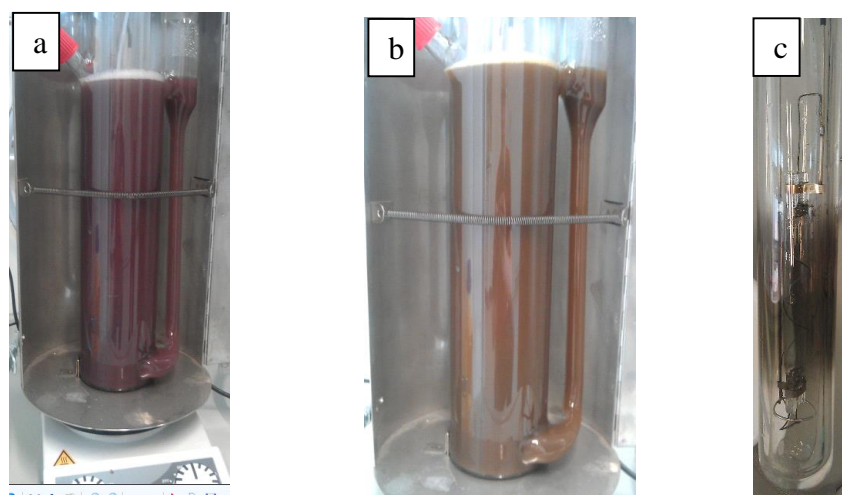


Figure 4.27 Hybrid microgel loaded with the copper nanoparticles (a), hybrid microgel with the Cu@Ag nanoparticles and sedimentation of the copper on the UV lamp.

To investigate the morphology and distribution of the metal nanoparticles in the hybrid microgel, synthesized using the UV method, a TEM analysis was performed (Figure 4.28). For this a diluted microgel dispersion was dropped on the TEM grid and dried at room temperature.

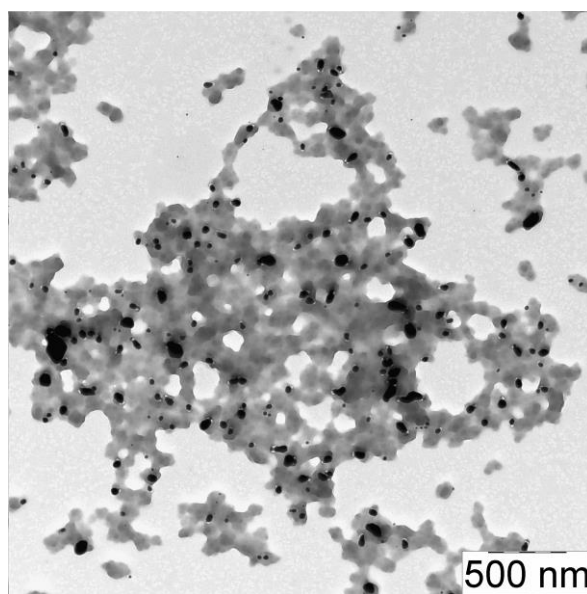


Figure 4.28 TEM image of the hybrid microgel loaded with Cu@Ag nanoparticles synthesized using the UV method.

From the TEM analysis, the metal nanoparticles show a broad size distribution. The metal nanoparticles are situated only on the surface of the microgel, no loose metal was detected on the grid. However, the big diameter of the metal nanoparticles and low yield by the synthesis affected their total distribution in the microgel. Moreover, even at high content of the metal no

#### 4. Microgel Based Conductive Films

constant contact between metal nanoparticles was reached. This makes this system not suitable for the production of conductive inks.

Besides the loading of the microgels with the copper@silver nanoparticles, hybrid microgels loaded with pure silver nanoparticles were studied in this work (Figure 4.29). The hydrazine was chosen as a reduction agent for the metal ions, due to the previous results. For the synthesis of silver loaded hybrid microgels, (Table 4.9) the water dispersion of the VCL-AAEM-AAC microgel, containing 25 mg of microgel, was mixed for 5 minutes with the calculated amount of silver nitrate. After mixing, the hydrazine solution was slowly added to the mixture using a syringe pump.

The color of the dispersion turned from the milky white to the brown-gray. Finally, the hybrid microgel was purified using dialysis for over 3 days.

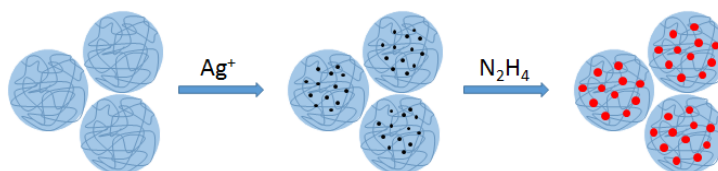


Figure 4.29 Schematic demonstration of hybrid microgel synthesis.

Table 4.9 Reaction mixture composition for the hybrid microgel loaded with silver nanoparticles.

Sample	$\omega_{\text{Metall}}$ %	$n_{\text{AgNO}_3}$ [mmol]	$m_{\text{AgNO}_3}$ [mg]	$n_{\text{N}_2\text{H}_4}$ [mmol]	$V_{\text{N}_2\text{H}_4}$ [mL]
12.1	0.1	0.025	4.4	0.002	0.1
12.2	0.2	0.058	9.9	0.003	0.15
12.3	0.3	0.100	17.0	0.005	0.25
12.4	0.4	0.155	26.4	0.007	0.35
12.5	0.5	0.233	39.7	0.01	0.5
12.6	0.6	0.350	59.5	0.015	0.75
12.7	0.7	0.545	92.6	0.02	1
12.8	0.8	0.9346	158.8	0.02	1
12.9	0.9	2.1028	357.4	0.02	1

As in case of the incorporation of copper nanoparticles in the VCL-AAEM-AAC microgel, AAEM and AAC act as a stabilizing agent for the silver ions and nanoparticles. To prove fulfillment of the reduction of the silver ions, the composition of hybrid microgels with different silver nanoparticles content was analyzed using ICP-AES. For the measurements

#### 4. Microgel Based Conductive Films

hybrid microgels were dialyzed and dried. A certain amount of the dried microgel was dissolved in nitric acid. The results of the measurements are listed in figure 4.30. The measured data corresponded to the theoretical values. This creates a good possibility in creation of silver loaded hybrid microgels.

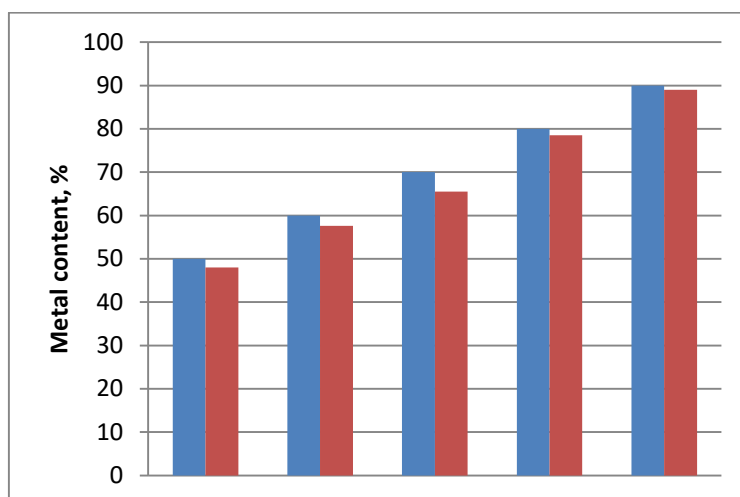


Figure 4.30 Theoretical (blue) and with IPC-AES measured silver content in VCL-AAEM-AAC hybrid microgel.

For the further investigation of the silver loaded hybrid microgel, TEM analysis of the microgel loaded with 65% of silver (Figure 4.31) was performed. As in the standard procedure, the diluted, dialyzed microgel was dropped on the TEM grid and dried at room temperature. The hybrid microgels in the dried state have a diameter of 250 nm and consist of a mixture of the complete, silver covered microgel, and the uncovered microgel particles. However, from the next results that were obtained in this work such mixture of the particles is conductive. Apparently, the covering of each single microgel particle is not necessary and the metallic silver of one microgel particle is in contact with the silver of other particles. The empty microgel particles act in this case as a bounding and a film-building agent.



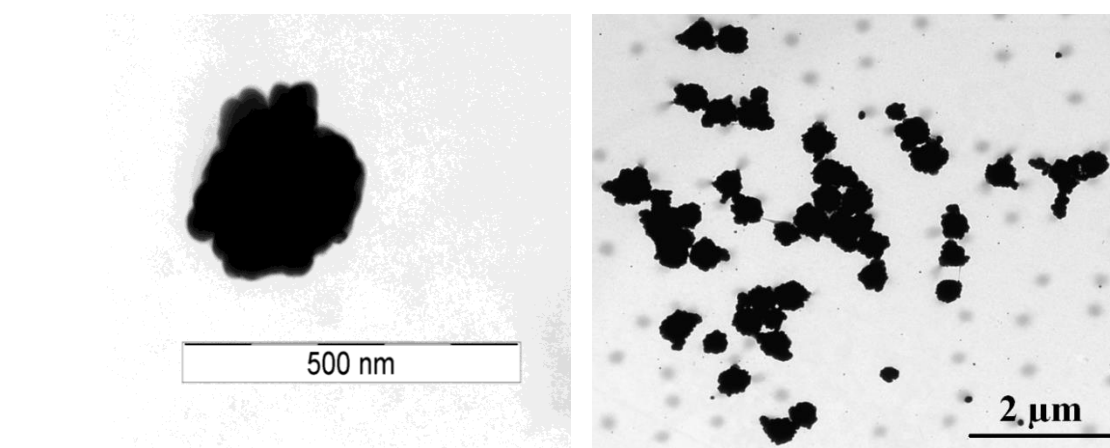


Figure 4.31 TEM image of the hybrid microgel loaded Ag nanoparticles synthesized using the hydrazine method.

To summarize, in this chapter hybrid microgels loaded with the metal nanoparticles were synthesized. As reducing agents for the hybrid microgels synthesis, UV light with photo initiator and hydrazine were used. It was shown, that the usage of hydrazine as a reducing agent is preferable. Moreover, the metal nanoparticles content is easily controlled, by choosing the starting ratio of microgel to metal salt. The hybrid microgels are stable against the sedimentation by metal loading up to 50 %. Due to the successful synthesis of the copper core silver shell metal nanoparticles and their immobilization in the VCL-AAEM-AAC microgel, a good possibility is created to invent a new price efficient alternative to using pure silver nanoparticles as an electricity conductive agent.

#### 4.5 Design and characterization of composite films

In this work model conductive inks containing different amounts of metal nanoparticles for casting of composite films were produced. The printing was performed on different surfaces. For the production of the conductive inks hybrid microgels after dialysis were concentrated up to 10 times using the evaporator at 30 °C and vacuum of 50 mbar. After the concentration, the hybrid microgels achieved the right viscosity and sedimentation stability. After casting the hybrid microgels using different methods on a surface and drying of the inks, the films were analyzed using light and electron microscopy. All composite films were tested for conductivity using the Van-der-Pauw four-point measuring method. Moreover, the conductive films were tested for mechanical stability.



#### 4. Microgel Based Conductive Films

---

For the printing on the model substrates, the first step is the production of the conductive inks. As an example for production of conductive inks based on VCL-AAEM-AAC microgel loaded with various amounts of silver nanoparticles, 2 liters of hybrid microgel was synthesized. After the cleaning procedure using dialysis, the hybrid microgels were concentrated to 100 mL of model inks. As a result, 100 mL of hybrid microgel with approximately 8 wt-% of solid state was obtained. These inks were used in all experiments of conductive films production, using spin coating, casting, doctor blade, ink jet and screen-printing.

As a first method for producing conductive films in this work, spin coating was used (Figure 4.32). As substrate for the spin coating only the glass plates were used. This was done because of the stability of glass against the rotation at high speed compared to textiles and polymer film substrates. For the spin coating, 25  $\mu$ l of the standard ink was dropped on the glass plate and rotated for 1 minute at 1000 rpm. As a result, a homogeneous film with an average thickness of 1  $\mu$ m was achieved.



Figure 4.32 Hybrid microgel ink on the glass substrate (left) and the spin coating device (right).

Another possibility to obtain the composite films is casting the hybrid microgel films on the surface. By casting, the inks were dropped on the surface and dried at room temperature. The advantage of this method is that all kinds of the surfaces can be used. The method is convenient but the thickness of the film is not homogeneous. This method is good for fast fabrication and the analysis of the conductive films. For the production of the films using the casting method 0.1 mL of the ink was dropped on the surface and dried. As a result, stable films with the average thickness of 2  $\mu$ m were produced (Figure 4.33).

#### 4. Microgel Based Conductive Films

---

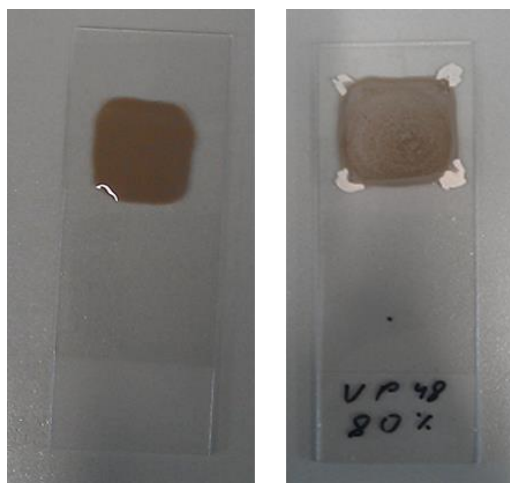


Figure 4.33 Casting of the conductive inks on the glass substrate. Wet sample directly after casting (left) and dried sample of VCL-AAEM-AAC microgel containing 80 % of silver nanoparticles (right).

For the producing of the composite films using the doctor blade method (Figure 4.34) the inks were passed inside of the 4 walls frame. One wall of the frame is higher than the other walls and by moving the frame the liquid trace stays on the surface. In figure 4.34 (right) the results of the PET films coating with the inks are shown. The resulting films have high fluctuations in the film thickness, which can be explained through the low density and viscosity of the inks.



Figure 4.34 Frame for film building (left) and the composite films on PET substrate (right)

For the precise printing of the inks, ink-jet printing was used. In this work, a commercial ink-jet printer was used. The printing nozzle of the cartridge in this case was only 10  $\mu\text{m}$  and because of the high viscosity of the hybrid microgel inks, using this method was not possible.

#### 4. Microgel Based Conductive Films

---

As an alternative for the commercial printers, industrial printers with height nozzle diameter and pressure in the cartridge could be used.

The last approach in producing the composite films was screen-printing (Figure 4.35). The frame for printing consists of an aluminum body and the mesh. Some parts of the mesh are closed with polymer film. Using this method, the hybrid microgels were pulled out through the uncoated mesh on the printing surface.



Figure 4.35 Frame for the screen printing.

For the screen printing 1 mL of conductive ink was placed on the mesh (in the covered zone) and pulled through the mesh using a plastic blade. After the printing process, the mesh was removed and the hybrid microgel was dried at room temperature. The results of the screen printing show a homogeneous film without cracks (Figure 4.36). The average thickness of the film is 2  $\mu\text{m}$ .

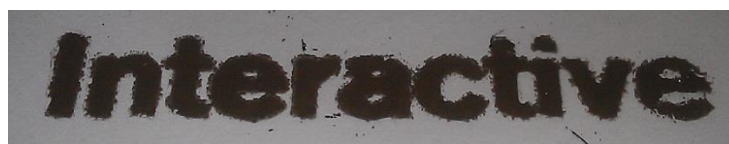


Figure 4.36 Glass coated with the composite film produced using screen printing.

To compare the different approaches and methods of film preparation, all results were summarized in table 4.10.

#### 4. Microgel Based Conductive Films

Table 4.10. Comparison of the different printing technics of the hybrid microgels applied on different surfaces.

Printing method	Substrate	Film sickness	Film quality
Spincoating	Glass	< 1 $\mu\text{m}$	No cracks, homogeneous
Casting	Glass, PET, textile	2 $\mu\text{m}$	No cracks, relatively homogeneous
Doctor blade	PET	2 - 25 $\mu\text{m}$	No cracks, not complete homogeneous
Screen printing	Glass, textile	2 $\mu\text{m}$	No cracks, homogeneous

From the comparison of different methods, it was determined that it is possible to get good printing results of the high viscosity hybrid-microgel inks on different coating surfaces. It was shown that the homogeneity of the films depends on the surface polarity of the substrate. In the case of polar substrates such as glass, the hybrid microgel distributes equally on the surface and produces a homogeneous film without cracks. In opposite to the hydrophilic surfaces, hydrophobic surfaces caused cracks in the composite films, and not equal distribution of the film thickness over the coating. The hydrophobic surfaces can be easily transformed to the hydrophilic form using plasma treatment. For example, by applying the plasma treatment to the PET film, it was possible to get a mechanically stable composite film without cracks on the PET surface. All these results create good possibilities in creating robust conductive films with continuous contact between the metal nanoparticles in the hybrid microgels.

To look closer to the hybrid-microgels film structures, light microscope measurements were performed. As an example, the film samples containing 65 wt-% of metals, prepared using casting techniques on the glass plates, were analyzed (Figure 4.37). From the images it can be seen that the films have a smooth surface without visible cracks which insures the continuous contact between the metal nanoparticles in the microgel. The difference in the surfaces of the two films comes from the different dimensions of the Cu@Ag and Ag nanoparticles loaded hybrid microgel particles.

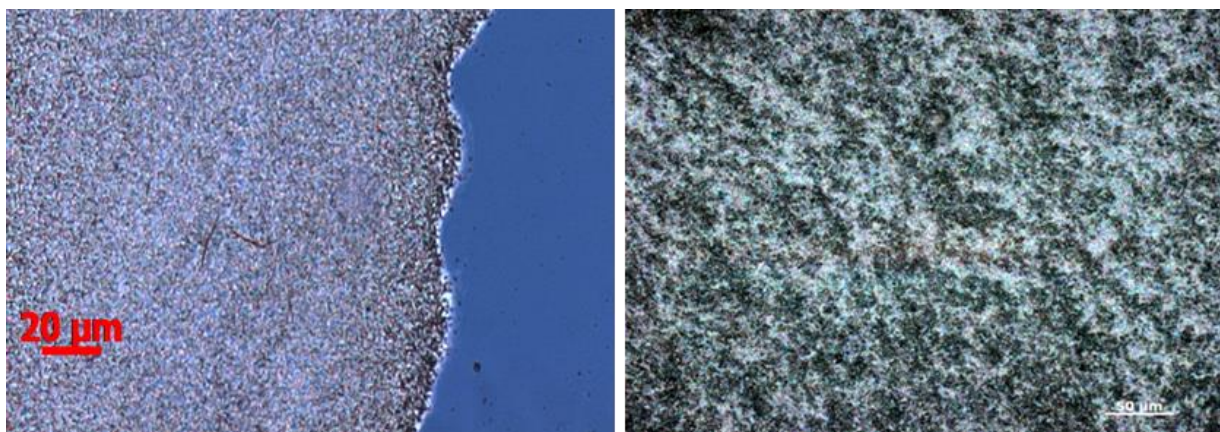


Figure 4.37 Light microscope images of the composite films VCL-AAEM-AAC microgel loaded with 65 wt-% of Cu@Ag nanoparticles (left) and VCL-AAEM-AAC microgel loaded with 65 wt-% of Ag nanoparticles (right).

In addition to all it was proven that the conductive inks based on water dispersion of the hybrid VCL-AAEM-AAC microgels loaded with metal nanoparticles are suitable for printing and after the drying procedure building the homogeneous crack free film with defined film thickness. Only one exception is the high viscosity of the inks, which make it impossible to print it using a conventional ink-jet printer. Using the industrial ink-jet printer with a bigger nozzles diameter may solve this issue. All other printing techniques are suitable for printing the conductive inks on all types of substrates with or without previous modification of the surface.

After the successful printing of the conductive inks on the model substrates, the possibility to print on fabric was tested. During the AiF project, the project partner supplied the fabric samples. The samples were made from different materials and have different polarities. Besides the samples made of cotton, fabrics made of PET and PET/elastane fibers were used as a surface for printing (Figure 4.38).



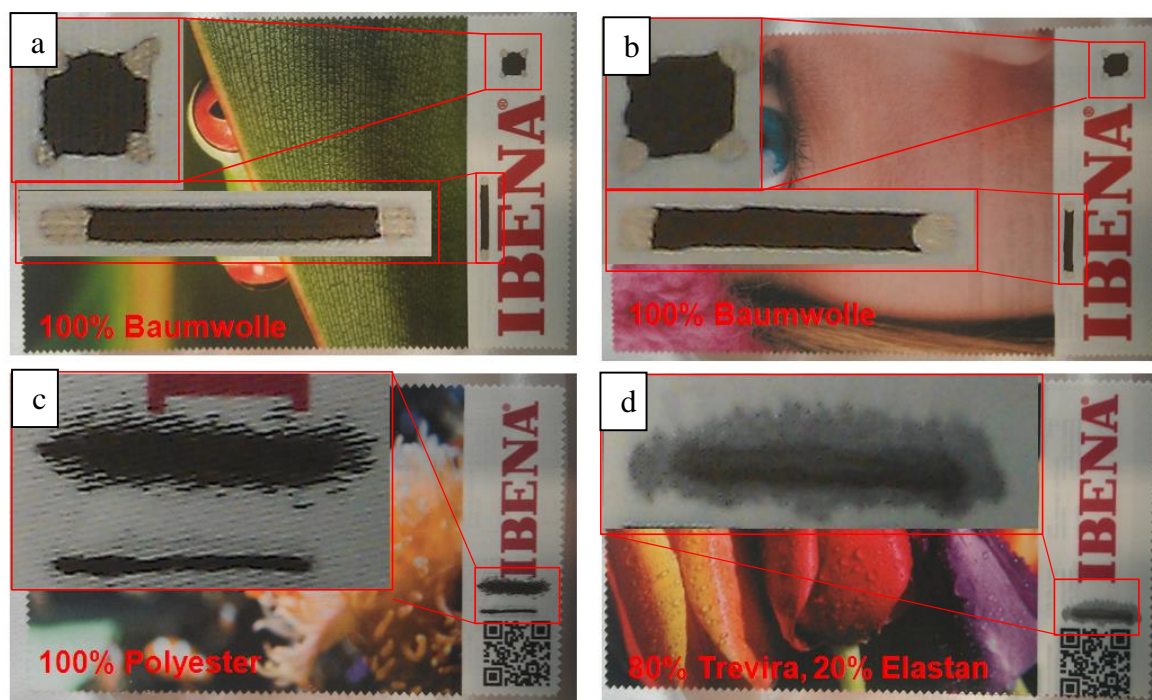


Figure 4.38 Results of the casting on the fabric samples made of cotton (a, b), PET (c) and PET/elastane (d)

The printing procedure was performed using inks made of VCL-AAEM-AAC microgel loaded with 60 wt-% of silver nanoparticles. As printing techniques, casting and screen-printing were used. The results of the casting printing are shown in figure 4.38. As a result, on both cotton samples (Figure 4.38 a, b) a homogeneous film (with height-defined edges) made of conductive ink was achieved. In the case of non-polar polyester, the height defined and the homogeneous thickness distribution of the conductive film was not achieved (Figure 4.38 c, d). This shows that the printing on the non-treated hydrophobic fabric is not possible and the process has to be optimized.

The samples of the PET fabric printed with conductive inks were further analyzed using electron microscopic analysis (FESEM). The figure 4.39 shows the PET sample with the dried conductive ink.

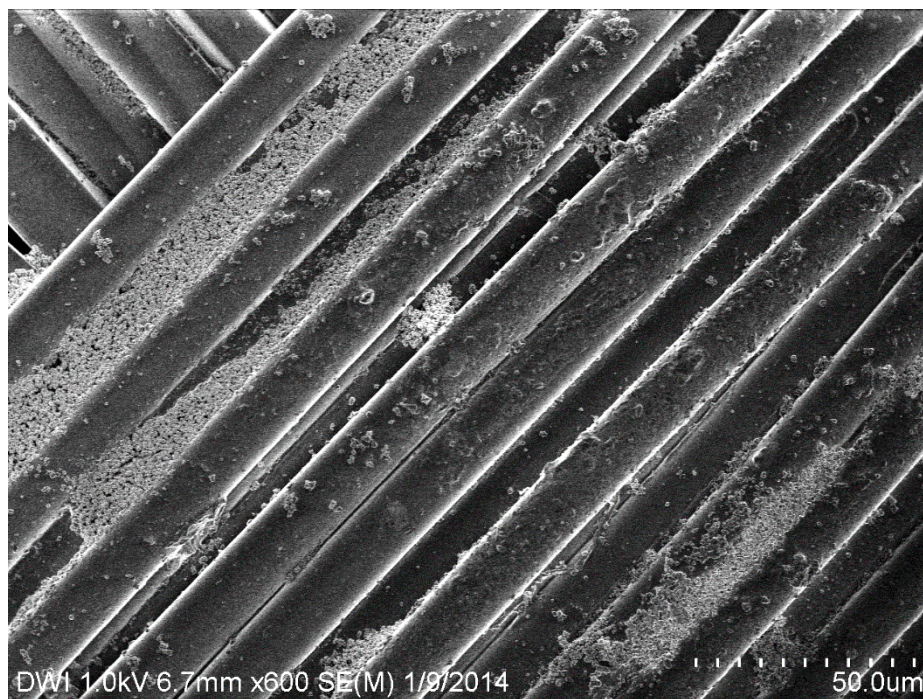


Figure 4.39 FESEM image of the VCL-AAEM-AAC microgel loaded with the 60 wt-% of silver nanoparticles on the PET fabric.

From this image it was concluded that due to the capillary forces the hybrid microgel dispersion prefers to settle in the holes between the fibers and does not make a film on the surface of the fabric. This prevents the continuous contact between the metal nanoparticles and as a result, the printed PET fabric is not conductive. Moreover, the edges of the printed hybrid microgel are undefined and it was not possible to get the shaped print.

Printing the conductive inks on a fabric shows good results in the case of using the polar fabric such as cotton, and creates a new possibility to produce smart textiles. In the case of the hydrophobic fabric, new procedures and preparation of the fibers before the printing must be performed.

#### **Electrical conductivity measurements.**

For the evaluation of the electrical conductivity of the hybrid microgels, resistance measurements of the composite films using four-point Van-der-Pauw method were performed. To perform these measurements, conductive inks based on VCL-AAEM-AAC microgels loaded with different amounts of metal nanoparticles were printed on the glass plates using the casting approach. The edges of conductive films were catted with a blade in order to get a perfect square. In order to get stable electrical contact, the corners of the square were covered with the silver glue. The resistances of the composite films were measured

#### 4. Microgel Based Conductive Films

using the equations  $R_{12,34}=V_{34}/I_{12}$  and  $R_s=\pi R/\ln 2$  where the resistance is  $R$ ,  $V$  is the voltage and  $I$  is the amperage.

The results of the conductivity measurements of the composite films consisted of VCL-AAEM-AAC microgels coated with the different content (from 10 to 90 wt-%) of silver nanoparticles, and are as follows (Figure 4.40). From the results it can be seen that at low metal content, the resistance is high and the samples are not conductive. With the metal nanoparticles content higher than 50 wt-% the resistance decreases dramatically, that means that the sample become conductive. After the 50 wt-% loading the samples stay conductive and the conductivity values stay constant over all concentration. The samples with low silver content are cheaper on one hand and are more flexible on another hand. The conductivity of the composite films with a silver content more than 50 wt-% are comparative with the conductivity of pure silver.

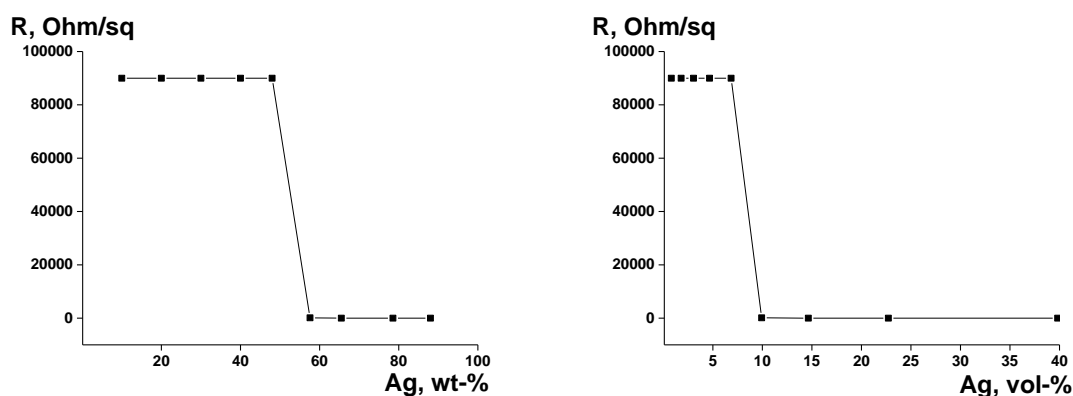


Figure 4.40 Dependence of the square resistance on the metal content in the hybrid microgels. Left weight percent of the silver, right volume percent of the silver.

The conductivity of the composite film may change with changing the environmental conditions. Especially the temperature and humidity have an influence on the swelling of the hybrid microgel. The swelling of the microgels changes the distance between the metal nanoparticles. To study the impact of this parameters, measurements in the climatic oven (Figure 4.41) were performed.



#### 4. Microgel Based Conductive Films

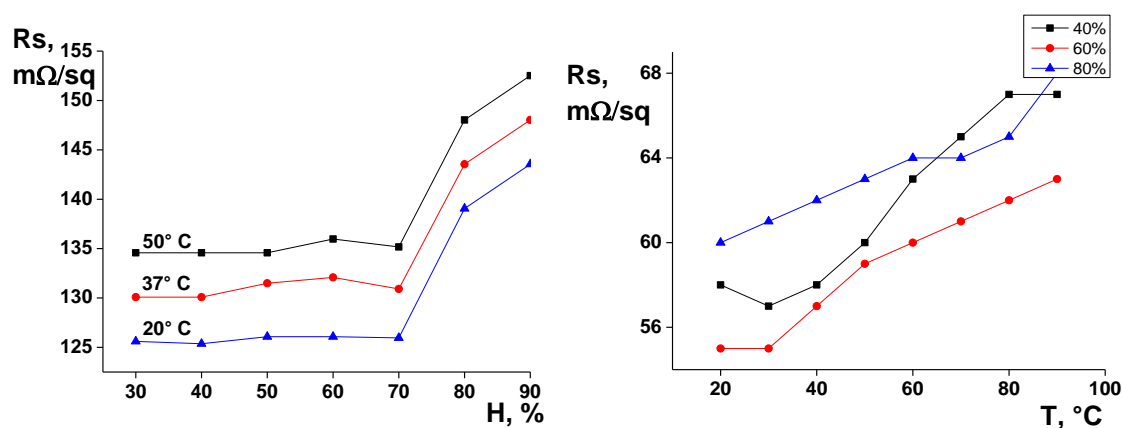


Figure 4.41 Resistance of the VCL-AAEM-AAC hybrid microgel loaded with 65 wt-% of silver nanoparticles depending on humidity (left) and the temperature (right).

From the resistance measurement at different humidity, it is to conclude that the square resistance of the composite film stays unchangeable for a humidity up to 70 %. For a humidity higher than 70% the microgels in the film start to swell, changing the distances between the metal nanoparticles at the same time, which leads to the increase of the square resistance. That's why for the application of the conductive films at high humidity, in order to get constant conductivity, it is necessary to protect the microgels from swelling. The solution of this problem may be the application of a protective layer over the conductive film. The same is with the protection of the film against direct contact with water. The resistance of the conductive films is also affected by temperature (Figure 4.41 right). With the increasing of temperature, it is also noticeable a slight increase in the resistance of the films, this increase is normal for all simple metals.

Another interesting point in the study of the composite films properties is the mechanical properties. With the application of hybrid microgels on textiles, they will always be in motion with bending and stretching. To study these influences, special devices and techniques were used. For the bending experiments, conductive inks were casted on the PET film; the ends of the conductive films were covered with silver glue, to insure the stable contact between the hybrid microgel film and the resistance-measuring device. The resistance of the conductive film was measured in 3 positions (Figure 4.42). In the first position, the composite film is deformed outside. This leads to the increase of the distances between single metal nanoparticles and leads to an increase of the resistance. In the second position, the film is in a normal straight position (no influence on the resistance). In the third position, the microgel is deformed inside, what leads to a decrease of the distances between metal nanoparticles and a decrease of the film resistance (Figure 4.42). The results of the measurements correlate well

#### 4. Microgel Based Conductive Films

with the theory. After a slight increase of resistance over 100 bending cycles, the resistance stays unchangeable even after more than 5000 cycles, which is very important for using the inks on textiles.

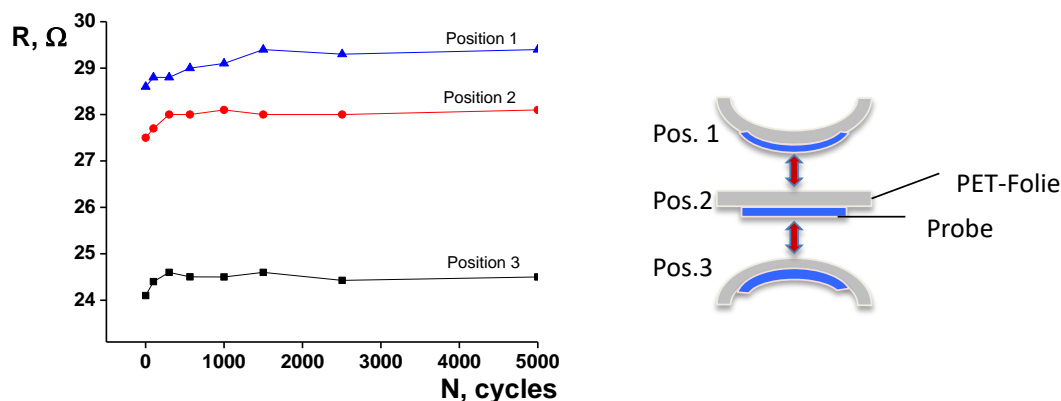


Figure 4.42 Resistance of the conductive film casted on the PET film in different bending states.

Another important factor for the hybrid microgel based conductive films is the stability against stretching (Figure 4.43). As was mentioned before stretching of the hybrid microgels leads to an increase of the distance between the metal nanoparticles and an increase of the electrical resistance.

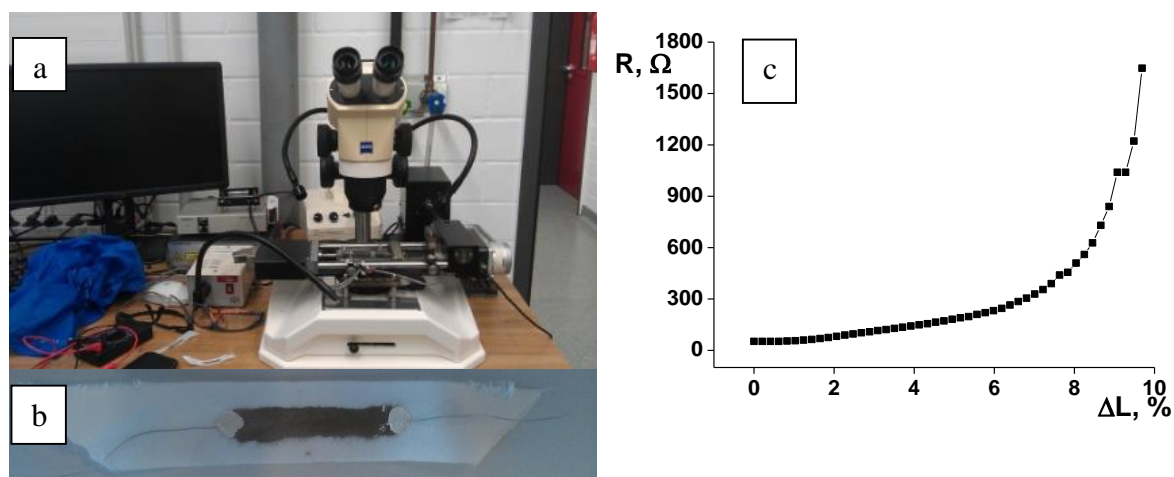


Figure 4.43 Device for the measuring of the electrical resistance during stretching (a), cotton fabric covered with VCL-AAEM-AAC microgel loaded with 60 % of silver nanoparticles (b), dependence of stretching on the electrical resistance (c).

For this experiment hybrid microgels were casted on the diagonally cut cotton fabric (Figure 4.43 b). The ends of the conductive film were combined with the wires using silver glue. The textile with conductive layer was placed between two moving parts of the stretching device. During the slow stretching, resistance values were recorded (Figure 4.43 c). From the

#### 4. Microgel Based Conductive Films

stretching results it can be seen that the hybrid microgel can be stretch up to 8 % without significant loss of conductivity. After 8 % a huge increase in the resistance can be seen in the system, after 10 % cracks occur in the films and the layer is no longer conductive.

The influence of water on the conductive films was also studied. By using the conductive films on textiles, the films should stay conductive after a washing procedure. For this experiment, conductive inks were casted on the PET film and textile samples. The samples were placed in aqueous media by continuous measuring of the electrical resistance. One part of the samples was uncovered, another part of the samples was covered with the silicon to prevent the swelling of the microgels. The results of the conductivity measurement are shown in figure 4.44. As a result, the samples without protective layer swell in water, which leads to the loss of conductivity. At the same time, the samples covered with silicon are protected from the swelling and show constant conductivity over a long period.

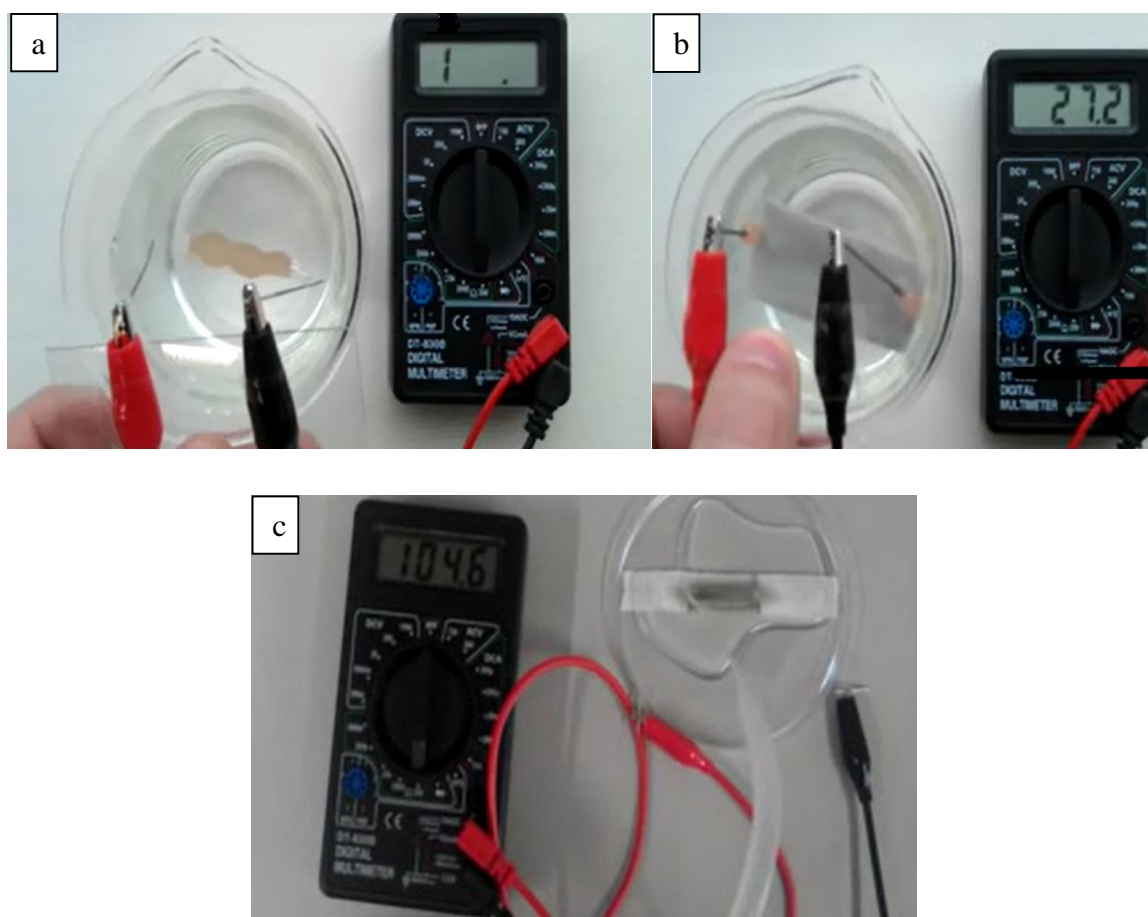


Figure 4.44 Conductivity measurement of the hybrid microgels casted on the PET film uncovered (a), covered (b) and on the textile, covered (c)

#### 4. Microgel Based Conductive Films

---

For the demonstration of the principal possibility of using the hybrid microgels as conductive arrays, circuits on the different substrates were printed. As conductive inks, 8% hybrid microgel dispersions containing 60 wt-% of silver nanoparticles were used. A first example was FRID chip printed on cotton substrate using screen printing. Second example was electrical circuit consisting of battery, switch and LED light. It was possible to get electrical contact and light the LED lamp (Figure 4.45 a, b).

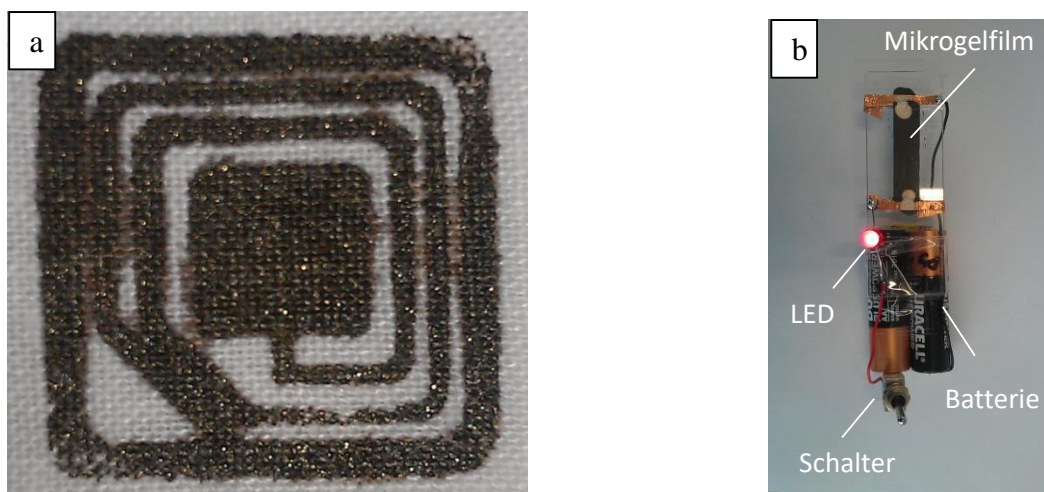


Figure 4.45 Examples of printed conductive films: FRID on cotton (a) and conductive film for lightning a LED (b).

## 5 Conclusions and outlook

In the first part of the work stimuli responsive, thermo-sensitive, hybrid microgels loaded with metal complexes and nanoparticles for application in catalysis were synthesized. The microgels exhibit a critical aggregation temperature (CAT) behavior in different alcohols. At temperatures above the CAT all microgels described in this part of the work are well redispersed and swollen in the solvent giving stable dispersion. By temperatures near and below CAT microgel particles started to collapse and aggregate, building solid sediments which can be removed from the solvent using decantation or mild centrifugation. Thermo-responsive properties were possible by application of the thermo-responsive ethyl acrylate as a main monomer.

It was shown that ethyl acrylate microgels can be easily modified with different comonomers giving new functionalities to the resulting microgels. First described system were EA-HEMA microgels with different comonomer ratios. Presence of the HEMA in the system due to the hydrophilicity of HEMA lead to the shifting of the CAT to the low temperature region. Additionally, presence of the hydroxyl group in HEMA molecule give opportunity for further modification. The second, third and fourth systems were based on AAEM and AAC comonomers, which can make strong complexes with metal nanoparticles. Acrylic acid was able to shift the CAT point in low temperature region; AAEM in contrast shifts the CAT to high temperature region.

The system based on EA:AAEM (90:10) was loaded with variety of metal nanoparticles. It was possible to form iridium, rhodium, platinum, ruthenium and palladium nanoparticles using environmentally friendly in-situ reduction of the metal salts in microgel dispersions using hydrogen under high pressure. Hybrid microgels loaded with very small (2-3 nm) noble metal nanoparticles exhibited high catalytic activity and recyclability.

Besides the metal nanoparticles, EA based microgels were modified with metal complexes directly during the polymerization, using functional comonomers or post-modification using –OH groups EA-HEMA microgels. In this work, microgels were successfully modified with iridium and rhodium complexes. Resulting microgels show thermosensitive properties and are active in catalysis.

## 5. Discussion and Outlook

---

As a further investigation of the catalytically active thermosensitive microgels can be the design of a catalytic systems, which exhibit CAT properties in other solvents, by replacing ethyl acrylate with other temperature sensitive monomers. In addition, the incorporation of the catalytic active organic molecules or enzymes are of big interest for the creation of highly active and selective modern catalysts.

In the second part of this work, adhesive, highly flexible and geometrically defined conductive films were produced. It was possible to design water-based inks based on metal nanoparticles loaded microgels (hybrid microgels). After the drying procedure of the hybrid microgels, metal nanoparticles have contact to each other insuring the electrical conductivity of the printed areas at metal loading of 50 wt-%.

As microgel systems in this part of the work two microgels were successfully synthesized and characterized. First system was based on *N*-Vinylcaprolactam (VCL), 2-(Methacryloyloxy)ethyl acetoacetate (AAEM), 1-Vinyl-2-pyrrolidone (VP) and [2-(Methacryloyloxy)ethyl]trimethylammonium chloride (MEAK) as a functional comonomers and *N,N'*-Methylenebisacrylamide (BIS) as a crosslinker. The MEAK and AAEM were used for the stabilization of the microgel during the synthesis and for complexation of the metal ions and nanoparticles, VP was used as photo initiator for reduction of the copper ions. The second microgel system was based on *N*-vinylcaprolactam (VCL) as a main monomer, 2-(methacryloyloxy)ethyl acetoacetate (AAEM) and acrylic acid as a functional comonomers and on *N,N'*-methylenebisacrylamide (BIS) as a crosslinker. The complexation of the metals was possible with application of AAEM and AAC.

The loading of the microgels with metal nanoparticles and their incorporation was performed by reduction of the metal salts directly in water-based microgel dispersions using chemical or UV-light reduction. The usage of chemical reduction agents for the reduction of the metals in microgel dispersions was more preferable. Chemical reduction leads to the complete reduction of the metal ions and the metal nanoparticle loading can be easily set by setting the start ion concentration.

It was possible to perform a controlled loading of the microgels with metal nanoparticles up to 50 wt-%. The high loaded hybrid microgels exhibit high colloidal stability and good film formation properties.

Especially interesting and commercially efficient is the application of the core-shell metal particles for the production of the conductive inks. In this work core-shell particles consisting

## 5. Discussion and Outlook

---

of copper core and silver shell were synthesized. The synthesis of core-shell particles performed by reducing of the copper salts in-situ in microgels dispersions with additional treating with silver salt, which lead to the reduction of the silver ions on the copper nanoparticles surface. As an alternative to this system silver nanoparticle loaded hybrid microgel can be used.

The printed areas show high mechanical stress tolerance. Electric paths produced in this work were able to get through 5000 bend cycles. Even by stretching of the sample up to 8 % the conductivity stays in place. Because of the swelling behavior of the microgel in water, metal nanoparticles can lose contact to each other and as a result, a loss of the conductivity occurs, therefore it is necessary to prevent the contact of the hybrid microgels with water by using covering films. The hybrid microgel films in this work were protected using polysiloxanes as a protective layer, which prevent not only swelling of the microgels but also metal leaching from the film.

## References

- [1] W. Funke, O. Okay and B. Joos-Müller, Microencapsulation/Microgels/Iniferters, edited by S. DiMari, W. Funke, M. A. Haralson, D. Hunkeler, B. Joos-Müller, A. Matsumoto, O. Okay, T. Otsu, A. C. Powers, A. Prokop, T. G. Wang and R. R. Whitesell (Springer Berlin Heidelberg, 1998), Vol. 136, 139-234;
- [2] R. Pelton, *Advances in Colloid and Interface Science* 2000, 85 (1), 1-33;
- [3] Z. Li, W. Richtering, T. Ngai, *Soft Matter*, 2014, 10, 6182-6191;
- [4] K. Geisel, L. Isa, W. Richtering, *Angew. Chem.*, 2014, 126, 5005-5009;
- [5] B. R. Saunders and B. Vincent, *Advances in Colloid and Interface Science* 1999, 80 (1), 1-25;
- [6] K. Geisel, W. Richtering, L. Isa *Soft Matter*, 2014, 10, 7968-7976;
- [7] S. Nayak and L. A. Lyon, *Angewandte Chemie* 2005, 117 (47), 7862-7886;
- [8] Y. Hertle, T. Hellweg, *J. Mater Chem.* 2013, 1, 5874-5885;
- [9] M. Das, E. Kumacheva, *Chem. Mater.* 2008, 20, 7157-7163;
- [10] W. Richtering, A. Pich, *Soft Matter*, 2012, 8(45), 11423-11430;
- [11] V. Koula, R. Mohameda, D. Kuckling, H.-J. P. Adler, V. Choudhary, *Colloids and Surfaces B: Biointerfaces* 2011, 83, 204-213;
- [12] A. Pich and H.-J. P. Adler, *Polymer International* 2007, 56 (3), 291-307;
- [13] A. V. Kabanov, S. V. Vinogradov, *Angew. Chem. Int. Ed.* 2009, 48, 5418;
- [14] D. J Siegwart, J. K. Oh, K. Matyjaszewski, *Prog. Polym. Sci.* 2012, 37, 18;
- [15] M. Ballauff and Y. Lu, *Polymer* 2007, 48 (7), 1815-1823;
- [16] Y. Lu, Y. Mei, M. Drechsler, M. Ballauff, *Angew. Chem. Int. Ed.*, 2006, 45 , 813;
- [17] Y. Lu, S. Proch, M. Schrunner, M. Drechsler, R. Kempe, M. Ballauff. *J. Mater. Chem.*, 2009, 19, 3955;
- [18] A. Döring, W. Birnbaum, D. Kuckling, *Chem. Soc. Rev.* 2013, 42, 7391-7420;



## References

---

- [19] L. Shen, A. Pich, D. Fava, M. Wang, S. Kumar, C. Wu, G. D. Scholes and M. A. Winnik, *Journal of Materials Chemistry* 2008, 18 (7), 763-770;
- [20] S. Nayak and L. A. Lyon, *Angewandte Chemie International Edition* 2005, 44 (47), 7686-7708;
- [21] S. Lehmann, S. Seiffert, W. Richtering *Journal of Colloid and Interface Science* 2014, 431, 204-208;
- [22] A. Pich, W. Richtering: *Microgels by precipitation polymerization: Synthesis, characterization, and functionalization. Chemical Design of Responsive Microgels*, volume 234, pages 1–37. Springer Berlin Heidelberg, Berlin, Heidelberg, 2010;
- [23] RH. Pelton, P. Chibante, *Colloids. Surf.* 1986 20, 247;
- [24] M. Panayiotou, C. Pöhner, C. Vandevyver, C. Wandrey, F. Hilbrig, R. Freitag, *React Funct Polym* 2007, 67, 807;
- [25] A. Imaz, JI. Miranda, J. Ramos, J. Forcada, *Eur. Polym. J.* 2008, 44, 4002;
- [26] K. Kratz, A. Lapp, W. Eimer, T. Helweg, *Colloids Surf. A Physicochem. Eng. Asp.* 2002, 197, 55;
- [27] W. McPhee, KC. Tam, R. Pelton, *J. Colloid Interface Sci.*, 1993 156, 24;
- [28] M. Luther, C. Heuck, *Chem. Abstr.*, 1932, 26, 4505;
- [29] W.D. Harkins, *J. Am. Chem. Soc.*, 1949, 69, 1428;
- [30] A. Ravve, *Organic Chemistry of Macromolecules*, Dekker, New York, 1967;
- [31] MJ. Snowden, BZ. Chowdry, B. Vincent, GE. Morris, *J. Chem. Soc. Faraday Trans.*, 1996, 92, 5013;
- [32] K. Kratz, T. Helweg, W. Eimer, *Colloids Surf. A Physicochem Eng. Asp.*, 2000, 170, 137;
- [33] S. Peng, C. Wu, *Macromolecules*, 2001, 34, 568;
- [34] V. Boyko, S. Richter, W. Burchard, KF. Arndt, *Langmuir*, 2007, 23, 776;
- [35] JD. Debord, LA. Lyon, *Langmuir* 2003, 19, 7662;

## References

---

- [36] V. Boyko, A. Pich, Y. Lu, S. Richter, KF. Arndt, HJ. Adler, *Polymer*, 2003, 44, 7821;
- [37] T. Hoare, D. McLean, *J. Phys. Chem. B*, 2006, 110, 20327;
- [38] T. Hoare, R. Pelton, *Langmuir*, 2004, 20, 2123;
- [39] J. I. Amalvy, E. J. Wanless, Y. Li, V. Michailidou, S. P. Armes, Y. Duccini, *Langmuir*, 2004, 20, 8992;
- [40] G. Eichenbaum, P. Kiser, A. Dobrynin, S. Simon, D. Needham, *Macromolecules*, 1999, 32, 4867;
- [41] A. Garcia, M. Marques, T. Cai, R. Rosario, Z. Hu, D. Gust, M. Hayes, SA. Vail, CD. Park, *Langmuir*, 2007, 23, 224;
- [42] J. Xu, R. Pelton, *J. Colloid Interface Sci.*, 2004, 276, 113;
- [43] T. Hu, Y. You, C. Pan, C. Wu, *J. Phys. Chem. B*, 2002, 106, 6659;
- [44] N. Greinert, W. Richtering, *Colloid Polym. Sci.*, 2004, 282, 1146;
- [45] J.E. Wong, A.M. Diez-Pascual, W. Richtering, *Macromolecules*, 2009, 42, 1229;
- [46] J. Kleinen, W. Richtering, *Macromolecules*, 2008, 41, 1785;
- [47] N. Häntzschel, M. Schrunner, H. Hund, RD. Hund, C. Lück, A. Pich, *Macromol Biosci.* 2009, 9, 444;
- [48] C. Cheng, X. Zhu, A. Pich, M. Möller, *Langmuir*, 2010, 26, 4709;
- [49] Y. Gong, M. Gao, D. Wang, H. Möhwald, *Chem. Mater.*, 2005, 17, 2648;
- [50] M. Kuang, D. Yang, H. Bao, M. Gao, H. Möhwald, M. Jiang, *Adv. Mater.*, 2005, 17, 267;
- [51] I. Gorelikov, LM. Field, E. Kumacheva, *J. Am. Chem. Soc.*, 2004, 126, 15938;
- [52] A. Biffis, N. Orlandi, B. Corain, *Adv. Mater.*, 2003 15, 1551;
- [53] G. Zhang, D. Wang, Z. Gu, J. Hartmann, H. Möhwald, *Chem. Mater.*, 2005, 17, 5268;
- [54] G. Zhang, D. Wang, Z. Gu, H. Möhwald, *Langmuir*, 2005, 21, 9143;
- [55] J. Zhang, S. Xu, E. Kumacheva, *Adv. Mater.*, 2005, 17, 2336;

## References

---

- [56] F. Tang, N. Ma, L. Tong, F. He, L. Li, *Langmuir*, 2011 28, 883;
- [57] D. Suzuki, H. Kawaguchi, *Langmuir*, 2005, 21, 12016;
- [58] S. Tehrani, W. Lin, S. Rosenfeldt, G. Guerin, Y. Lu, Y. Liang, M. Drechsler, S. Förster, M. Winnik, *Chem. Mater.*, 2016, 28, 501;
- [59] A. Pich, A. Karak, Y. Lu, A.K. Ghosh, H. Adler, *Macromol. Rapid Commun.*, 2006, 27, 344;
- [60] A. Pich, J. Hain, Y. Lu, V. Boyko, Y. Prots, H. Adler, *Macromolecules*, 2005, 38, 6610;
- [61] S. Schachschal, A. Pich, *Langmuir*, 2008, 24, 5129;
- [62] H. Jia, D. Schmitz, A. Ott, A. Pich, Y. Lu, *J. Mater. Chem. A*, 2015, 3, 6187;
- [63] A. Contin, A. Biffis, S. Sterchele, K. Dörmbach, S. Schipmann, A. Pich, *J. of Colloid and Interface Sci.*, 2014, 414, 41;
- [64] Llopis, J., Albert, A., Usobinaga P.: *Eur. Polym. J.* 1967, 3, 259;
- [65] Sander, U., Wolf, B.A.: *Angew. Makromol. Chem.* 1986, 139, 149;
- [66] Herold, F.K., Schulz, G.V., Wolf, B.A.: *Materials Chem. Phys.* 1983, 8, 243;
- [67] Dusek, K.: *Coll. Czech. Chem. Commun.* 1969, 34, 3309;
- [68] Jenckel, E., Gorke, K.: *Z. Naturforsch.* 1950, 5, 556;
- [69] H. Feil, Y. Bae, J. Feijen, S. Kim, *Macromolecules*, 1993, 26, 2496;
- [70] E. Makhaeva, L. Thanh, S. Starodoubtsev, A. Khokhlov, *Macromol. Chem. Phys.*, 1996, 197, 1973;
- [71] S. Peng, C. Wu, *Macromol. Symp.*, 2000, 159, 179;
- [72] M. Panayiotou, R. Freitag, *Polymer*, 2005, 46, 615;
- [73] S. Peng, C. Wu, *Macromolecules*, 2001, 34, 6795;
- [74] C. Jones, L. A. Lyon, *Langmuir*, 2003, 19, 4544;

## References

---

- [75] V. Pinkrah, M. Snowden, J. Mitchell, J. Seidel, B. Chowdhry, G. Fern, *Langmuir*, 2003, 19, 585;
- [76] T. Hoare, R. Pelton, *Macromolecules*, 2004, 37, 2544;
- [77] S. Peng, C. Wu, *Polymer*, 2001, 42, 6871;
- [78] B. Saunders, N. Laajam, E. Daly, S. Teow, X. Hu, R. Stepto, *Adv. Colloid Interface Sci.*, 2009, 147, 251;
- [79] H. Crowther, B. Vincent, *Colloid Polym. Sci.*, 1998, 276, 46;
- [80] K. Mukae, M. Sakuri, S. Sawamura, K. Makino, S. Kim, I. Ueda, K. Shirahama, J. *Phys. Chem.*, 1993, 97, 737;
- [81] M. Mielke, R. Zimehl, *Prog. Colloid. Polym. Sci.*, 1998, 111, 74;
- [82] B. Saunders, H. Crowther, B. Vincent, *Macromol.*, 1997, 30, 482;
- [83] P. Zhu, D. Napper J. *Colloid. Interface Sci.*, 1996, 177, 343;
- [84] M. Moniruzzaman, G. Fernando, J. Talbot, *Journal of Polymer Science Part A- Polymer Chemistry*, 2004, 42, 2886;
- [85] D. Kungwatchakun, M. Irie, *Makromolekulare Chemie Rapid Communications*, 1988, 9, 243;
- [86] L. Chen, S. Li, Y. Zhao, Y. Wang, Q. Wang, *Journal of Applied Polymer Science*, 2005, 96, 2163;
- [87] H. Cui, H. Chen, R. Qu, C. Wang, C. Sun, W. Zhou, M. Yu and H. Jiang, *J. Appl. Polym. Sci.*, 2009, 111, 3144;
- [88] V. Butun, A. Atay, C. Tuncer, Y. Bas, *Langmuir*, 2011, 27, 12657;
- [89] J. Clarke, B. Vincent, *J. Chem. Soc., Faraday Trans.*, 1981, 77, 1831;
- [90] H. Nur, M. Snowden, V. Cornelius, J. Mitchell, P. Harvey, L. Benee, *Colloids Surf. A*, 2009, 335, 133;
- [91] M. Antonietti, W. Bremser, M. Schmidt, *Macromolecules*, 1990, 23, 3796;
- [92] L. Cragg, J. Manson, *J. Polym. Sci.*, 1952, 9, 265;

## References

---

- [93] L. Nie, W. Jiang, W. Yang, C. Wang, S. Fu, J. Macromol. Sci., Part A: Pure Appl.Chem., 2005, 42, 623;
- [94] R. Frank, J. Downey, K. Yu, H. Stover, Macromolecules, 2002, 35, 2728;
- [95] H. Jiang, H. Chen, Y. Liang, X. Liu, Polym. Adv. Technol., 2011, 22, 1555;
- [96] X. Lu, D. Huang, X. Yang, W. Huang, Polym. Bull., 2006, 56, 171;
- [97] J. Downey, G. McIsaac, R. Frank, H. Stover, Macromolecules, 2001, 34, 4534;
- [98] E. Goh, H. Stover, Macromolecules, 2002, 35, 9983;
- [99] J. Machotova, J. Snuparek, Z. Cernosek, L. Svoboda, Prog. Org. Coat., 2008, 62, 71;
- [100] N. Leadbeater, M. Marco, Chem. Rev., 2002, 102, 3217;
- [101] D. Bergbreiter, J. Tian, C. Hongfa, Chem. Rev., 2009, 109, 530;
- [102] T. Terashima, M. Kamigaito, K. Baek, T. Ando, M. Sawamoto, J. Am. Chem. Soc., 2003, 125, 5288;
- [103] T. Terashima, M. Ouchi, T. Ando, M. Kamigaito, M. Sawamoto, J. Polym. Sci., Part A: Polym. Chem., 2006, 44, 4966;
- [104] T. Terashima, M. Ouchi, T. Ando, M. Kamigaito, M. Sawamoto, Macromolecules, 2007, 40, 3581;
- [105] T. Terashima, M. Ouchi, T. Ando, M. Sawamoto, J. Polym. Sci., Part A: Polym. Chem., 2010, 48, 373;
- [106] T. Terashima, M. Ouchi, T. Ando, M. Sawamoto, J. Polym. Sci., Part A: Polym. Chem., 2011, 49, 1061;
- [107] T. Terashima, M. Ouchi, T. Ando, M. Sawamoto, Polym. J., 2011, 43, 770;
- [108] T. Terashima, A. Nomura, M. Ito, M. Ouchi, M. Sawamoto, Angew. Chem., Int. Ed., 2011, 50, 7892;
- [109] T. Terashima, A. Nomura, M. Ouchi, M. Sawamoto, Macromol. Rapid Commun., 2012, 33, 833;
- [110] J. Deng, C. Lu, G. Yang, Z. Chen, React. Funct. Polym., 2012, 72, 378;

- [111] N. Haraguchi, A. Nishiyama, S. Itsuno, *J. Polym. Sci., Part A: Polym. Chem.*, 2010, 48, 3340;
- [112] Y. Lu, Y. Mei, M. Ballauff, M. Drechsler, *J. Phys. Chem. B*, 2006, 110, 3930;
- [113] Y. Mei, Y. Lu, F. Polzer, M. Ballauff, M. Drechsler, *Chem. Mater.* 2007, 19, 1062;
- [114] J. Zhang, G. Wei, T. Keller, H. Gallagher, C. Stötzl, F. Müller, M. Gottschaldt, U. Schubert, K. Jandt, *Macromol. Mater. Eng.*, 2010, 295, 1049;
- [115] N. Sahiner, O. Ozay, *React. Funct. Polym.*, 2011, 71, 607;
- [116] S. Kanaoka, N. Yagi, Y. Fukuyama, S. Aoshima, H. Tsunoyama, T. Tsukuda, H. Sakurai, *J. Am. Chem. Soc.*, 2007, 129, 12060;
- [117] A. Biffis, *J. Mol. Catal. A: Chem.*, 2001, 165, 303;
- [118] A. Biffis, E. Sperotto, *Langmuir*, 2003, 19, 9548;
- [119] P. Steward, J. Hearn, M. Wilkinson, *Adv. Colloid Interface Sci.*, 2000, 86, 195;
- [120] J. Bieleman, J. Hajas, K. Dören, Flow-levelling and coalescing agents, in: *Additives for coatings*, Wiley-VCH Verlag GmbH, 2007, pp. 163–200;
- [121] G.L. Brown, *J. Polym. Sci.*, 1956, 22 423;
- [122] F. Dobler, Y. Holl, *Trends Polym. Sci.*, 1996, 4, 145;
- [123] J. Keddie, A. Routh, Molecular diffusion across particle boundaries, in: *Fundamentals of Latex Film Formation*, Springer, Netherlands, 2010, pp. 151–183;
- [124] O.L. Wheeler, H.L. Jaffe, N. Wellman, *Off. Digest*, 1954, 26, 1239;
- [125] F. Dobler, Y. Holl, *American Chemical Society*, 1996, 648, 22;
- [126] D. Sheetz, *J. Appl. Polym. Sci.*, 1965, 9, 3759;
- [127] M. Yue, Y. Hoshino, Y. Ohshiro, K. Imamura, Y. Miura, *Angew. Chem. Int. Ed.*, 2014, 53, 2654;
- [128] C. Sorrell, M. Carter, M. Serpe, *Appl. Mater. Interfaces*, 2011, 3, 1140;
- [129] O. Zavgorodnya, M. Serpe, *Colloid Polym Sci*, 2011, 289, 591;

- [130] M. Serpe, K. Yarmey, C. Nolan, A. Lyon, *Biomacromolecules*, 2005, 6, 408;
- [131] C. Nolan, M. Serpe, A. Lyon, *Biomacromolecules*, 2004, 5, 1940;
- [132] C. Sorrell, A. Lyon, *J. Phys. Chem. B*, 2007, 111, 4060;
- [133] M. Serpe, C. Jones, L. A. Lyon, *Langmuir*, 2003, 19, 8759;
- [134] C. Sorrell, A. Lyon, *Langmuir*, 2008, 24, 7216;
- [135] A. South, R. Whitmire, A. Garcí'a, A. Lyon, *Appl. Mater Interfaces.*, 2009, 1, 2747;
- [136] Y. Xia, X. He, M. Cao, C. Chen, H. Xu, F. Pan, J. Lu, *Biomacromolecules*, 2013, 14, 3615;
- [137] K. Horigome, D. Suzuki, *Langmuir*, 2012, 28, 12962;
- [138] S. Schmidt, T. Hellweg, R. Klitzing, *Langmuir* 2008, 24, 12595;
- [139] S. Schmidt, M. Zeiser, T. Hellweg, C. Duschl, A. Fery, H. Möhwald, *Adv. Funct. Mater.*, 2010, 20, 3235;
- [140] J. Wei, J. Cai, Y. Li, B. Wu, X. Gong, T. Ngai, *Colloids and Surfaces B: Biointerfaces*, 2015, 132, 202;
- [141] S. Berger, R. Singh, J. Sudha, H. Adler, A. Pich, *Polymer*, 2010, 51, 3829;
- [142] S. Bhattacharya, F. Eckert, V. Boyko, A. Pich, *Small*, 2007, 3, 650;
- [143] A. Pich, S. Bhattacharya, Y. Lu, V. Boyko, H. Adler, *Langmuir*, 2004, 20, 10706;
- [144] Y. Xia, Y. Gu, X. Zhou, H. Xu, X. Zhao, M. Yaseen, J. Lu, *Biomacromolecules*, 2012, 13, 2299;
- [145] A. L. Dearden; P. J. Smith; D.-Y. Shin; N. Reis, B. D.; P. O'Brien. *Macromol. Rapid Commun.* 2005, 26, 315;
- [146] K. F. Teng; R. W. Vest. *IEEE Trans. Comp. Manufact. Tech.* 1988, 11, 291;
- [147] Y. Byun; E.-C. Hwang; S.-Y. Lee; Y.-Y. Lyu; J.-H. Yim; J.-Y. Kim; S. Chang; Pu, L. S.; J. M. Kim. *Materials Science and Engineering B* 2005, 117, 11;

## References

---

- [148] M. Y. Park; J.-H. Son; Rhee, S.-W. *Electrochemical and Solid-State Letters* 1998, 1, 32;
- [149] G. G. Rozenberg; J. H. G. Steinke. *Organometallics* 2001, 20, 4001;
- [150] D. Kim; J. Moon. *Electrochemical and Solid-State Letters* 2005, 8, 30;
- [151] P. Buffat, J.-P. Borel. *Phys. Rev.* 1976, 13, 2287;
- [152] J. B. Szczech; C. M. Megaridis; J. Zhang; D. R. Gamota. *Microscale Thermophysical Engineering* 2004, 8, 327;
- [153] M. Grouchko, A. Kamyshny, S. Magdassi, *Journal of Materials Chemistry*, 2009, 19, 3057;



---

## Danksagung

An dieser Stelle möchte ich mich bei all denen bedanken, die mich bei der Anfertigung der Doktorarbeit unterstützt haben:

Zuerst möchte ich Prof. Dr. Andrij Pich für die Aufnahme in seine Arbeitsgruppe und die Vergabe der sehr spannenden Forschungsthemen recht herzlich bedanken. Seine Kommentare und Anmerkungen haben mich darin unterstützt meine Horizonte in der Polymer- und Kolloidchemie zu erweitern.

Weiter möchte ich mich bei den BMBF SKY Projekt Kollegen aus dem Institut für organische Chemie: Prof. Dr. Magnus Rueping, Dr. Rüdiger Borrmann, Marta Fernandes und den Mitarbeiter von Evonik Industries: Dr. Renat Kadyrov, Dr. Dorit Wolf und Dr. Cornelius Friedrichs für die gute und fruchtbare Zusammenarbeit bedanken.

Ein Dank gilt auch den Auszubildenden und Studenten, welche ihre Bachelor- und Diplomarbeiten unter meiner Anleitung erstellt, sowie als wissenschaftliche Hilfskraft für mich gearbeitet haben. Dazu gehören: Marcella Blees, David Schroeter, Richard von Goetze und Michel Waringo.

Weiterhin gilt mein großer Dank der Arbeitsgruppe Pich. Vielen Dank für die fachlichen Gespräche über die Arbeitszeit hinaus und die gemeinsam verbrachte Freizeit. Darüber hinaus möchte ich meine besondere Verbundenheit zu Andreea Balaceanu, Christian Willems, Dominic Kehren, Sebastian Kühl, Thorsten Palmer, Jason Zografou und Karla Dörmbach ausdrücken. Ihr seid nicht nur Kollegen für mich, sondern richtige Freunde, auf die man sich immer verlassen kann.

Besonders danke ich Familie Graefenstedt für die kontinuierliche Unterstützung und die nette Freizeitgestaltung.

Und natürlich danke ich meiner lieben Familie, meinen Eltern und Geschwistern, für ihre Unterstützung und Liebe. Ich danke Euch sehr.

---

## **Versicherung**

Hiermit versichere ich, dass ich die vorliegende Arbeit ohne unzulässige Hilfe Dritter und ohne Benutzung anderer als der angegebenen Hilfsmittel angefertigt habe; die aus fremden Quellen direkt oder indirekt übernommen Gedanken sind als solche kenntlich gemacht. Die Arbeit wurde bisher weder im Inland noch im Ausland in gleicher oder ähnlicher Form einer anderen Prüfungsbehörde vorgelegt.

Volodymyr Palchyk